AN ABSTRACT OF THE THESIS OF

Laxmikant Dhage for the degree of Master of Science in Ocean, Earth and Atmospheric Sciences presented on March 20, 2014.

Title: Intra-seasonal Sea Level Variability along the West Coast of India

Abstract approved: ______________________________

P. Ted Strub

The importance of local versus distant forcing is studied for the wind driven intra-seasonal (30-120 day) sea level anomaly (SLA) variations along the west coast of India. Three locations on the continental slope are chosen to represent the west coast. Two more locations, one east of Sri-Lanka and another on the south east coast of India are chosen to investigate their remote contributions to the intra-seasonal SLA variability along the west coast of India. Significant correlations of altimeter derived SLA on the west coast are found with the SLA east of Sri-Lanka and SLA as far as Sumatra and the Equator, with increased lags. These correlations are consistent with remote forcing from the Equator in the form of reflected Rossby waves originating along the Sumatra coast. Correlations of SLA on the west coast with the SLA on the south-east coast of India are significant, but lower in magnitude than signals arriving from Sumatra. This suggest that signals on the south-east coast of India (generated locally or along the wave guide between there and the Equator) are significantly weakened as they propagate around Sri-Lanka, the tip of India, in comparison to signals propagating westward from the coast of Sumatra.

The highest correlations between SLA on the west coast and winds are found with the winds from the southern tip of India, suggesting the importance of remote

wind forcing from south of India. This supports the contribution of the coastal trapped wave signals to the west coast of India, although lags between winds at tip of India and SLA on the west coast are longer than expected (6-7 days). An idealised model is used to explore the possibility that the apparent 6-7 day lag in simple correlation is caused by the arrival and combination of several signals, which were generated simultaneously at different locations by the large scale winds.

Extending the 2-point correlations, multivariate linear regression models and coherence calculations identify the remote winds from south of India and the sea level anomalies east of Sri-Lanka as the major contributors to intra-seasonal SLA variability on the west coast of India, with a minor contribution from the south-east coast of India. Use of correlation techniques is complicated by the fact that winds at the bottom of India are correlated with winds throughout the basin-scale system. Some clarification is provided by coherence and phase calculations, which demonstrate the importance of the 40-60 day band in the intra-seasonal (30-120 day) period. Use of the 40-60 day band pass filter eliminates an unrealistically long (5 day) lag between local winds and sea level response on the west coast of India. Hovmoller diagrams help to illustrate the propagation of signals to the west coast of India for two different pathways: A Rossby wave pathway from Sumatra and an East coast pathway from the south-east coast of India. These pathways are consistent with the above statistical analysis.

Intra-seasonal Sea Level Variability along the West Coast of India

by

Laxmikant Dhage

A THESIS

submitted to

Oregon State University

in partial fulfillment of
the requirements for the
degree of

Master of Science

Presented March 20, 2014
Commencement June 2014

Master of Science thesis of Laxmikant Dhage presented on March 20, 2014.

APPROVED:

Major Professor, representing Ocean, Earth and Atmospheric Sciences

Dean of the College of Earth, Ocean and Atmospheric Sciences

Dean of the Graduate School

I understand that my thesis will become part of the permanent collection of Oregon State University libraries. My signature below authorizes release of my thesis to any reader upon request.

Laxmikant Dhage, Author

ACKNOWLEDGEMENTS

First and foremost, I would like to express sincere thanks to my advisor Ted Strub, without whom this work would have never come together. Being an international student from a non-native English speaking country, it was difficult in the beginning but his constant support and encouragement helped and motivated me through out my research. He has been far more than an advisor, providing help, directions and guidance even at the personal level. His patient nature and his belief on me gave me a lot of flexibility in my research. I would also like to express my earnest thanks to Ted Durland, whose constant feedback and direction helped in the gradual progress of my research. I would also like to thank the other members of my committee who read the thesis and provided feedback on the work. A large thank you goes to Corinne James who helped in processing and making available the different datasets used in this research. I would like to thank my fellow graduate students and officemates who have been supportive with useful feedback and discussion. Lastly, a bucket of thanks goes to my parents and my family members for being patient and providing me constant support and motivation. It would have not been possible without them.

TABLE OF CONTENTS

LIST OF FIGURES

LIST OF FIGURES (Continued)

Figure Page

LIST OF FIGURES (Continued)

Figure Page

LIST OF FIGURES (Continued)

Figure Page

Figure Page

LIST OF TABLES

LIST OF APPENDIX FIGURES

Chapter 1: Introduction

Over the past twenty years, progress has been made in defining the seasonal circulation along the east and west coasts of India: in the East India Coastal Current (EICC) and the West India Coastal Current (WICC) as well as in the Bay of Bengal (BOB)-that part of Indian Ocean directly east of the Indian continent. This has been accomplished through traditional oceanographic hydrographic cruises *Shetye et al.* 1996, analytic and numerical modeling studies [*McCreary et al.* 1996; *Shankar* 1997; *McCreary et al.* 1999 and (more recently) using satellite altimeter data [*Babu et al.* 2003; *Durand et al.* 2009; *Vialard et al.* 2009; *Shenoi* 2010; *Rao et al.* 2010].

Sea level variability serves as an indicator of upwelling and downwelling along the west coast of India and is of particular interest because this is an important fisheries region, with increased productivity in upwelling periods. Upwelling events have significant intra-seasonal variability, and in contrast to the more thoroughly understood seasonal variability, the coastal circulation on these shorter time scales is only now being addressed [*Amol et al.* 2012; *Suresh et al.* 2013; *Girishkumar et al.* 2013].

After a brief review of our current understanding of the coastal circulation on annual and inter-annual scales, this work focuses on improving our understanding of what drives the intra-seasonal SSH variability on the west coast of India. This is done by investigating correlations of altimeter sea level anomalies and ECMWF winds at various key locations and by building multivariate regression models to quantify which possible forcing mechanisms explain the greatest amount of the intra-seasonal variability of sea level along the west coast of India.

1.1 Seasonal Cycle

Winds in the northern Indian Ocean change directions twice a year. They blow from the southwest during May-September (summer monsoon) [Fig 1.1] and from the north-east during November-February (winter monsoon)[Fig 1.2]. March-April and October are transition months when winds are very weak. Coastal currents in the northern Indian Ocean show strong seasonal cycles, although not necessarily in phase with local winds. The hydrographic observations, ship-drift currents, surface drifter trajectories and eddy-resolving models show a clear picture of seasonality in the circulation of the northern Indian Ocean [*Shenoi*, 2010]. Along the west coast of India during June-September, the current is equatorward; during the winter monsoon (November-February), currents change to poleward, flowing against the prevailing winds along the coast. Along the east coast of India, the EICC transports are poleward and strongest during March-May, when the winds in the region are the weakest of the year [*Shenoi*, 2010]. During the winter monsoon, the EICC is equatorward, which can be determined using salinity as a tracer [*Shenoi*, 2010]. The EICC carries the fresh water originating in river runoff and transports it as far as the southwest coast of India, turning around Sri Lanka and continuing into the WICC northward along the coast. In this way the WICC and EICC sometimes work together to form a continuous flow beginning in the northern Bay of Bengal and extending to the Northern Arabian Sea.

1.1.1 Semi-annual Kelvin Waves

The circulation described above cannot be forced by local winds alone as, at times, the current flows in directions opposite to the winds. A framework for an explanation of the surface currents can be constructed from a combination of wind-forced and free coastal and equatorial trapped Kelvin and Rossby waves, which occur on scales from intra-seasonal to interannual [*McCreary et al.*, 1996]. Equatorial Kelvin waves are created when the Equatorial Indian Ocean comes under the influence of the annual monsoonal wind forcing. According to *Rao et al.* [2010], two semiannual upwelling Kelvin waves occur: during the winter monsoon (January-March) and the summer monsoon (July-September); and two downwelling Kelvin waves occur: during the summer monsoon transition (April-June) and winter monsoon transition (October-December). These Kelvin waves propagate along the equatorial wave guide until reaching the Sumatra coast. Some of their energy then follows the coastal waveguide counter-clockwise around the perimeter of the BoB. As the signals propagate around the BoB along the coast, they take the form of Coastal Trapped Waves (CTWs), more closely approximating coastal Kelvin waves where the shelf is negligible and the slope is nearly vertical. CTWs can also be created by local winds along the margins of the BoB, but the Equatorial Kelvin waves have been described most frequently in the literature.

Among these waves, only the winter transition downwelling Kelvin wave appears to reach the west coast of India, propagating along the equatorial region, around the coastal BoB and along the west coast of India to its northern edge. Thus, it affects India′s entire coastal circulation [*Rao et al.*, 2010].

1.1.2 Upwelling along the west coast of India

Neither of the semi-annual upwelling Kelvin waves (January-March and June-September) reach the west coast of India. Nor is the local seasonal upwelling-favorable wind-forcing strong along this coast. Winds along the west coast of India are almost perpendicular to the coast, except for a weak equatorward component along the southwest coast during the summer monsoon (June-September). However, a strong upwelling signal can be seen along the west coast of India, making the west coast a biologically productive region. The west coast of India accounts for 70% of the fish catch of the total Arabian Sea [*Bakun et al.*, 1998] and the southwest coast of India contributes about 20% of the total marine fish catch of India [*Manjusha et al.*, 2013]. This demonstrates the economic importance of the upwelling for the Indian marine fisheries and motivates our search for the factors that control its variability, since previous studies find only weak evidence for forcing by Equatorial upwelling Kelvin waves and local wind forcing .

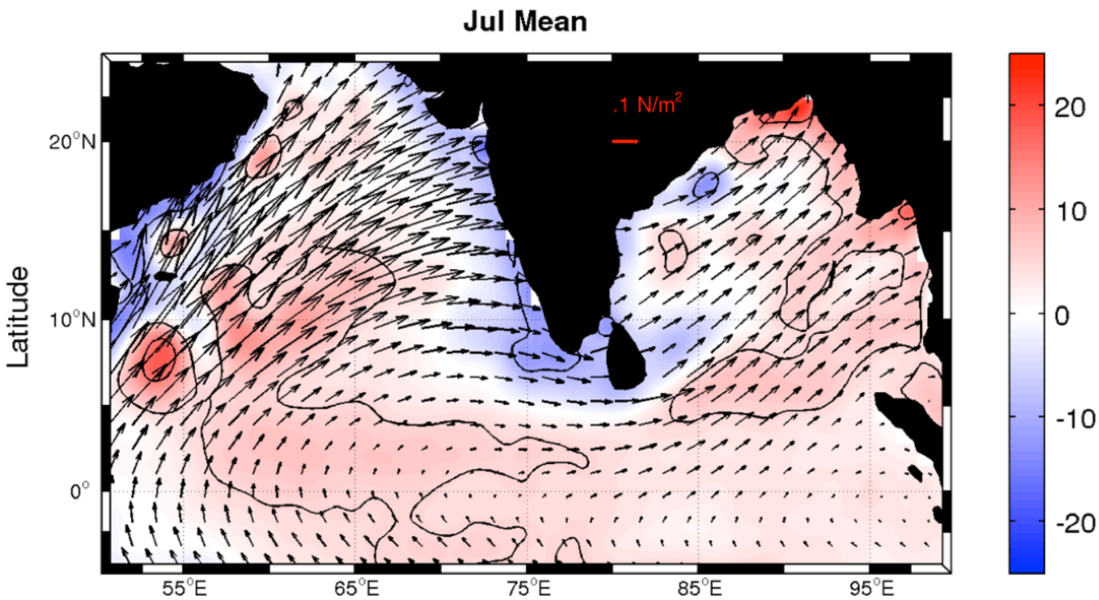

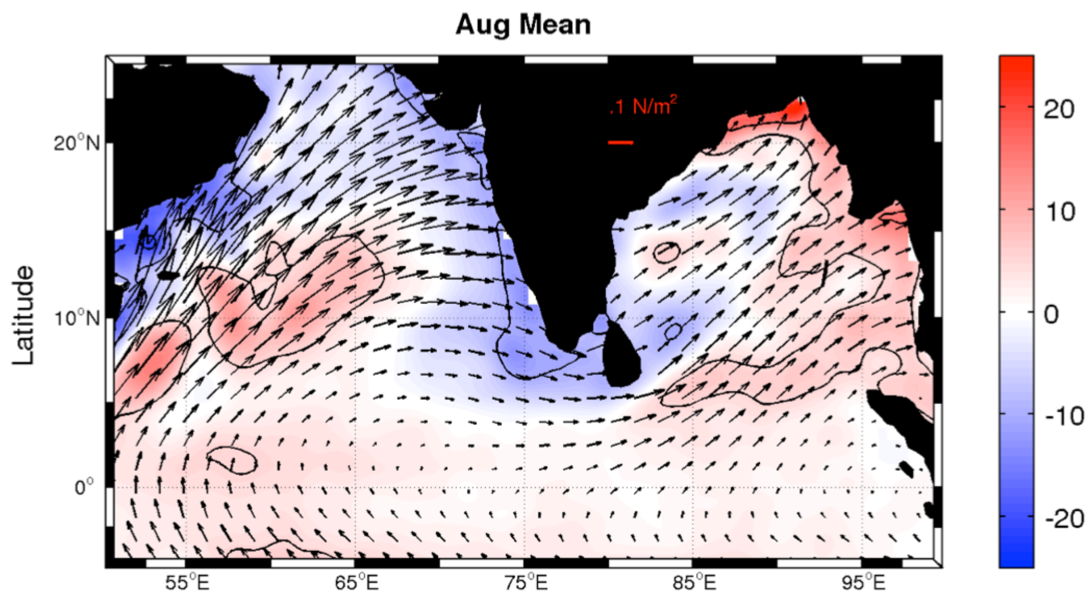

Figure 1.1: Monthly mean AVISO SLA (cm), overlaid are the ECMWF wind stress: Summer Monsoon

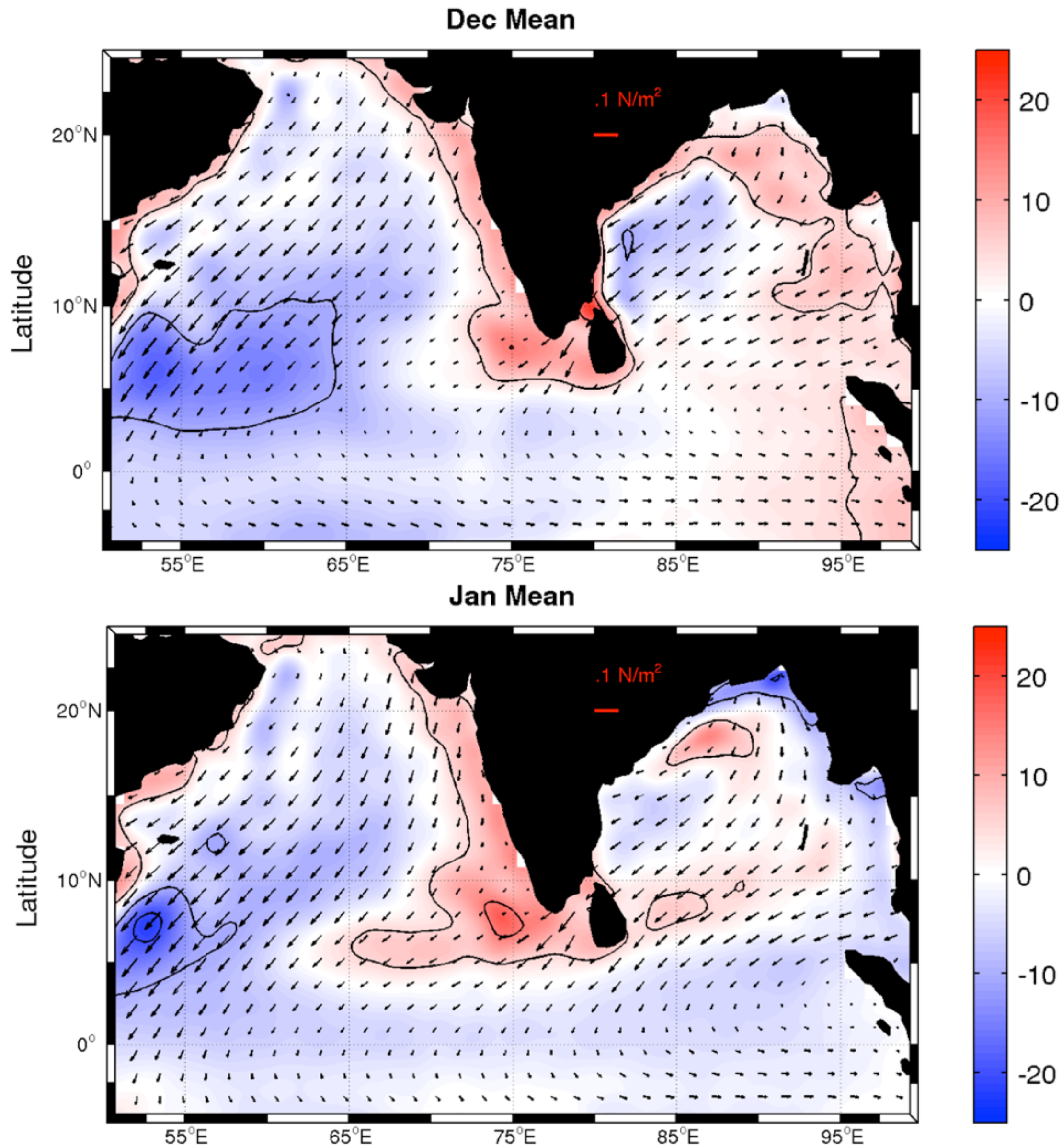

Figure 1.2: Monthly mean AVISO SLA (cm), overlaid are the ECMWF wind stress: Winter Monsoon

1.2 Interannual Variability

Although the focus of our study is the intra-seasonal time scale, we note that the circulation in the northern Indian Ocean includes a significant amount of interannual variability [*Shankar et al.* 2010; *Clarke et al* 1994], largely due to the Indian Ocean Dipole (IOD) events. The IOD is an interannual fluctuation associated with ocean-atmospheric interactions leading to out-of-phase fluctuations of western and eastern equatorial sea surface temperature anomalies (SSTA) [*Saji et al.* 1999; *Webster et al.* 1999]. During positive IOD events easterly wind anomalies occur over the equatorial region, which are replaced during the negative IOD event by westerly wind anomalies. Whether or not these events affect the upwelling along the west coast of India is not considered in this study.

1.3 Intra-seasonal Variability

Recent studies provide evidence of the importance of intra-seasonal variability in the coastal circulation [*Durand et al.* 2009; *Suresh et al.* 2013;*Vialard et al.* 2009;*Amol et al.* 2012; *Girishkumar et al.* 2013]. To investigate the intra-seasonal variability of the WICC, the National Institute of Oceanography (NIO) at Goa has deployed ADCP moorings at several locations along the west coast of India. Studies by *Vialard et al.* [2009] and *Amol et al.* [2012] used data from these ADCP moorings to investigate the propagation of CTW's along the west coast of India.

Data from the mooring off of Goa showed the dominance of intra-seasonal variability of currents in the WICC during 2006-2008 and revealed that the intra-seasonal sea level tends to be in phase with alongshore current variation, suggesting the existence of CTW's along the west coast of India[*Vialard et al.*, 2009]. *Amol et al.* [2012] used the mooring data from both the continental shelf and the slope along the west coast of India to investigate the propagation of CTWs at the intra-seasonal time scales. The propagation was seen on the shelf and also on the slope for a wide band of frequencies. However, the main focus of their study was on higher frequencies, with periods less than the 30-day cut-off used in our study.

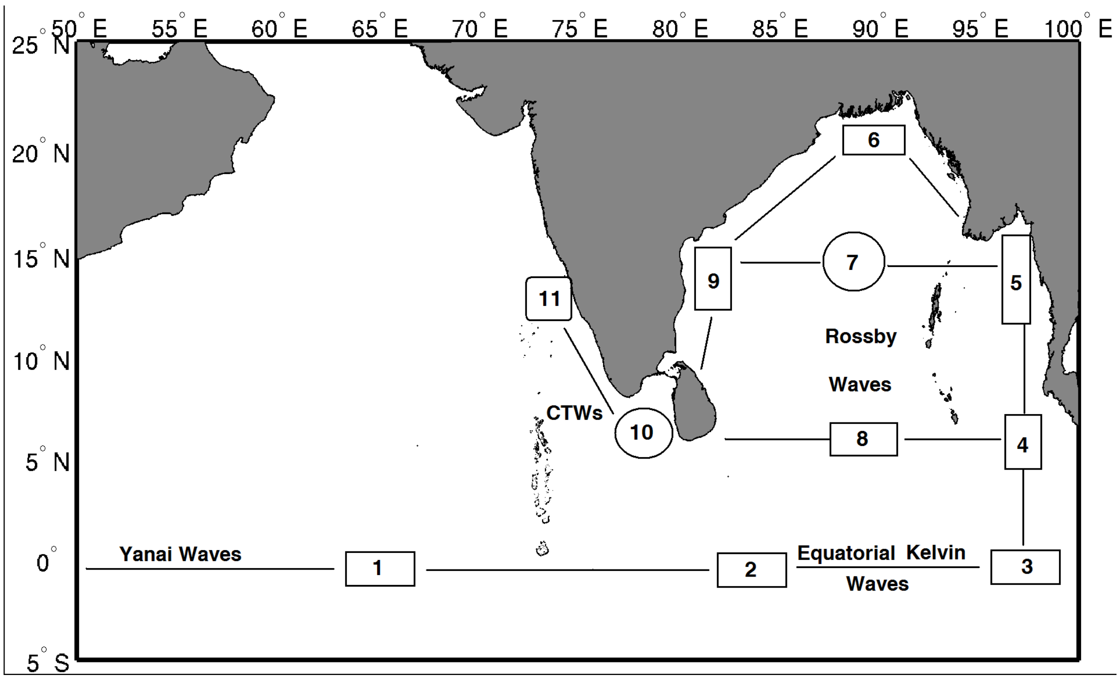

Figure 1.3: Broader picture of basin-wide scale dynamics in the Northern Indian Ocean

Recent modelling work from *Suresh et al.* [2013], suggests that most of the intra-seasonal variability in the Northern Indian Ocean is coming from the equator. In their model, the percentage of intra-seasonal variance attributable to an equatorially generated signal is 80-90% along the north-east coast of the BoB, decreasing to 50% north-east of Sri-Lanka along the wave guide next to south-east India, and then increasing to 60-70% along the west coast of India. The suggested source for this increase is from Rossby waves that are generated by the reflection of equatorial Kelvin waves from the coast of Sumatra, which arrive at the south-east tip of Sri Lanka after crossing the southern BoB. *Suresh et al.* [2013], also conclude that winds near the southern tip of India contribute significantly to the intra-seasonal variability in the WICC. These winds can either reinforce or weaken the incoming Rossby wave signal.

The mechanism through which these winds reinforce or weaken remotely generated signals is through the generation of the sea level signals that propagate as CTWs along the west coast of India. CTWs have been studied extensively during the past 50 years [*Brink*, 1991]. A typical time scale for their local generation is of order 1-2 days, with phase propagation speeds of 2 m/s, resulting in maximum correlations between currents and sea level at a given location and winds 200-500 km up the wave guide at lags of 2 days [*Denbo and Allen et al*, 1987]. As with the results of *Amol et al.* [2012], however, we note that the results of *Denbo and Allen et al* [1987] and most other CTW investigations apply to the higher frequencies.

The net result is that SLA variability along the Indian west coast can come from a combination of several different forcings and signals [Fig 1.3]. In discussing the expected lags between the forcing and response signals, we use standard theory of Kelvin, Rossby and Coastal Trapped Waves (*Appendix A.1*). In this study, we investigate the contribution to intra-seasonal SLA variations along the west coast of India from remote forcing that arrives either as a Rossby wave signal from Sumatra or in the form of CTW signals (generated along the east coast or southern tip of India), and from the local wind forcing.

Chapter 2: DATA AND METHODS

The primary data sets used are 10 years of altimeter sea level anomaly fields (SLA, also referred to as sea surface height anomaly, SSHA) from the Archiving, Validation and Interpretation of Satellite Oceanographic data project (AVISO), along with coincident surface vector winds over the ocean from the European Centre for Medium-Range Weather Forecasts (ECMWF). Both types of data are gridded with spatial separation of 0.25×0.25 degrees between grid points, at weekly and daily time steps. The effective temporal smoothing of the SSHA data from AVISO attenuates periods shorter than approximately 30 days; for consistency, we smooth the wind fields similarly. The means, trends and seasonal cycles (annual cycle plus first three harmonics) are removed prior to a 120-day high pass filter, leaving our intra-seasonal signals in a band-passed data set retaining periods of approximately 30-120 days.

2.1 SLA and Wind Data

2.1.1 SLA

The altimeter sea level anomaly data were obtained from the AVISO, web site (http: //www.aviso.altimetry.fr/). The ten-year period of the data is from October 1999 to November 2009). The standard gridded data are available as weekly fields, while an experimental daily data set is also available and used in this study. Both are optimally interpolated to a 0.25×0.25 degree grid, using all available altimeters as inputs, using the methods described by *LeTraon et al* [2000] and *Ducet et al* [2000]. The effective temporal smoothing of the final gridded product is approximately 30 days [*Chelton et al*, 2011]. No additional temporal smoothing was performed on these data except to eliminate periods greater than 120 days for intra-seasonal analysis.

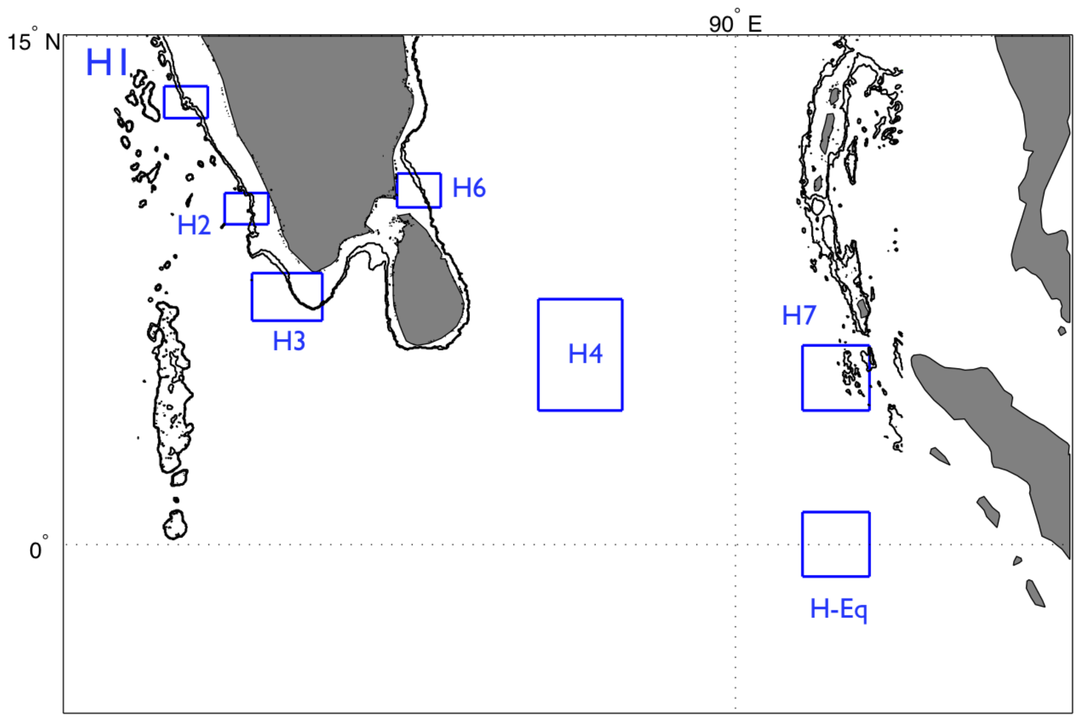

Figure 2.1: Height Boxes H1, H2, H3, H4, H6, H7, H-eq (in blue)

2.1.2 Surface Vector Winds

Ocean surface vector winds are available from the ECMWF, web site (http://data-portal.ecmwf.int). Winds from the ERA-40 reanalysis are available every six hours on a 0.25×0.25 degree grid, similar to that of the SLA. To match the temporal smoothing of the SLA data, the data were smoothed with a cosine square weight function with a cut-off frequency of 30 days, centered on the AVISO weekly time points. This insures that both AVISO SLA and ECMWF winds have the same timing. Similar filtering and timing was used in constructing the daily wind fields for comparison to the daily SLA fields.

2.2 Creation of Spatially Averaged Time Series

Both SLA and surface wind data are averaged over the rectangular areas shown in Fig 2.1 - Fig 2.3 to create the time series used in our analyses. Three boxes for SLA are located over the continental slope along the Indian west coast (H1-H3) [Fig 2.4], with another (H6) over the slope along the Indian southeast coast and two along a zonal pathway between Sumatra and Sri-Lanka (H4 and H7) [Fig 2.1. H1 is centered at $\sim 14^o$N (100-200 km south of Goa) and is our primary interest is predicting SLA variability at this location. We investigate whether the SLA and wind data reveal the forcing mechanisms proposed in the modelling work of *Suresh et al.* [2013]. The three height boxes on the western Indian continental slope (H1, H2 and H3) are chosen such that they are over the reference altimeter tracks on the west coast of India (those occupied by TOPEX/Poseidon, Jason-1 and Jason-2), as depicted in Fig 2.4. Even though we have not used the along track data for this analysis, choosing the boxes over the altimeter tracks insures that the more precise altimeter data is included in our primary time series. Box H6 is located on the southeast coast of India, along the pathway that would be followed by CTW signals moving around the Bay of Bengal (BoB) before passing the tip of India and moving up the west coast. The final two boxes for SLA are chosen east of Sri-Lanka (H4), and near Sumatra (H7) to represent the zonal pathway that would be taken by Rossby waves crossing the southern BoB after being generated by equatorial Kelvin wave reflection. Wind stress curl within the BoB can also contribute to the Rossby wave signal at H4 [*Han et al.*, 1999], and we asses the likely importance of equatorial contributions to H4. All the grid- points inside boxes H1, H2, H3, H4, H6 and H7 are spatially averaged with equal weights to obtain a single SLA time-series for each box. The box sizes are chosen to provide adequate statistical reliability of the averaged SLA signal. H1, H2 and H6 are chosen such that they can capture the CTW signal on the slope. However boxes H3 and H4 are comparatively larger in size as they represent SLA at the tip of India and a Rossby wave signal coming from east of Sri Lanka (which is better represented if averaged over larger spatial domains).

In a similar way, wind boxes are chosen along the west coast near the SLA boxes (Fig 2.2- Fig 2.3). One surrounds box H1 (TA1), one surrounds box H2 (TA2) and one lies in between the SLA boxes (TA12). The choice of larger boxes for the winds was found to reduce the smaller-scale noise in the data and improve the correlations with the SLA. The directions of the winds are chosen to obtain spatially averaged alongshore wind stress time-series for each box, representing variations of alongshore winds in that particular region. Alongshore wind stress in the downwelling sense are assumed to be positive, as they lead to positive SLA values next to the coast. Three additional wind boxes represent different areas near southern India: on the southern tip of India TA3 surrounds SLA box H3, TA5 stretches around the western side of Sri-Lanka and TA4 covers the region south of Sri-Lanka and along its east coast. The single time-series for each box is constructed to represent variations of alongshore wind stress (even away from the coast), positive in the downwelling sense . Wind boxes TA3, TA4 and TA5 involve more than one sub-box which have different angles for computing the alongshore wind stress at each ECMWF grid point, taking into account the corresponding alongshore angle nearest to each grid point. The alongshore wind stresses for all the grid points falling inside the corresponding wind boxes are then spatiality averaged with equal weights to obtain a single time-series for each TA3, TA4 and TA5 box. Time-series of wind stress curl for each of the wind boxes are obtained in a similar fashion, and labelled similarly to the time series (C1, C12, C2, C3, C4, C5, C6).

An investigation is first carried out with the help of along-track altimeter data to test whether the SLA data over the shelf are contaminated with the tides. Fig 2.5 shows the correlation between the SLA and the total tides for track 181, which passes through box H1, the time-series of our interest. Low correlations between the SLA and the total tide correction, suggest that tides do not contaminate the data over the shelf. Although this is just a preliminary analysis, it provides some confidence for the use of gridded AVISO data over the shelf.

The seasonal cycle is removed from each of these time-series by subtracting

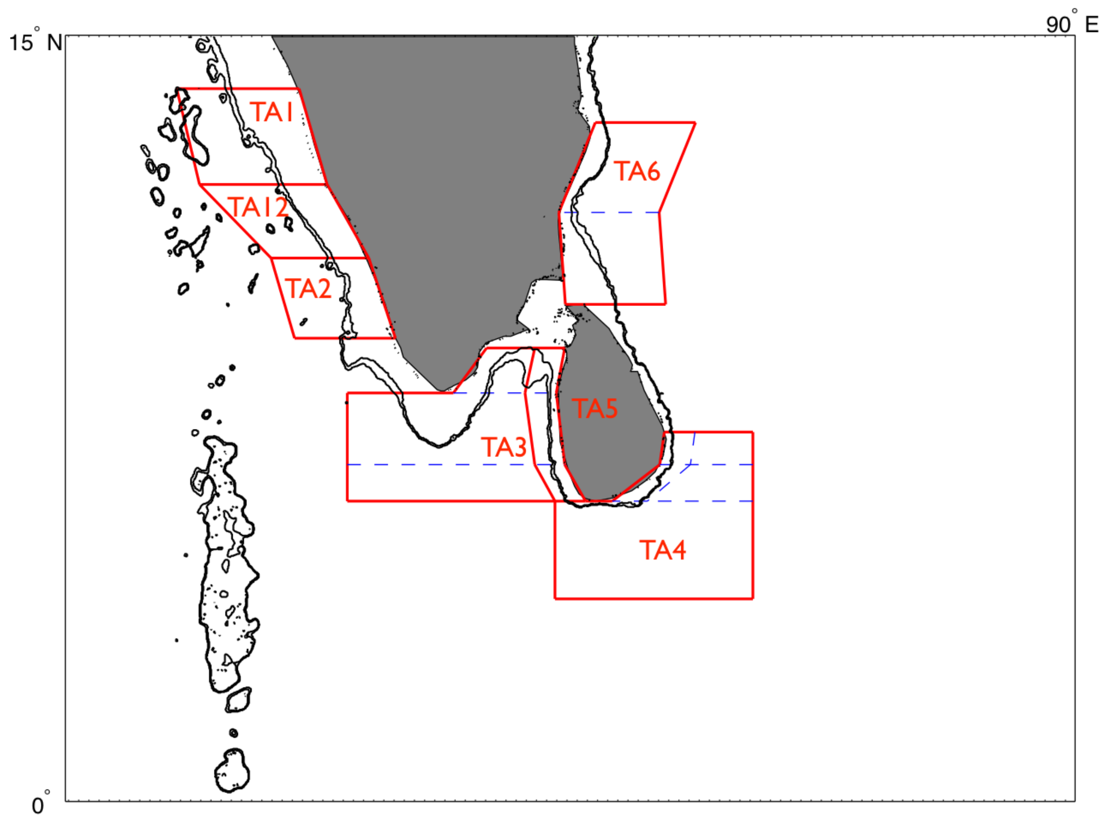

Figure 2.2: Wind Boxes TA1, TA12, TA2, TA3, TA4, TA5, TA6 (in red); – blue lines represent sub-boxes part of the big box

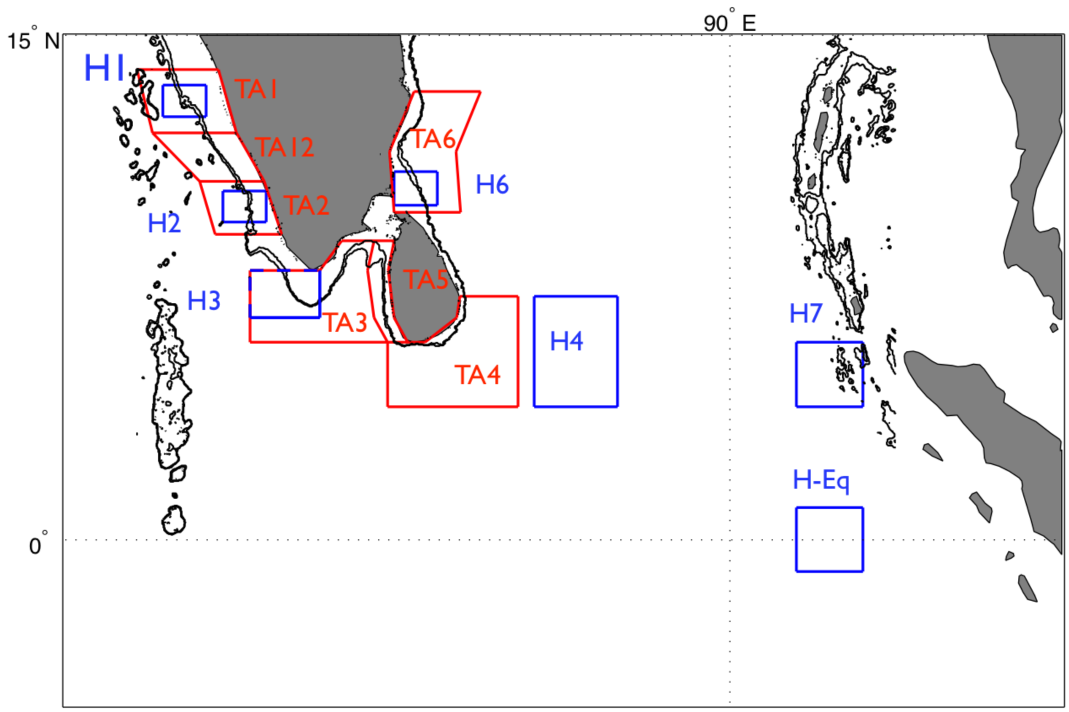

Figure 2.3: Wind Boxes(in red) and Height boxes(in blue) in close up

the annual signal and it's first three harmonics, i.e. ($f1 = 1/365.24$ days, $f2 = 2\times f1$, $f3 = 3\times f1$, $f4 = 4\times f1$), along with the removal of the mean and the trend. The remaining time-series is then filtered with a 120 day high pass filter using a Lanczos filter [*Emery et al*, 2004]. The final time-series is referred to as intra-seasonal and retains periods between 30-120 days. For most of the analyses, the intra-seasonal time-series for SLA, alongshore wind stress and wind stress curl are then normalized with their standard deviations from each box.

2.3 Spectra of the Time Series

Power Spectral Density (PSD) functions are calculated for each time series. The PSD identify the periods with the most energy in each of the time series, both before and after normalizing with the standard deviation of each time series. Nor-

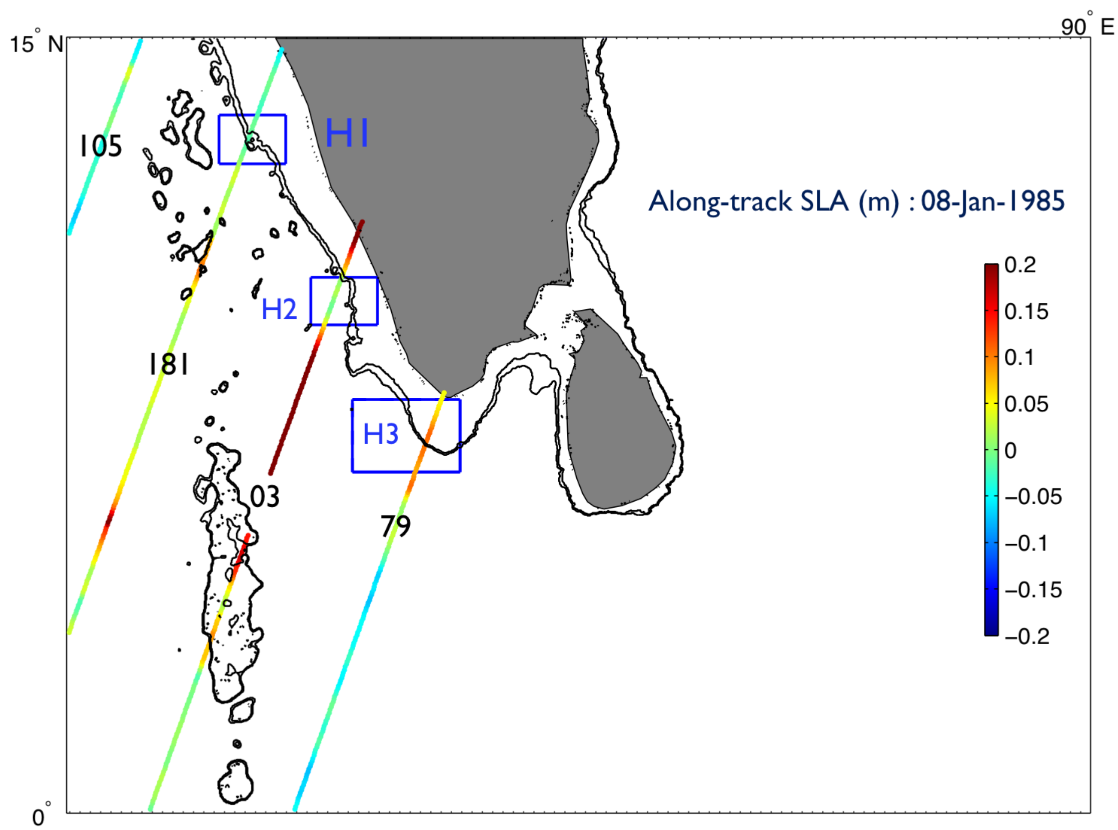

Figure 2.4: Boxes H1, H2, H3; Black contour lines represent 500m and 1000m iso-baths; Colourful lines are the satellite tracks from Jason1, during a single pass, with heights represnted by the colors

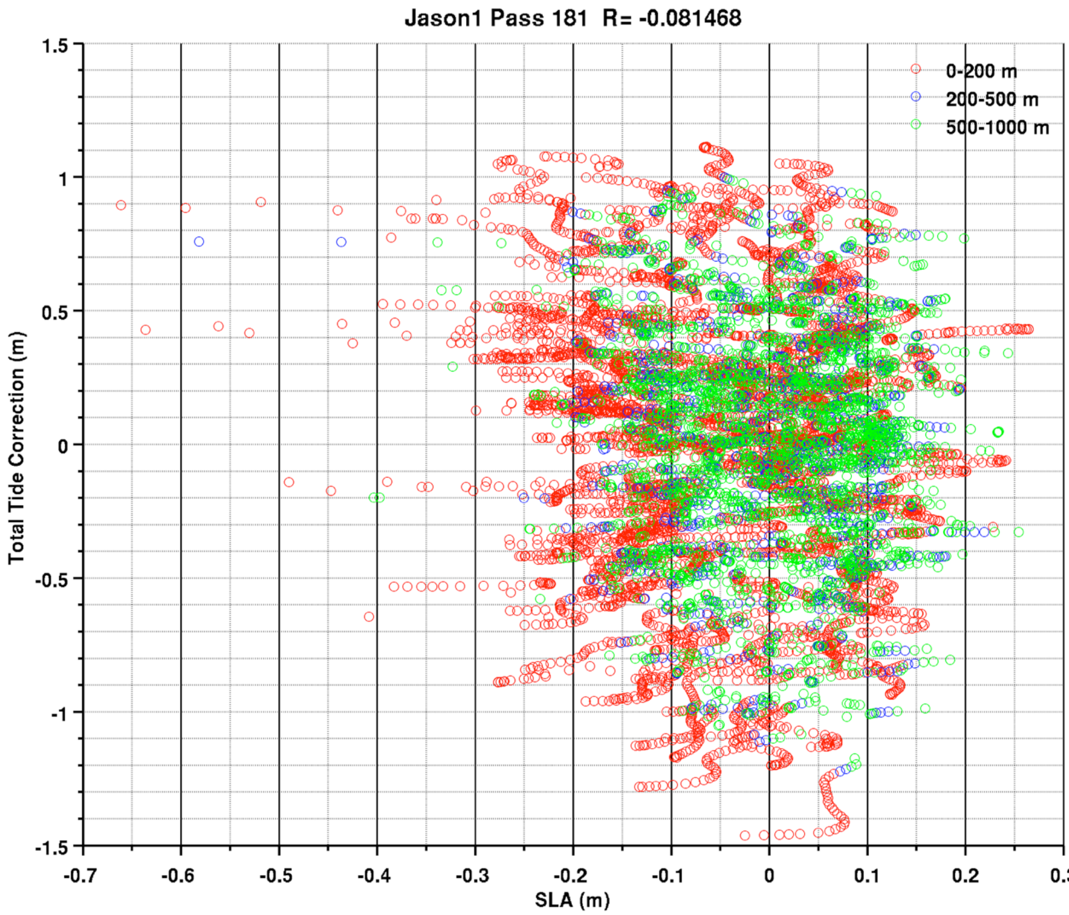

Figure 2.5: Scatter plot of SLA and total Tide corrections: Jason 1 Track 181 Figure 2.4, passing over box H1

malization allows more direct comparisons of the peaks and rates of roll-off for the time series of different parameters.

2.4 Lagged Correlations

Between any two time series, correlation co-efficients are obtained for different lags. The 95% confidence level for each lag is calculated using the significance test for sample cross correlation [*Chelton*, 1983]. The number of independently occurring events/degrees of freedom (N*) is computed using the Artificial Skill Method(ASM) [*Chelton*, 1983] (*Appendix A.2*. The value of N* is used in the computation of 95% confidence levels instead of N (the actual number of time points in the series). Due to the 7-day sampling of the standard AVISO SLA products, lags with these products can only be calculated in 7-day increments. In correlation verses lag plots, the skewness about the maximum calculated correlation often suggest an optimum lag that lies part way between 7-day increments. For this reason, we extend our analysis to the experimental daily SLA fields from AVISO, with good results. Although it may seem inconsistent to search for temporal lags of less than a week in data that have been filtered to remove periods of 30-days and less, we are looking for differences in timing of these longer-period signals, inferring the movement of the signals from location to location from lags in the arrival of the signals.

2.5 Regression Models

A hierarchy of linear regression models is built to predict the SLA on the west coast of India from SLA, alongshore wind stress and wind stress curl at other locations. For most comparisons, the SLA in box H1 is the estimand. Each series of models is built starting with the input variable which gives the highest correlation with the estimand (Model 1). The lag corresponding to the highest contribution to the model skill is identified by systematically lagging the time-series in the regression models.

$$\widehat{Y} = \beta_0 + \beta_1 \; F_1(t - \tau) \tag{2.1}$$

$\widehat{Y}$ is the estimated time-series with just one input field F_1 where τ represents the lag at which F_1 has the highest correlation with the estimand Y. The skill of a regression model is fraction of variance explained by the estimated time-series.

$$Skill = \frac{variance(\widehat{Y})}{variance(Y)} \tag{2.2}$$

After the determination of the variable and lag which produce the maximum Skill, a search is carried out for the variable and lag that produces the largest increase in Skill (explained variance). This becomes Model 2. In this search, the previous values of lagged correlations serve as guidance. However, the final choice of variables that are sequentially added to the model are based on the increased Skill and the robustness of that variable′s regression coefficient as more variables are added. In some cases, several variables produce a similar increase in Skill when added singly to the model; but when all are added, only one produces a regression coefficient much larger than the others (for the normalized time series). This is chosen as the next addition to the model.

As described by [*Chelton*, 1983], the addition of more input parameters to a regression model always explains more of the variance. However, the increase in the percentage of variance explained must be significant, in that the addition of the variable explains more of the variance than would be explained by the addition of a random variable. The significance of this increment in the percentage of variance explained is tested with an extra sum of squares test to determine whether the observed increase for a given variable is truly significant after adding an extra input parameter [*Chelton*, 1983]: If the skill for Model 1 with one input parameter is $\widehat{S}1$ and the skill for Model 2 with the addition of one extra input parameter is $\widehat{S}2$, then:

$$\widehat{S21} = \frac{(\widehat{S2} - \widehat{S1})}{(1 - \widehat{S2})} \tag{2.3}$$

$$S_{Crit} = \frac{(M2 - M1)}{N^* - M2 - 1} q_F(\alpha, M2 - M1, N^* - M2 - 1) \tag{2.4}$$

$$Prob[\widehat{S21} \geqslant S_{Crit}] = 1 - \alpha \tag{2.5}$$

where M2 and M1 are number of input parameters in Model 2 and Model 1 respectively, q_F is the Fisher distributed probability density function, and N^* is the number of independent events.

If $\widehat{S21}$ is greater than S_{Cri}, then the increment in the skill is significant with (1-α)% level of confidence (In most of our analysis a value of 95% is used). The value of N^* (number of degrees of freedom) used for this test is determined from lagged correlation between $\widehat{Y}$ and the estimand Y. Since the time-series used in this analysis are normalized, the absolute value of the regression coefficient corresponding to each of the input variables also gives a rough estimate of the importance of respective input variable for explaining the variance of the estimand.

The underlying problem common to analyses of geophysical signals occurs when there are significant correlations among the different input fields, which leads to high error bars on each of the regression coefficients in the regression models. In that case, it is difficult to estimate the importance of one factor over the other, as the error bars on each of those coefficients are large enough to include the others. By adding the input parameters in the order of decreasing explained variance, then testing the change in coefficients as other inputs are added, only the most important input parameters are kept in the model to explain the maximum variance of the estimand. The final test of the model is the extent to which its input parameters and lags are consistent with the dynamics which are thought to govern the physics of the processes.

2.6 Coherences

The calculation of two-point correlations and lags includes all time scales that are included in the time series. In our case the band-pass filtering includes periods from 30-120 days. Additional information about the correlations is provided by the calculation of frequency-dependent coherences between the same two time series. The magnitude of the coherence is a frequency-dependent correlation between the variables, while the phase of the coherence provides a frequency-dependent lag, for those coherences that have statistically significant magnitudes. Examination of the coherence magnitudes and phases allows us to determine which frequencies contribute the most to the previously calculated correlations and lags. These are considered in the discussion section, to aid in the interpretation of the correlations and regression models.

Chapter 3: RESULTS

In this Section we quantify the statistical connection of the coastal ocean′s response in sea level along the west coast of India to distant and local wind forcing and sea level signals. Two general approaches are used: simple two-point lagged correlations and multiple regression models. Significance levels of the statistics are determined as by using the effective degrees of freedom, N*, as described in the Methods Section. The brief comments on the interpretation of the results in this section are followed by a more detailed Discussion Section, in which we extend the correlations to frequency-dependent coherences and relate the results to the connections expected from dynamical relationships and also to previous studies.

3.1 The Intra-Seasonal Time Series

Time series of SLA in box H1 are shown in Fig 3.1 (weekly data) and Fig 3.2 (daily data) for the raw and filtered data: (1) Raw: Directly obtained from AVISO; (2) Non Seasonal: after removing trends, means and seasonal cycles (annual plus first three harmonics); and (3) Intra-seasonal: 120-day high pass filtered versions of the non-seasonal time series. The seasonal time scale is the most visually dominant aspect in both timeseries. The total variance of the raw signal at H1 is 72 cm^2. This drops to 14 cm^2 in the Non-Seasonal time series, which include both intra-seasonal and inter-annual variability. The inter-annual variability is removed with a high- pass filter that eliminates periods greater than 120 days, leaving only the intra-seasonal variability with a variance of 7 cm^2.

One of the primary types of information of interest in our analysis concerns the lags between local and distant signals, which are difficult to quantify at short time scales using the standard weekly data. This motivates the use of the experimental AVISO daily gridded SLA data set. Comparisons of Fig 3.1 and Fig 3.2 reveal

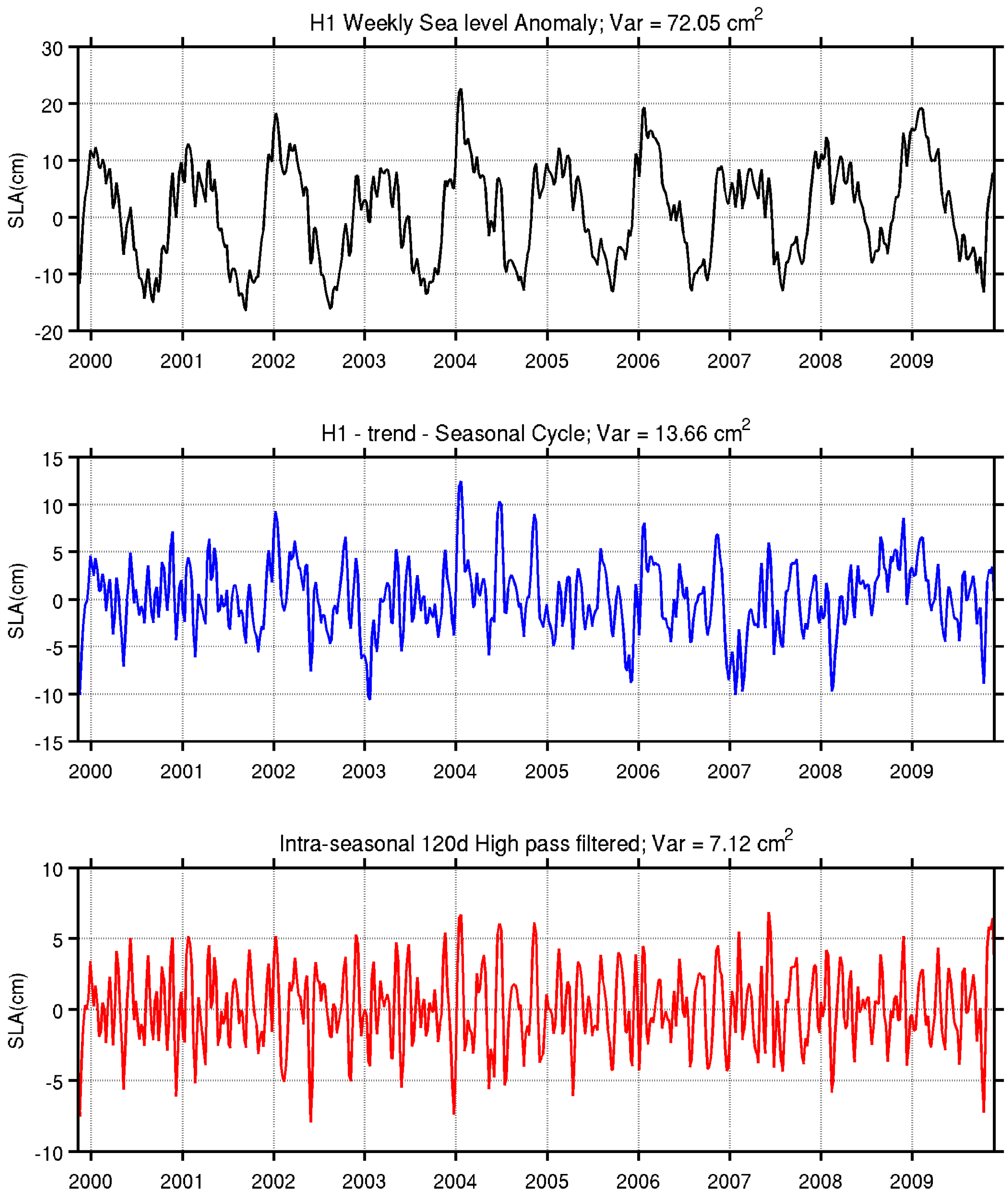

Figure 3.1: H1 SLA Time-series (AVISO weekly); Black: Raw; Blue: Seasonal Cycle and trend Removed; Red: Intra-seasonal 120 d high pass

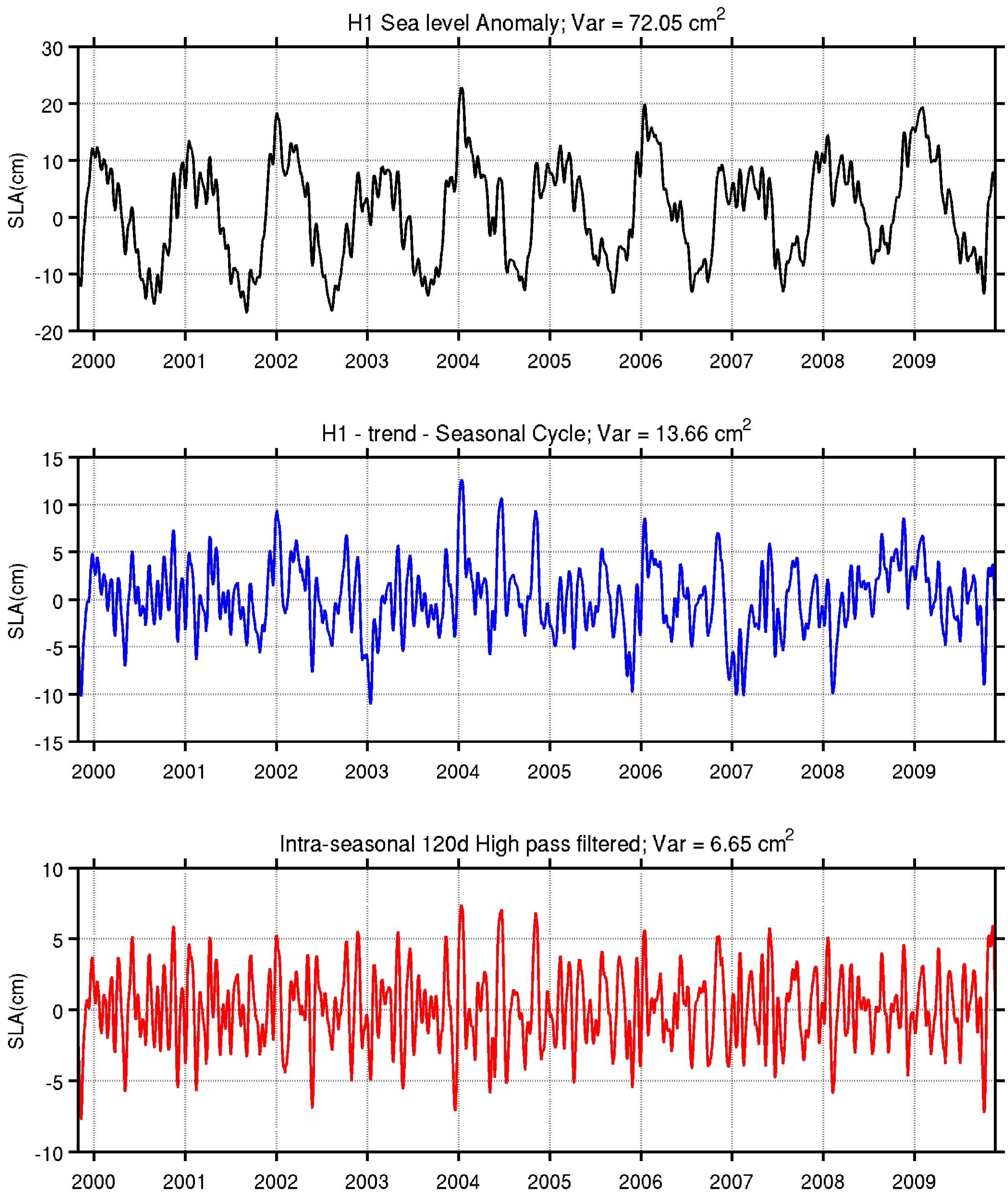

Figure 3.2: H1 SLA Time-series (AVISO daily); Black: Raw; Blue: Seasonal Cycle and trend Removed; Red: Intra-seasonal 120 d high pass

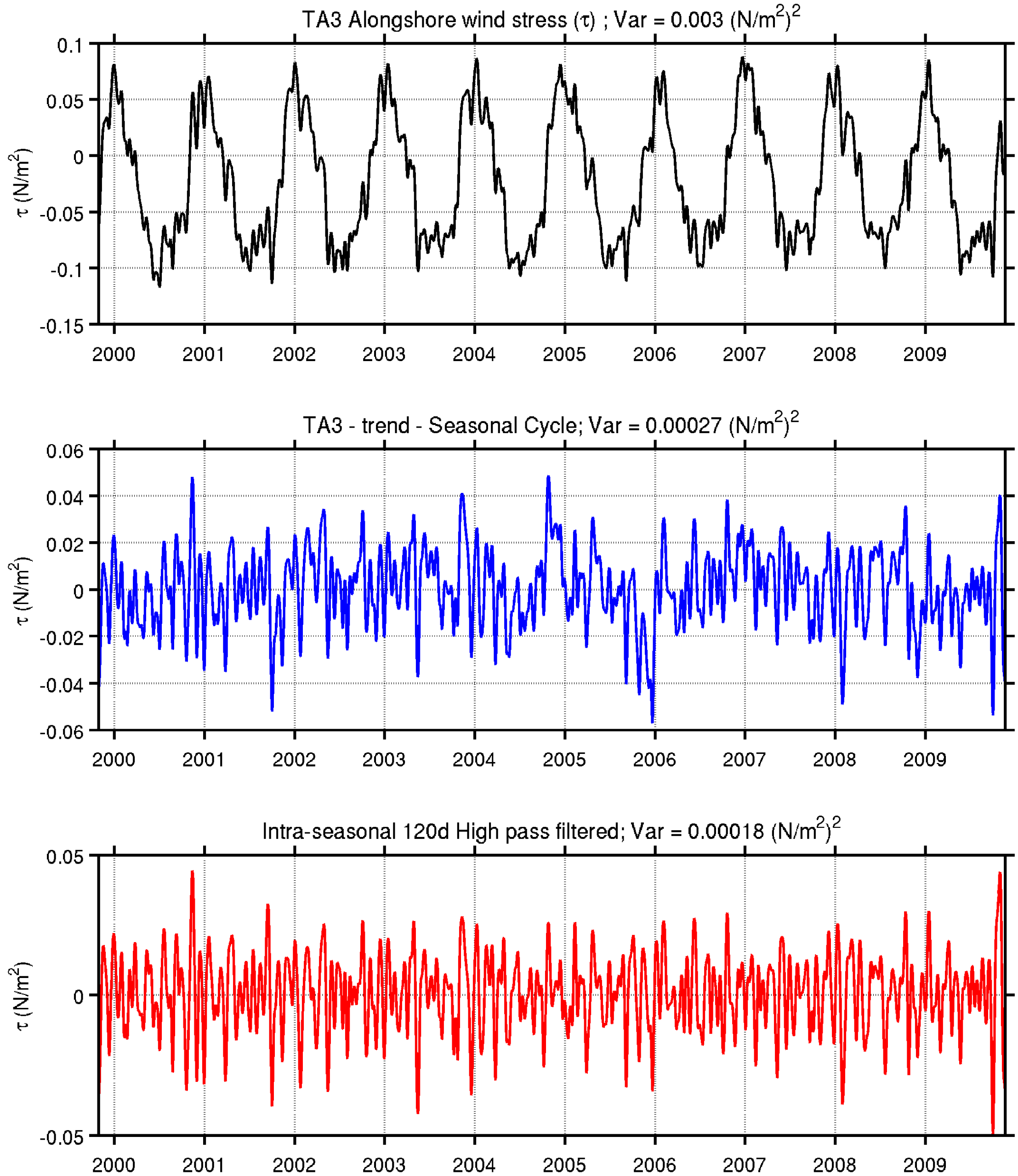

Figure 3.3: TA3 Alongshore Wind Stress; Black: 30d Low Pass; Blue: Seasonal Cycle and trend Removed; Red: Band-pass 30-120 days

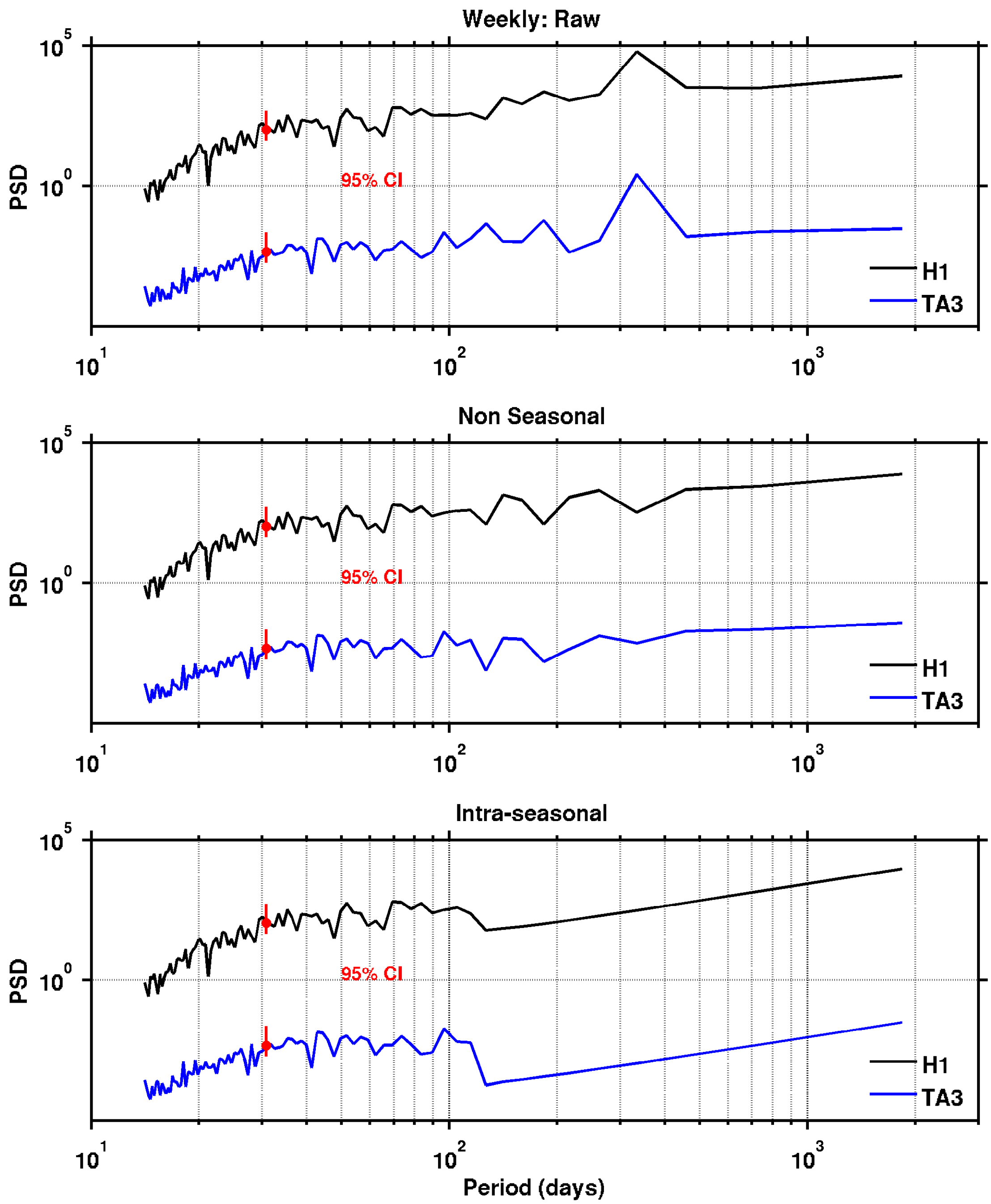

Figure 3.4: Power Spectrum of H1(AVISO Weekly) and TA3

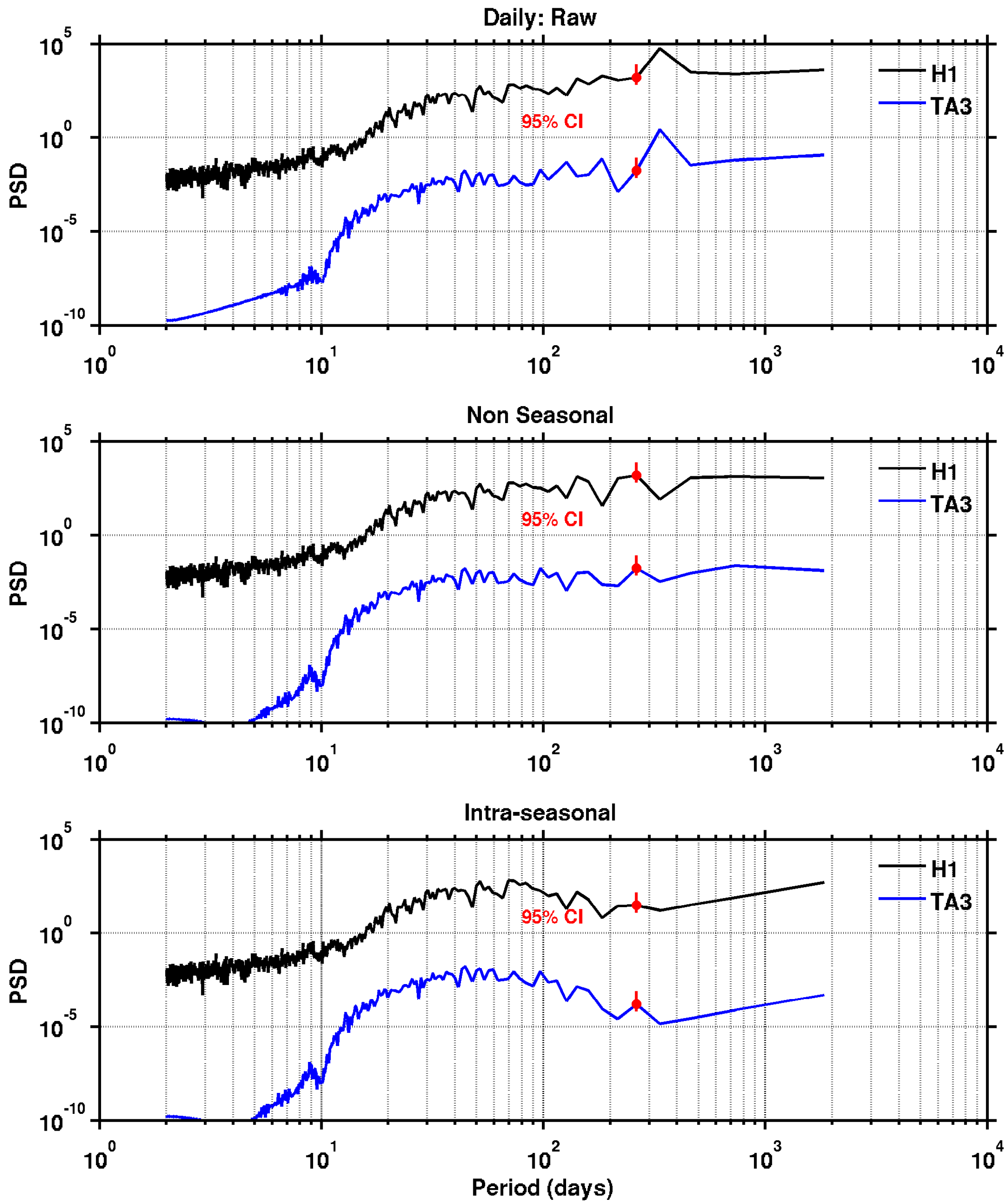

Figure 3.5: Power Spectrum of H1(AVISO daily) and TA3

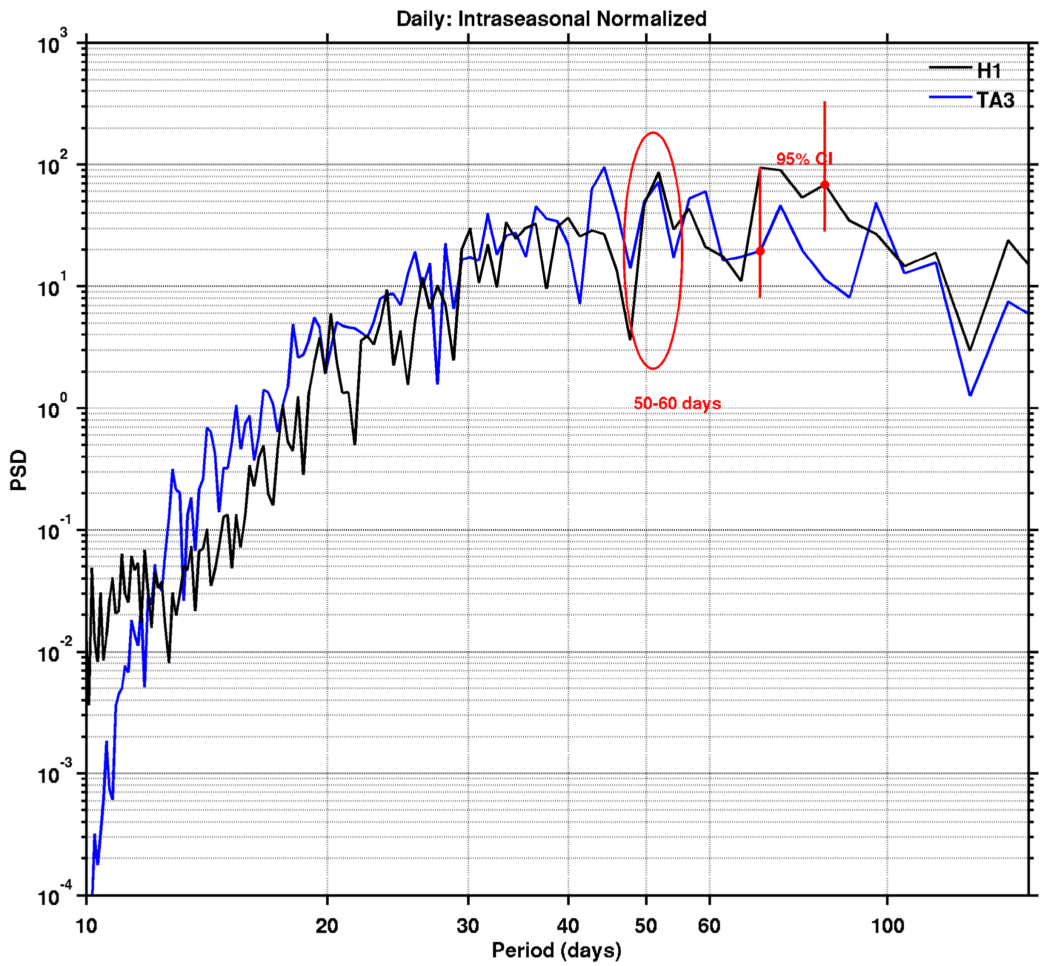

Figure 3.6: Power Spectrum of Normalized H1(AVISO daily) and Normalized TA3

nearly identical time series for the raw and non-seasonal time series, with only minor differences in the peak values for the intra-seasonal time series. For comparison, the similarly processed time series for ECMWF alongshore wind stress are shown in Fig 3.3. The annual cycle in the alongshore wind stress is very distinct. There is a significant drop in the variance as the annual cycle with first three harmonics and the trend are removed from the raw time-series. However, $2/3^{rd}$ of it's energy is retained at the intra-seasonal time scales [Fig 3.3]. In Fig 3.4 and Fig 3.5, the power spectra of H1 and TA3 time series confirm the dominance of seasonal cycles in daily as well as weekly time series. ECMWF winds have been smoothed with a period of 30 days on the assumption that AVISO SLA's have been smoothed with a period close to 30 days. Fig 3.4 and Fig 3.5 demonstrate that the drop in the PSD starts close to a period of 30 days for both winds and the SLA. However, the shape of the roll-off for AVISO SLA and the ECMWF winds are different; the power of ECMWF drops off more quickly than SLA. The analyses presented below have been repeated after filtering the SLA with the same filter used for the winds, with no significant change. Given the desire to preserve as much of the intra-seasonal signal as possible, we present the results without the additional smoothing to the SLA time series. The presence of a strong intra-seasonal signal on the west coast of India is consistent with the findings of [*Vialard et al.*, 2009].

Before further computations, the intra-seasonal time-series are normalized with their corresponding standard deviations. Fig 3.6 shows the power spectra of the normalized timeseries, allowing a more direct comparison between alongshore wind stress and SLA. We note that the 50-60 day period has coincident peaks in both winds and SLA. This is the period of Madden-Julian Oscillations (MJOs), well known signals in the ocean and atmosphere in the Indian Ocean. The 50-60 day signal will be seen to be a major contributor to intra-seasonal variability at periods of 30-120 days in our data sets.

3.1.1 Lagged Correlation Analysis

Intra-seasonal normalized SLA time-series from all other regions are correlated with weekly SLA in H1. Fig 3.7 and Table 3.1 show that the boxes on the west coast of India are highly correlated with H1 with a lag of 0 weeks, suggesting things happening almost at the same time all along the west coast. In Fig 3.7, these correlations are skewed, giving a hint of a slight phase lag between H1 and H2, and also between H1 and H3. The skewness is more evident in the correlation plot of H4, where the significant correlation of 0.32 suggests that the Rossby-wave mechanism proposed by *Suresh et al.* [2013], which is presumably represented by SLA variability in H4, is indeed important for estimating SLA variations in H1. Although the lag at which H4 has the highest correlation with H1 is 0 weeks, it is also slightly skewed toward the negative side, suggesting that H1 lags H4 with an actual lag of between 0 and 7 days. This is confirmed using the daily data, discussed below. The correlation between H1 and H6, along the east coast of India, is barely significant, with lags of 1-2 weeks. H7, off Sumatra, is significant with a longer lag of 3 weeks.

To asses the connection with SLA from Equator, SLA from H-Eq is correlated with all other boxes [Fig 3.8]. There is a significant correlation of H-Eq with H7 (off of Sumatra) with a lag of 0-1 week. The lag increases to 4 weeks as we go along the Rossby wave path(H7-H4-H1). The lag for H4 and H1 when correlated with H-Eq is 4 weeks; however the correlation plot show that they are skewed. Daily AVISO data are used for further analysis (below) to resolve lags less than 7 days.

Fig 3.9 shows the correlations of the alongshore wind stress with SLA in H1, using the weekly data. The highest correlation of H1 is with TA3 and the lowest correlation is with TA1, suggesting the importance of remote winds from tip of India over the local winds for intra-seasonal sea level variations in H1. These results are consistent with the study by *Amol et al.* [2012], suggesting the importance of distant winds from the tip of India for intra-seasonal SLA variations along the west coast of India, an indication of CTW dynamics. TA3 shows the maximum correlation for the lag of -1 week (TA3 leads H1). However, it is slightly skewed towards

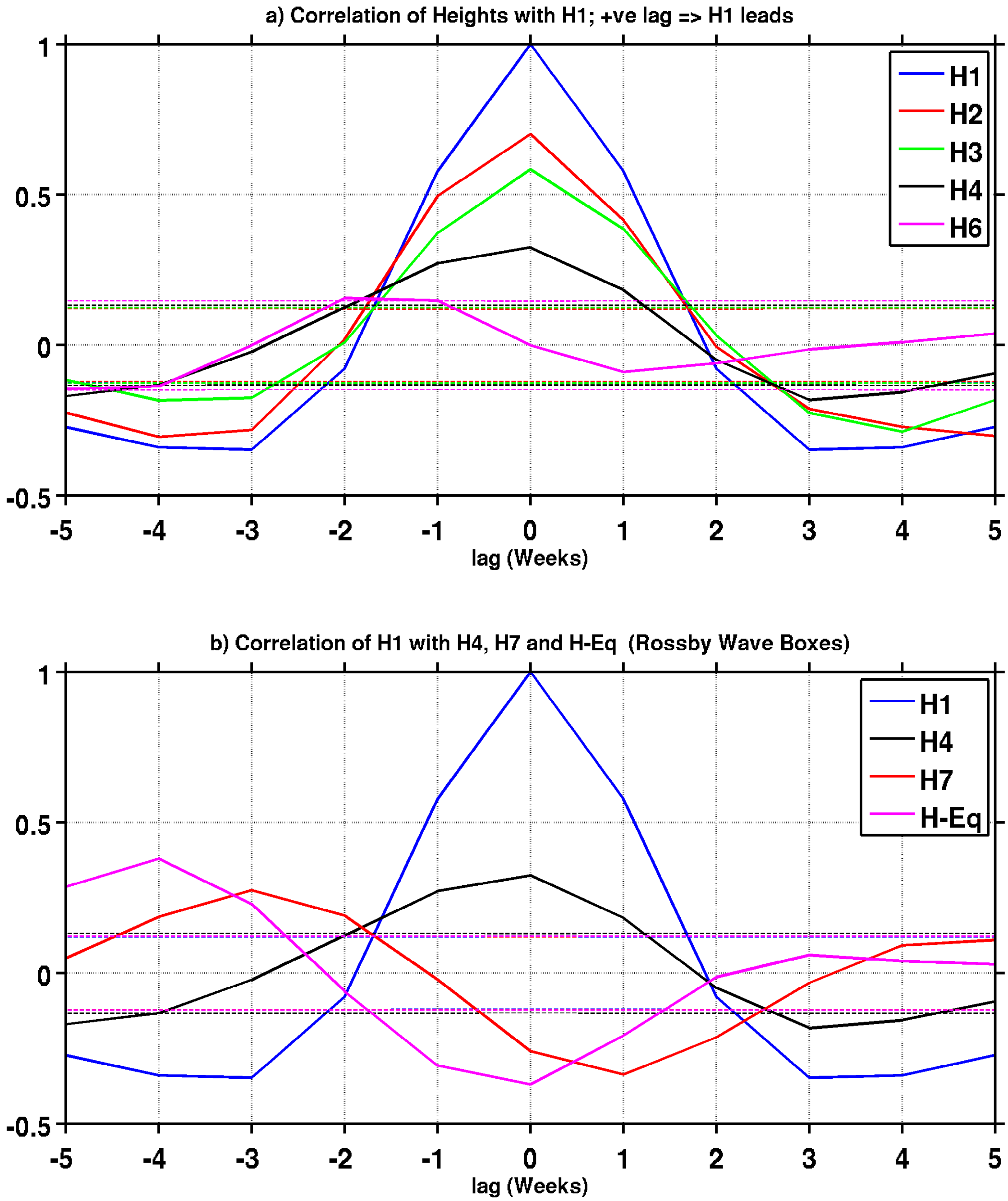

Figure 3.7: Correlation of weekly H1 with all other heights(Weekly AVISO); +ve lag means H1 leads

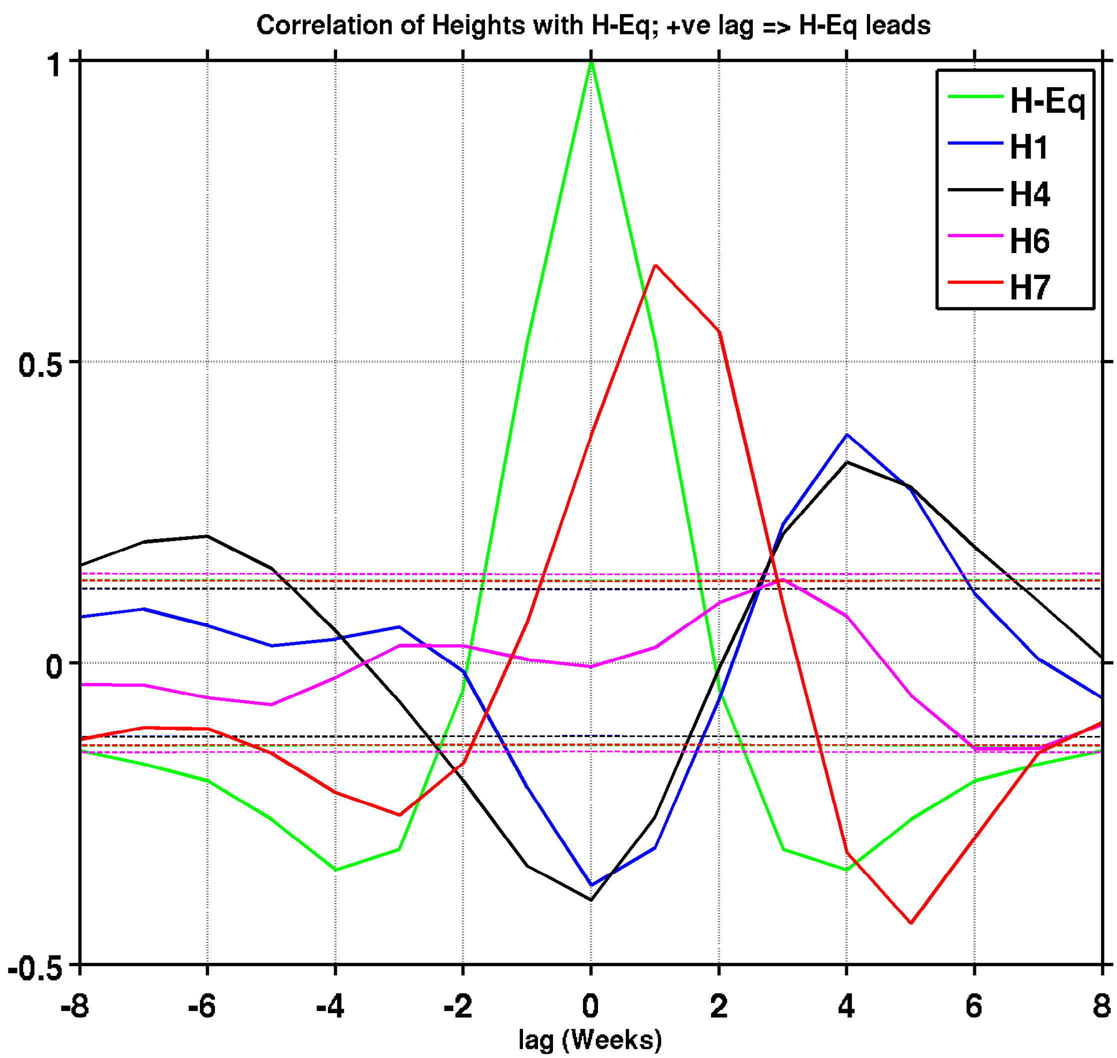

Figure 3.8: Correlation of weekly H-Eq with all other heights(Weekly AVISO); +ve lag means H-Eq leads

0, suggesting the exact lag is between 0 and -7 days. Alongshore wind stress at all of the boxes from TA1-TA4 have maxima at a similar lag of approximately 1 week and are skewed toward 0 weeks rather than 2 weeks, suggesting a true lag of less than a week.

The sign changes of correlations with TA5 along western Sri Lanka in Fig 3.9 are due to the fact that the same winds affect the tip of India and western Sri Lanka in an opposite sense (winds toward the southwest between India and Sri Lanka cause downwelling on the Indian coast and upwelling next to Sri Lanka). Since these winds produce negative wind stress in region TA5 (upwelling), the fact that they are negatively correlated with SLA in H1 indicates that SLA shows positive anomalies for winds to the SW, which produce positive wind stress in TA3 and downwelling next to India. Thus, the downwelling next to India caused by winds in TA3 affects the SLA along western India more strongly than the upwelling along western Sri Lanka, created by the same winds.

Fig 3.10 and Table 3.1 show the correlation of wind stress curl with H1 for the weekly time series, with similar results using the daily data sets (next section). The relationships between H1 and the curl of the wind stress in the different regions generally follow the same pattern as the wind stress but with opposite sign, due to the fact that negative wind stress curl causes positive (downwelling) SLA. The maximum correlation is found with C3 and C4, suggesting the importance of wind forcing to the south and southeast of India for predicting the SLA on the west coast of India, whether the more important forcing is alongshore wind stress or wind stress curl. There is also a significant correlation for the wind stress curl in C5 (along the west coast of Sri Lanka). This brings us back to the recent CTW modelling work by *Amol et al.* [2012], where the model solution suggests that forcing for the CTW's can extend beyond the west coast into the Gulf of Mannar. The significant correlation of wind stress curl from C5, along with the CTW model prediction from [*Amol et al.*, 2012], strengthens the argument that the winds near Sri Lanka may affect the SLA variability along the west coast.

The interpretation of the wind stress and wind stress curl correlations at differ-

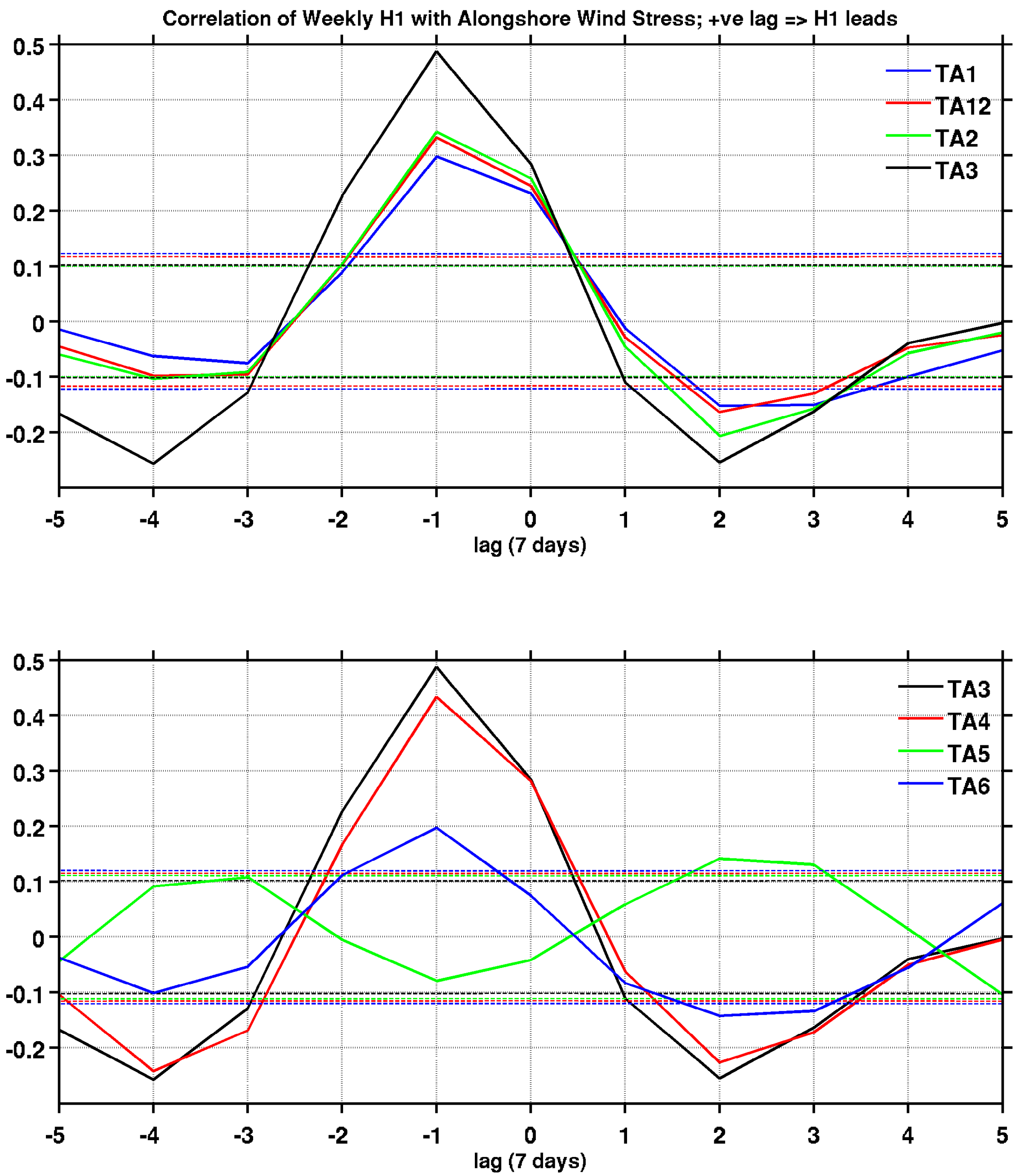

Figure 3.9: Correlation of weekly H1 with alongshore Wind Stress; +ve lag means H1 leads

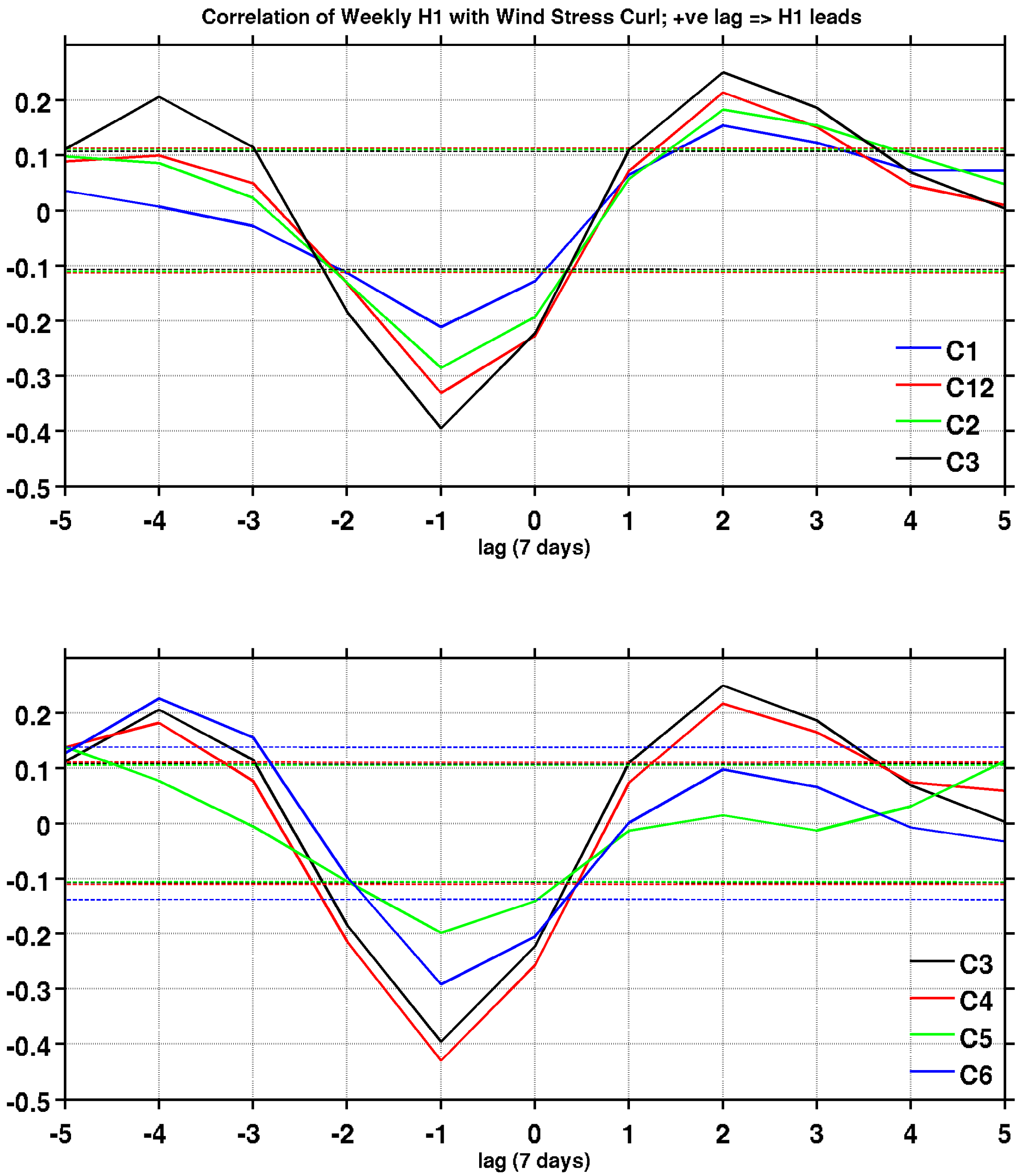

Figure 3.10: Correlation of weekly H1 with Wind Stress Curl; +ve lag means H1 leads

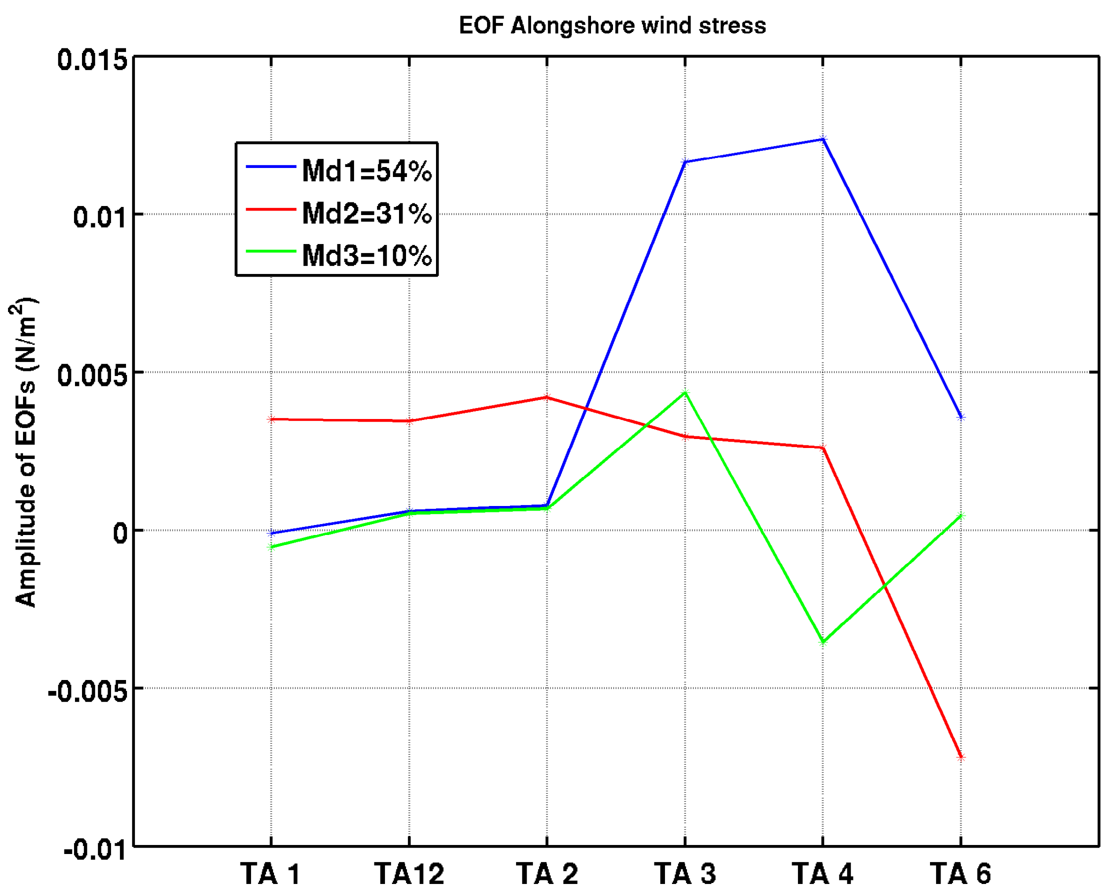

Figure 3.11: First 3 modes of EOFS for the weekly Alongshore Wind Stress: Suggesting TA3 and TA4 representing wide scale winds

ent locations is made difficult by the fact that the winds are large-scale in nature, due to the influence of the basin-wide monsoon systems. Table 3.2 shows the correlation of daily TA3 alongshore wind stress with wind stress and wind stress curl in all other wind boxes, quantifying the degree to which the different forcing functions are inter-correlated with each other. An EOF analysis is also carried out with the alongshore wind stress at these several location. Fig 3.11 shows the spatial amplitudes for the first three modes of the EOF′s. The first mode explains almost 54% of the total variance with highest amplitude coming from TA3 and TA4. This is consistent with our assumption of the large-scale nature of winds, which is mostly represented by TA4 and TA3 winds. This large scale nature of winds makes it difficult to interpret the correlations and their corresponding lags. As an example, the relatively large lags of local coastal sea level with the local winds (5-6 days) may be due to the fact that local winds are coherent with the remote winds, which are the true forcing factor. Differentiating wind stress from wind stress curl is further complicated by fact that coastal alongshore winds are slowed by processes next to the coast, causing high correlations between the coastal wind stress curl and the alongshore wind stress.

Even if the wind variables at different locations were independent, the weekly time increment makes it difficult to separate the local from distant forcing using the lags, since the height signals propagate quickly to H1 along the coastal wave guide, once signals are created or arrive at a distant coastal location. Thus, we next return to the daily time series.

3.1.2 Daily Gridded AVISO SLA Fields and Daily ECMWF Winds

Experimental daily AVISO gridded data are used to improve the resolution of the lags. Results are similar to those obtained with the weekly time series but with slightly higher correlations and greater resolution of the lags, presented in Table 3.3 and Fig 3.12 - Fig 3.15. The sea levels along the west coast (H1-H3) remain highly correlated (r$\sim$ 0.6-0.7) with lags of 0-1 days [Fig 3.12] . This is the regional signal of our interest. Outside of the west coast, the highest correlation is still with the alongshore wind stress at TA3, with a lag of 6 days [Fig 3.14]. Correlations with more local winds (TA1, TA12, TA2) are similar but slightly less, with maximum correlations at lags of 5-6 days. These lags are longer than expected for local upwelling and downwelling sea level responses to imposed wind stress, which are expected to be in the 1-2 day range [*Denbo and Allen et al*, 1987]. All of these wind signals with the longer lags may represent the large-scale variability in the intra-seasonal forcing, with multiple signals arriving at H1 and producing the appearance of 5-6 day lags (see the Discussion section).

The next highest correlation is with SLA at H4, east of Sri Lanka, with a 2-day lag [Table 3.3]. If this signal is travelling toward Sri Lanka, it should move quickly (1-2 days) from the coast of Sri Lanka to H1. Along the southeast coast of India at TA6, the alongshore wind stress is significantly correlated with with H1 with a lag of 8 days; the corresponding SLA along southeast India at H6 also significantly correlated with a lag of $\sim$ 11 days. These represent forcing and signals along the east coast of India. The lower correlation values are consistent with a decrease in coherence caused by the convoluted pathway around Sri Lanka and the southern tip of India. The lower lag for the TA6 winds compared to H6 can be thought of as produced by a high correlation of TA6 winds with TA3 winds, which have a lag of 6 days when correlated with H1. In a broader picture, all of the wind lags that we see in the point to point correlations may have been influenced by the basin wide scale wind signal, with a lag of 6 days with H1. Correlation of box H7 off of Sumatra to the west coast of India using daily AVISO SLA values are consistent with the results obtained from weekly correlations [Table 3.3, Fig 3.12]. Significant correlation of H-Eq, all along the Rossby wave path-way (H-Eq-H7-H4-H1,) with a gradual increment in the lag as we move along from H7 (off of Sumatra) to H4 (east of Sri-Lanka) to H1 (west coast of India) suggest the connection of equator with the west coast of India along the Rossby wave path-way [Fig 3.13]. Region next to Sumatra leads the SLA values along the Indian west coast by approximately 3 weeks (see the Hovmoller diagrams in the Discussion section below). The decrease in the correlation between the Equator and the southeast coast of India, with an

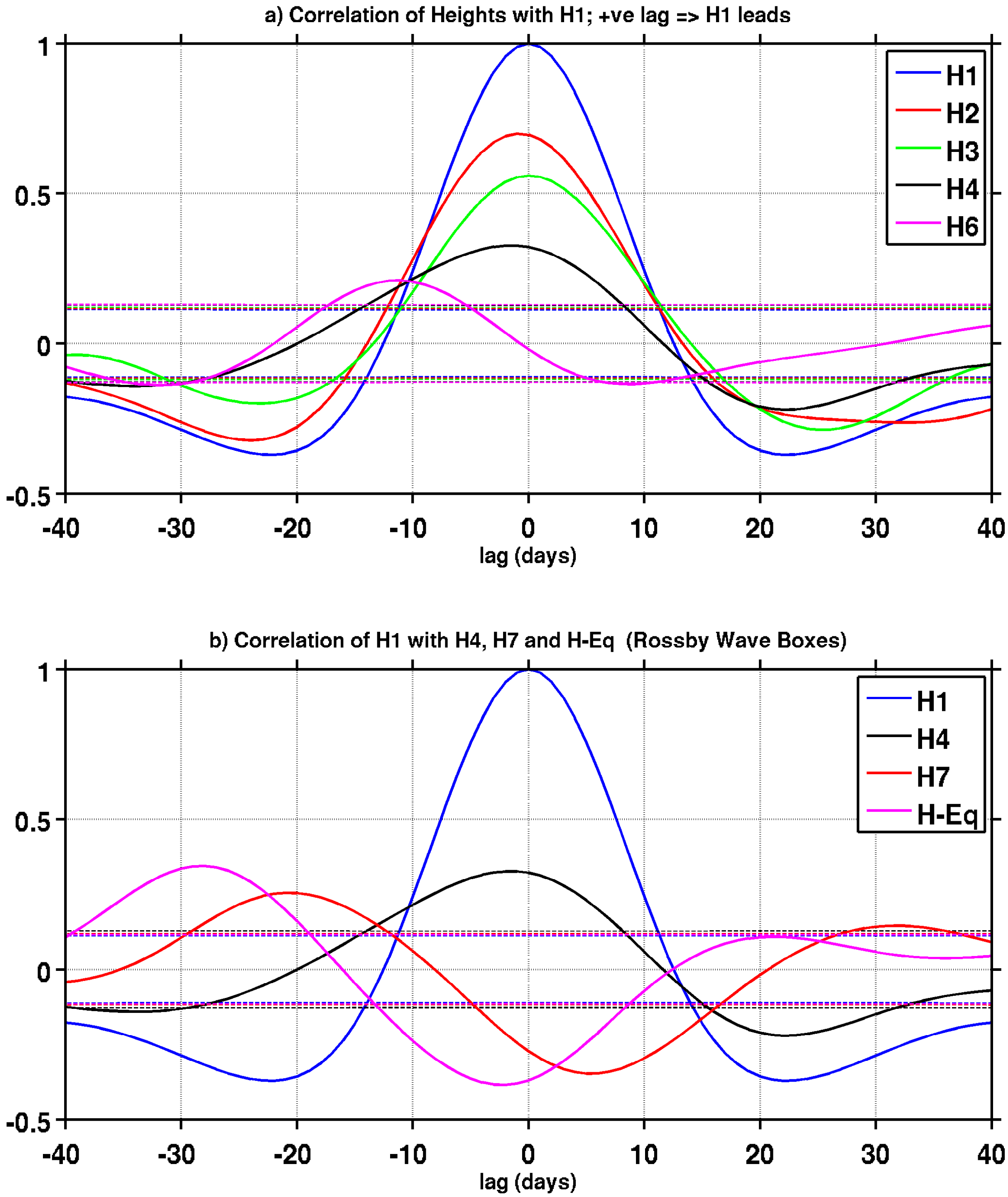

Figure 3.12: Correlation of daily AVISO H1 with all other heights(Daily AVISO); +ve lag means H1 leads

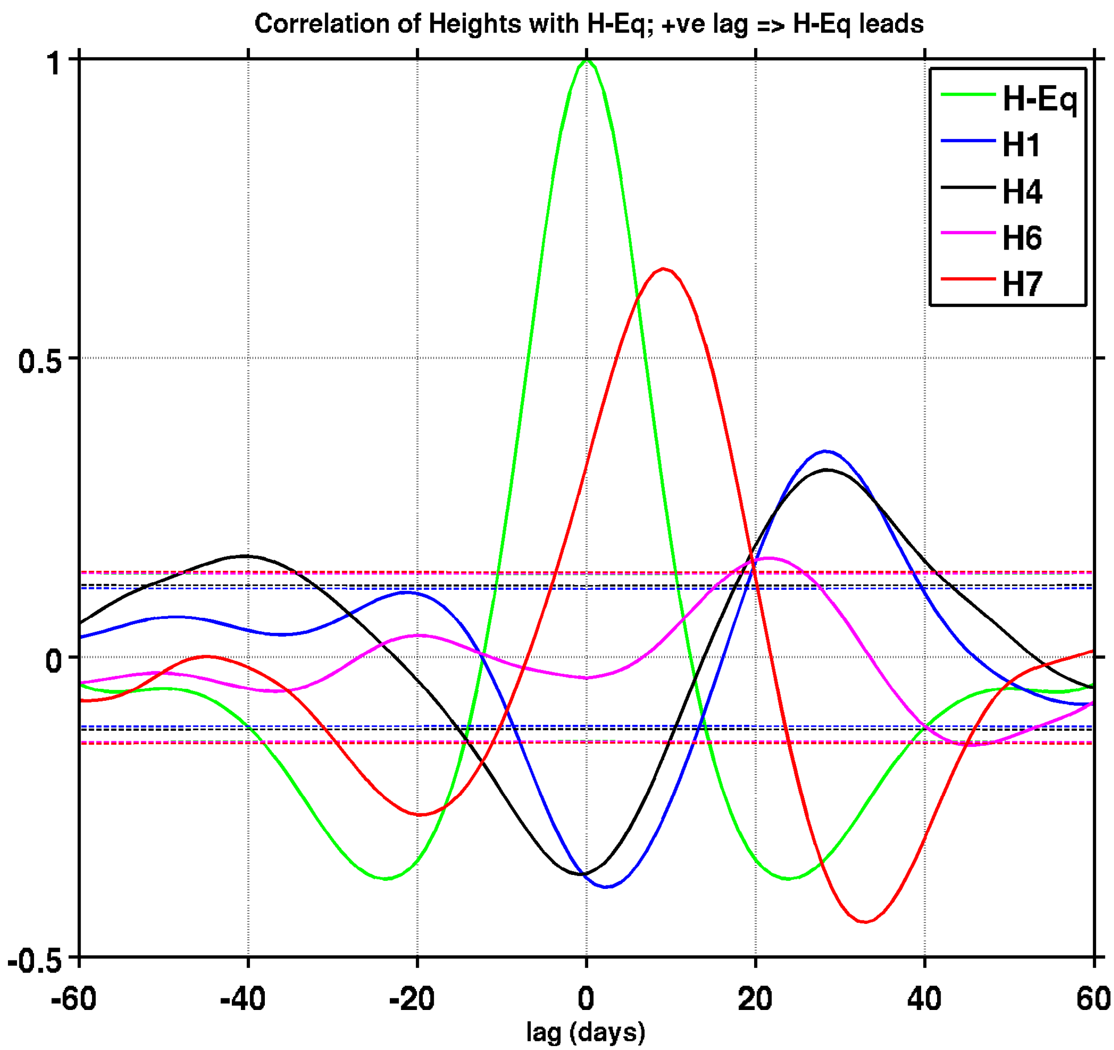

Figure 3.13: Correlation of daily H-Eq with all other heights(Daily AVISO); +ve lag means H-Eq leads

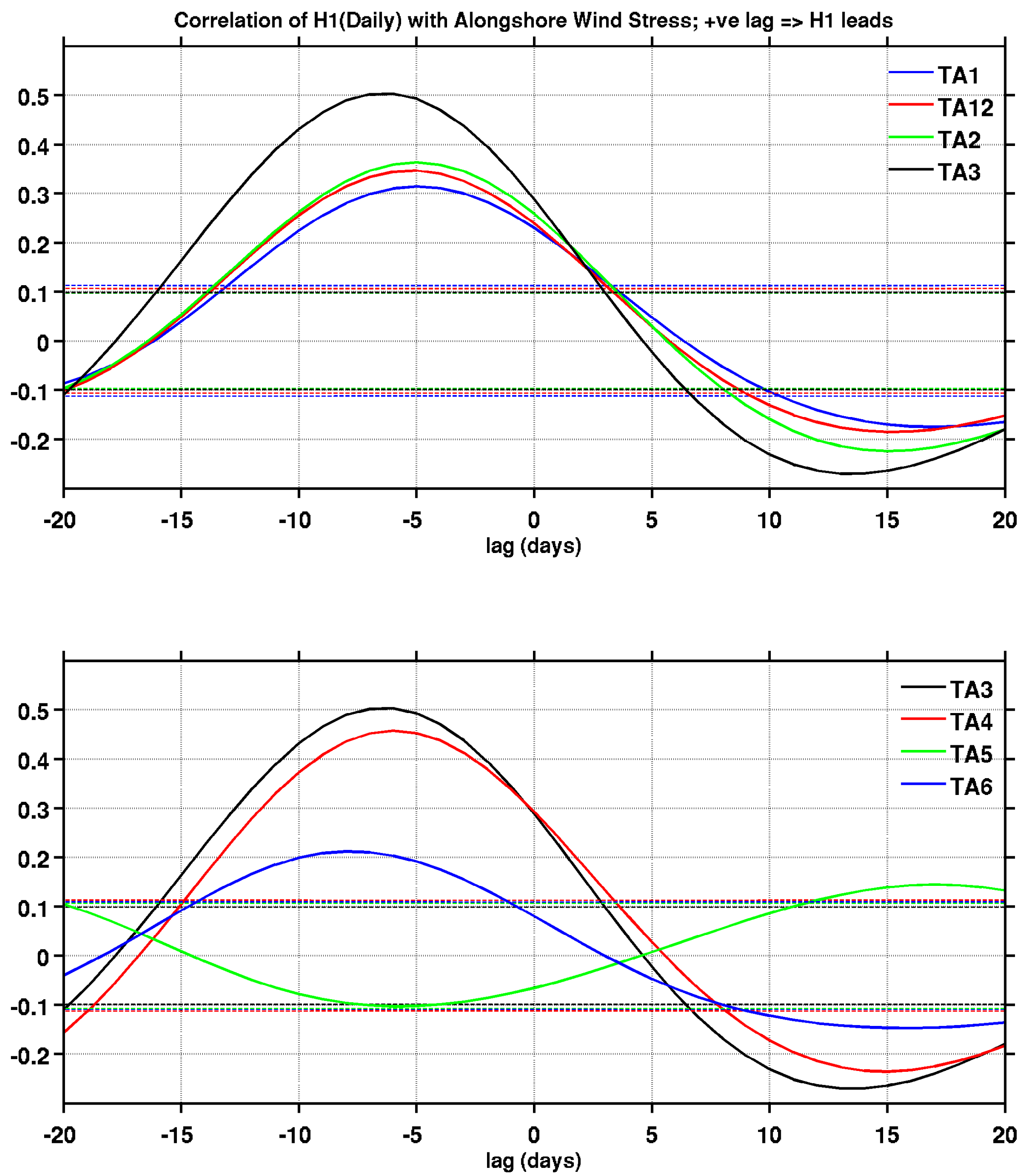

Figure 3.14: Correlation of daily AVISO H1 with alongshore Wind Stress; +ve lag means H1 leads

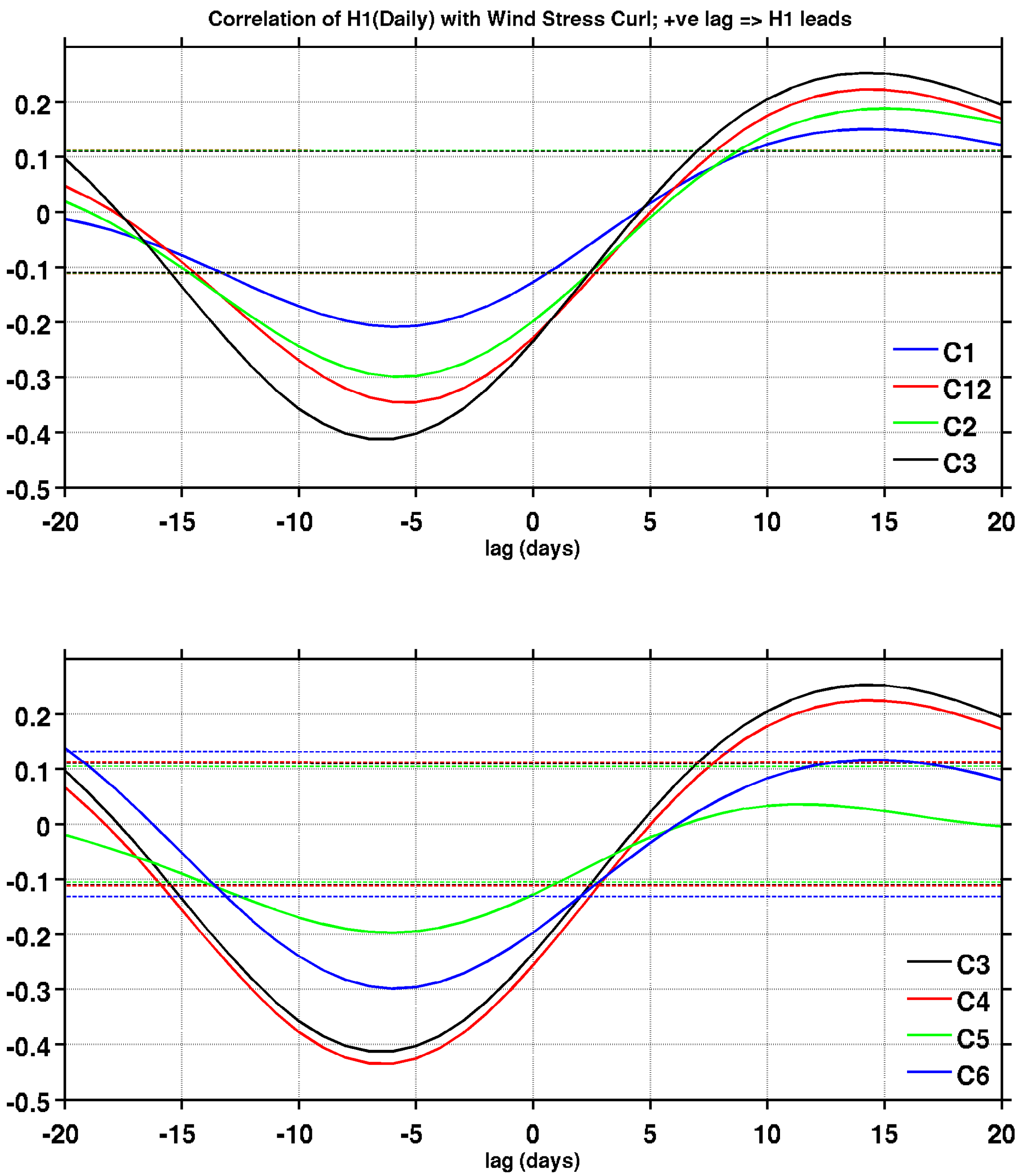

Figure 3.15: Correlation of daily AVISO H1 with Wind Stress Curl; +ve lag means H1 leads

increase of correlation along the west coast of India is consistent with the model results of *Suresh et al.* [2013]

As with the weekly data, the results of correlations of H1 with wind stress curl are similar to those with wind stress. Note that in both cases, there is greater similarity between regions 3 and 4 for curl (C3 and C4) than for wind stress (TA3 and TA4). This reinforces the interpretation of winds in these two regions as representing the large-scale wind fields, rather than the more local coastal winds.

3.2 Regression Models

In order to investigate the relative importance of multiple signals, we employ multivariate regressions, building models that use the variables (parameter, location and lag) that explain significant amounts of variance in H1, ordering these by the amount of additional variance explained. Although the above two-point correlations and their lags serve as a starting point, the final choice of variables and lags is based on the model regression analysis.

3.2.1 Weekly Time Series

A hierarchy of models is built by adding various inputs in the order of the highest percentage of variance explained. The first input parameter chosen is that with the highest correlation to H1, since this parameter explains the greatest amount of original variance. Table 3.1 shows the highest correlation and the corresponding lags for all of the possible inputs for predicting the SLA in H1, using the weekly data. The order of correlation for the first few variables with the correlation coefficients in parentheses is as follows: (1) H1(1.0), (2) H2(0.7), (3) H3(0.58), (4) TA3(0.48), (5) TA4(0.43), (6) C4(-0.43), (7) C3(-0.39), (8) TA2(0.34), (9) TA12(0.33), (10) C12(-0.33), (11) H4(0.32). The correlation of H7 with +7 day lag is not considered, as the positive lag represents H1 leading the SLA in H7 (not realistic, as discussed in detail in Discussion). Very high correlations among H1, H2 and H3 with a lag of near 0 days suggest that time-series of H1, H2 and H3 are quite similar, representing the regional west coast response, so H2 and H3 are not used as the input parameters for predicting the SLA in H1. The most distant signal, H7, is also not used in building a final statistical model, since we assume that Rossby wave signals from H7 must pass through H4 before reaching the west coast of India. Hence the first input parameter used to build up the model is TA3, which represents the winds at the tip of India. Every model is tested to determine whether the obtained skill (extra variance explained) is actually significant, with a 95% significance level [*Chelton*, 1983]. This is important because any random noise will also explain some percentage of variance but is purely artificial. Table 3.4 represents the stepwise addition of each input parameter to determine whether the addition is actually explaining more of the variance of the estimand, H1, than would be explained by a random variable.

The first Model uses only one input parameter, TA3 - the alongshore winds at the tip of India. The model is built with TA3 with a lag of -7 days (1 week) [Figure 3.16]. The skill of 0.2326, is significant in comparison to the threshold critical skill for this model of 0.0103. This model would suggest that almost 23% of H1 variance is coming just from the winds at tip of India, consistent with the study by *Amol et al.* [2012] that concluded that winds from the southern tip of India are important drivers for the intra-seasonal sea level variability along the west coast of India. However, as discussed above, the intraseasonal winds at many distant locations in the Indian Ocean basin are inter-correlated with each other [Table 3.2]. We believe that this large scale wind pattern is represented by TA3 and/or TA4 winds.

Once we have the first input variable, the choice of the next input parameter does not depend upon the order of correlations with H1, since the point to point correlations are highly influenced by the dominant basin wide signal. All other input parameters are tested for different lags with the additional hypothesis (and constraint) that the wind boxes on the west coast should have lower lags and winds on the east coast should have higher lags, compared to the winds from the tip of India. The final hierarchy of models is shown in Table 3.4 in the order of

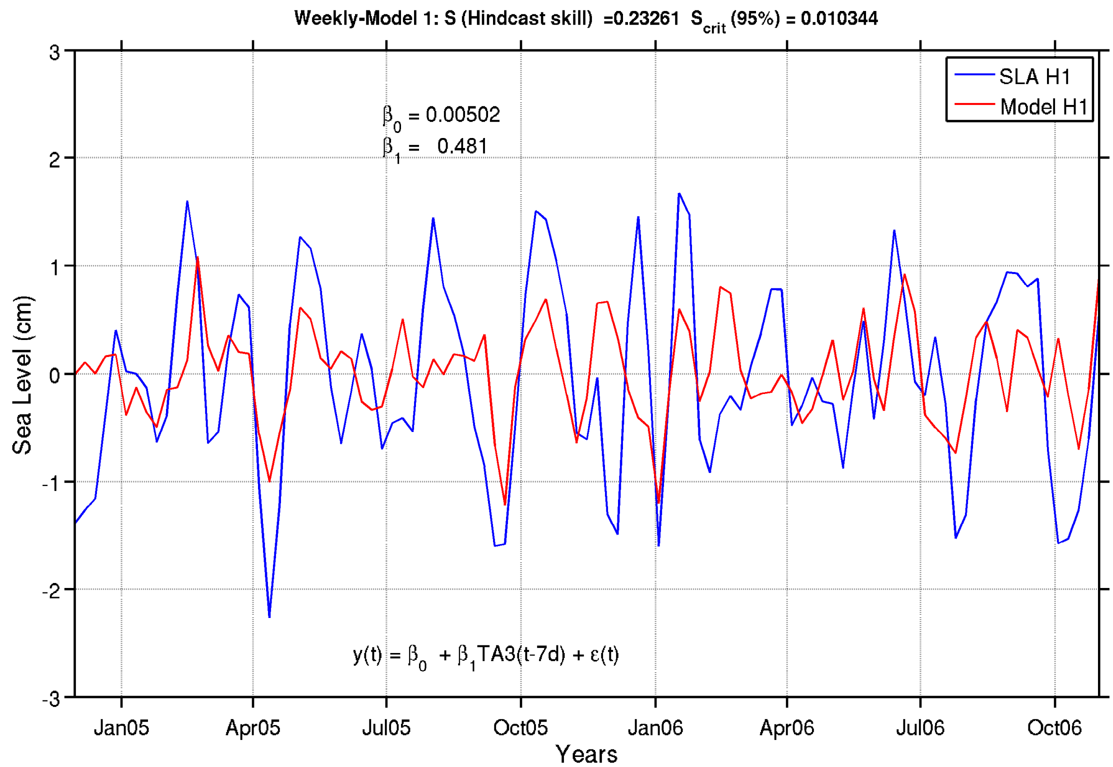

Figure 3.16: Weekly AVISO - Model 1 for Predicting H1; Input Parameters: TA3

decreasing increments in the proportion of variance explained. For the model to be significant, its Skill, S, must be greater than S_{crit}. For a new variable to be added, the increase in skill S_{nm} must be greater than S_{nmcrit} going from model n to model m.

For example, TA4 has a correlation of 0.43 with H1 (Table 3.1). Wind stresses in TA4 are mostly zonal, which cause upwelling (low sea level) on the southern coast of India when they are eastward. Even though there is such a high correlation with H1, the addition of TA4 into the Model 1, doesn′t really explain more skill as TA3 and TA4 are highly correlated [Table 3.2] with each other and most of the variance from these winds is already explained by TA3 winds. In a similar way, TA6 represents alongshore winds from the east coast of India. This does not

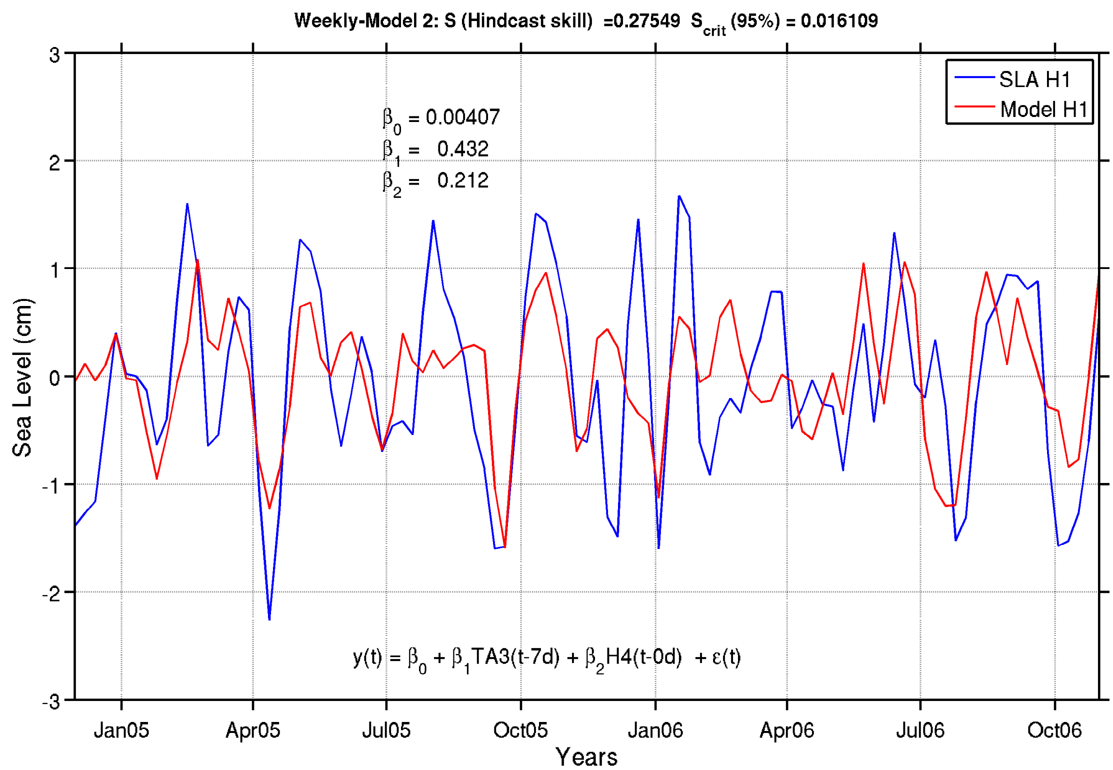

Figure 3.17: Weekly AVISO - Model 2 for Predicting H1; Input Parameters : TA3, H4

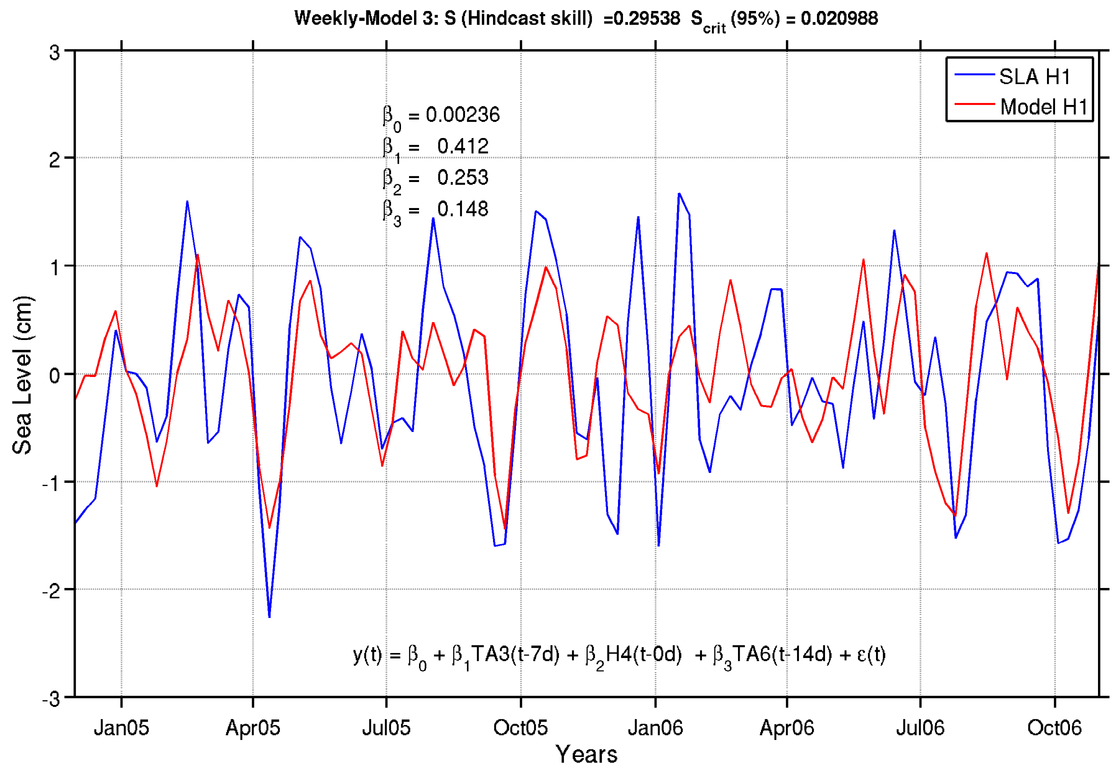

Figure 3.18: Weekly AVISO - Model 3 for Predicting H1; Input Parameters: TA3, H4, TA6

explain a significant increase in variance if added into the model with a lag of 7 days, even though the highest of correlation of TA6 winds is at the lag of 7 days. However, the model shows significant increment in the skill if TA6 winds are added with a lag of 14 days. This again suggests that the correlations and corresponding lags for almost all wind variables are influenced by the basin wide wind fields, with lags of 6 to 7 days with H1 (which we have not yet explained).

The final model consists of TA3 winds with a lag of 7 days, H4 with a lag of 0 days, TA6 winds with a lag of 14 days, C2 with a lag of 0 days and C5 with a lag of 14 days. Fig 3.16 - Fig 3.20 shows a two-year subset of the time series during 2005-2006, comparing the observed H1 to the model reconstructions of H1 for Models 1-4. This demonstrates how the additional input variables improve

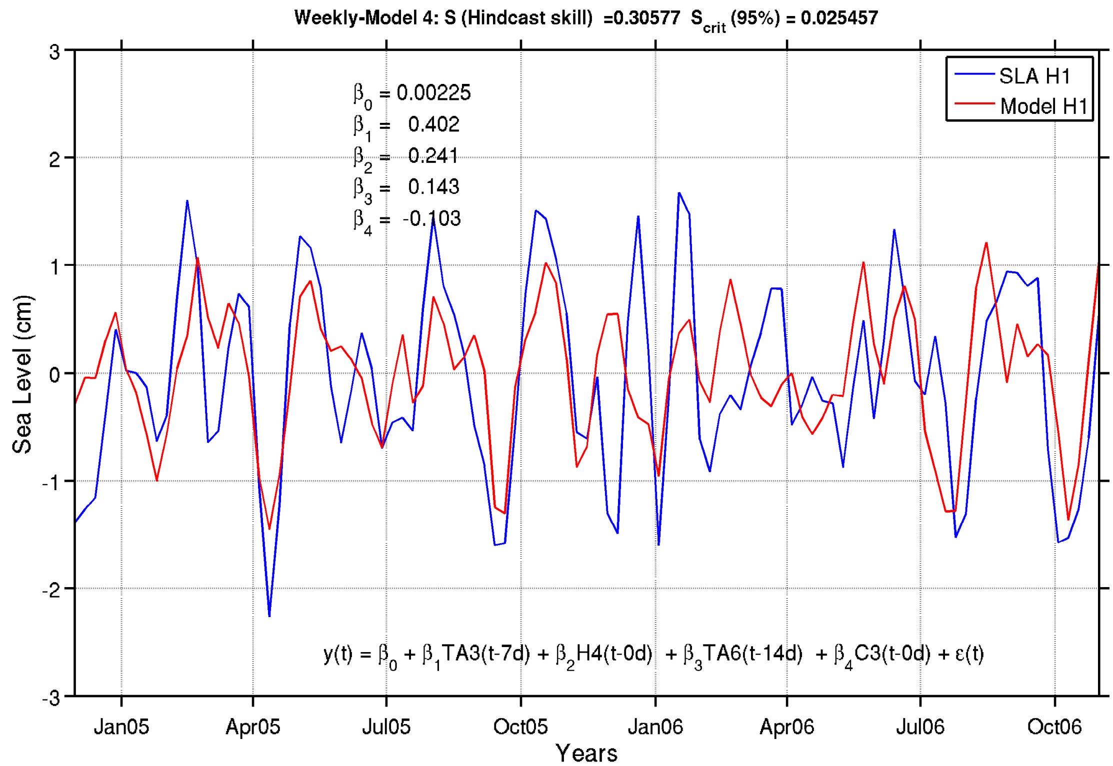

Figure 3.19: Weekly AVISO - Model 4 for Predicting H1; Input Parameters: TA3, H4, TA6, C3

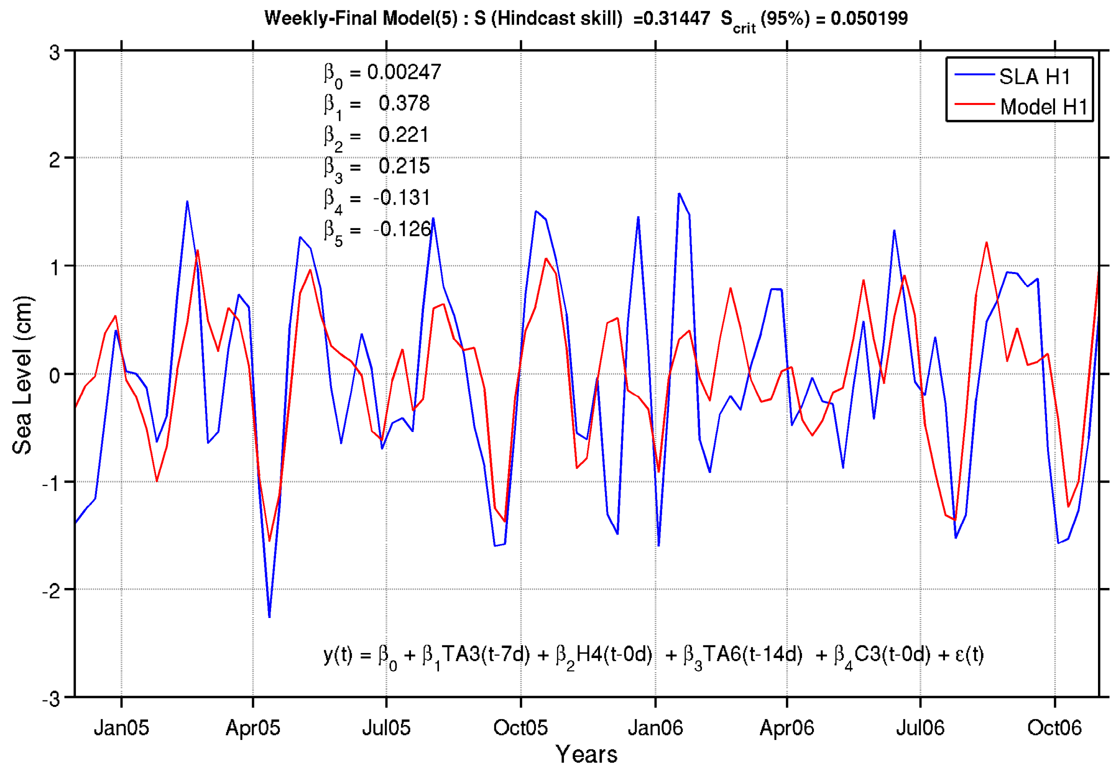

Figure 3.20: Weekly AVISO - Final Model for Predicting H1; Input Parameters : TA3, H4, TA6, C3, C5

the models representation of the intra-seasonal fluctuations. Even when the zero crossings are well represented (and not all are), however, many of the extrema are underestimated. Some of the unexplained variance is due to these underestimates. Addition of the final variable, C5, does little to improve the representation of the extrema. The final model can be thought of as a representation of 4 different signals; 1) local forcing: represented by C2 with a lag of 0 weeks; 2) Forcing from the tip of India: TA3 winds representative of basin wide scale signal with a lag of 1 week; 3) Forcing from the east-coast of India represented by TA6 winds with a lag of 2 weeks; and 4) Sea level from H4 representative of the Rossby wave signal with a lag of 0 to 1 week. The combined model explains almost one third of the variance.

3.2.2 Daily Time Series

Daily data have more symmetric correlations with a higher resolution of lags. The results of the regression models using daily SLA and winds refine those found using weekly data but do not change the general results [Table 3.5]. The daily model with just TA3 winds at the lag of 6 days explains almost 25% of the variance, suggesting the importance of the winds from the tip of India (which we again attribute to the basin-scale wind forcing of multiple signals, see the Discussion section). H4, with a lag of 3 days, explains the next largest amount of variance, increasing the total by 4-5% to 28.8%. The next most important is TA6, winds from east coast of India, with a lag of 13 days, increasing the variance by 2-3%. In the weekly time-series, TA6 with a lag of 2 weeks could not differentiate between itself and the H6 SLA signal which was also correlated with H1 at a lag of 2 weeks. Daily time series helps to differentiate between two signals along the Indian south-east coast: TA6 (alongshore wind stress with a lag of 13 days) and H6 (SLA, with a lag of 11 days). The final model of daily time-series has the same input variables as the weekly model, except an addition of the H6 signal with a lag of 11 days which increases the total variance by almost 1%, statistically significant but modest. The final model for daily time series consist of the following variable: 1) TA3 (-6 day) 2) H4 (-3 days) 3) TA6 (-13 day) 4) H6 (-11 day) 5) C2 (0 day) 6) C5 (-13 day). Figures 3.21 - 3.26 show a two-year subset of the time series during 2005-2006, comparing the observed H1 to the model reconstructions of H1 for Models 1-6.

Although, the high inter-correlations between input variables create large uncertainties in the regression coefficients (not shown here), we interpret correlations and regression models as identifying 5 regional input variables, with characteristic lags:

1) H1, H2 and H3 are well correlated with each other with short lags, representing the signal of interest on the west coast of India;

2) The strongest input is from winds south of India and Sri Lanka, which we regard as representative of basin-scale winds. The lag of 6 days is a puzzle that we investigate further in the Discussion section.

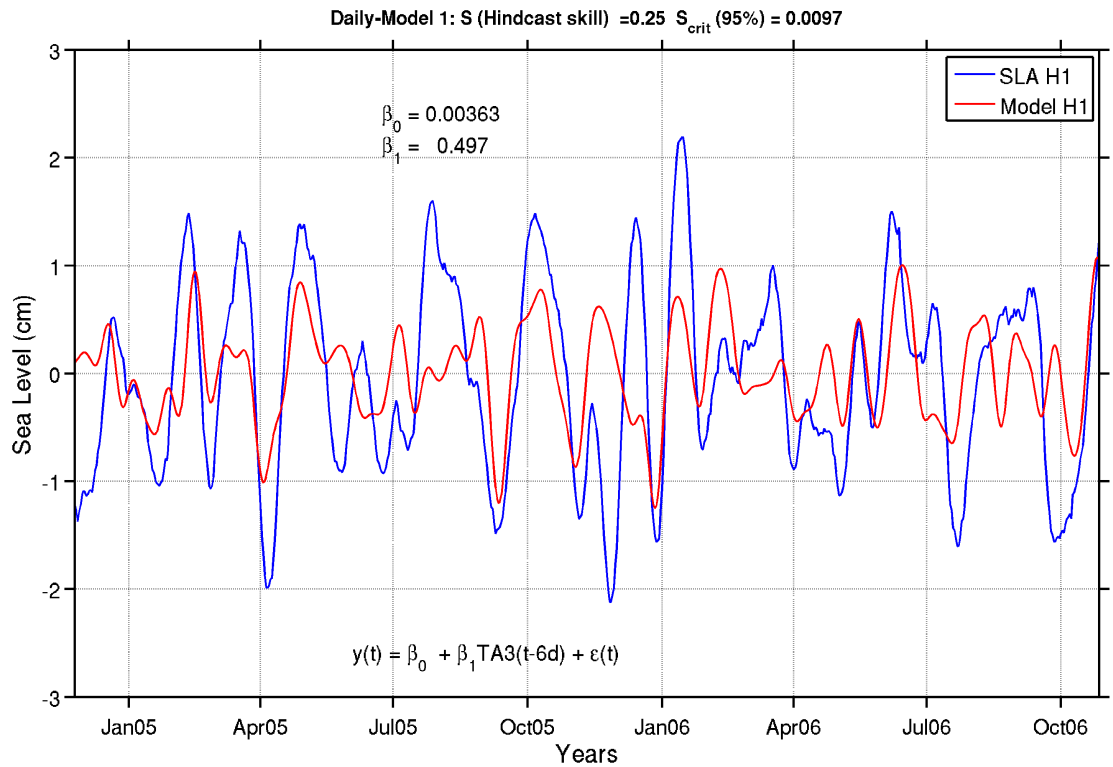

Figure 3.21: Daily AVISO - Model 1 for Predicting H1; Input Parameters: TA3

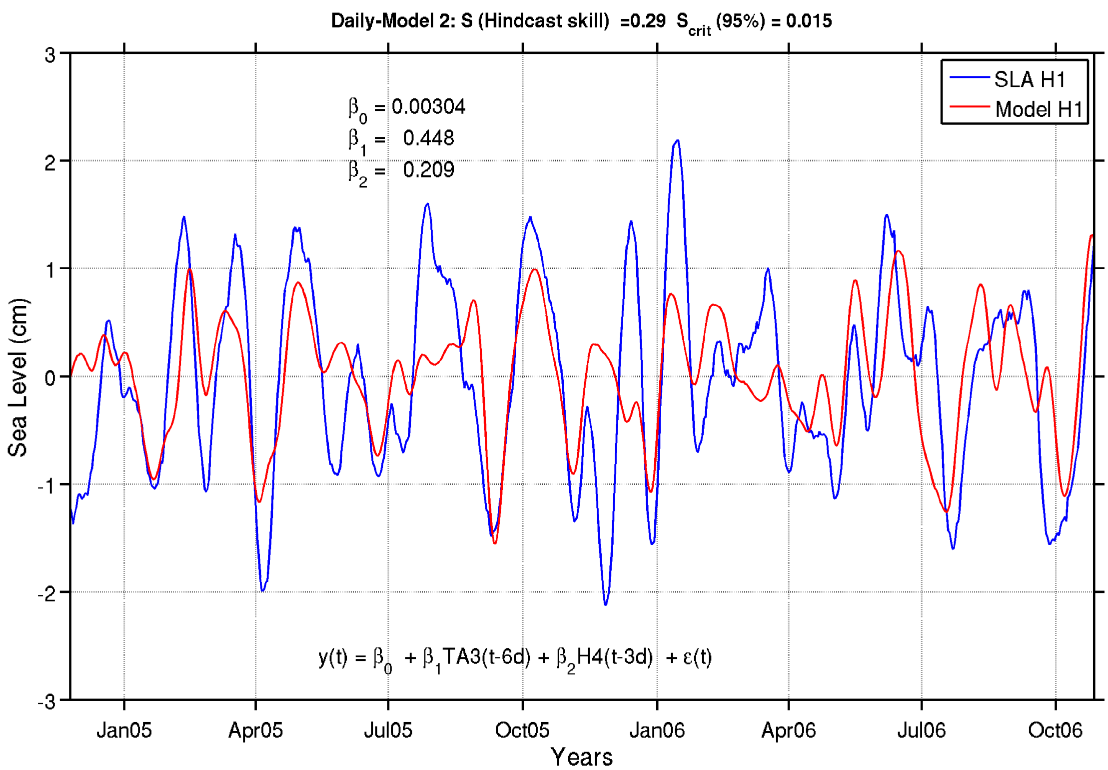

Figure 3.22: Daily AVISO - Model 2 for Predicting H1; Input Parameters : TA3, H4

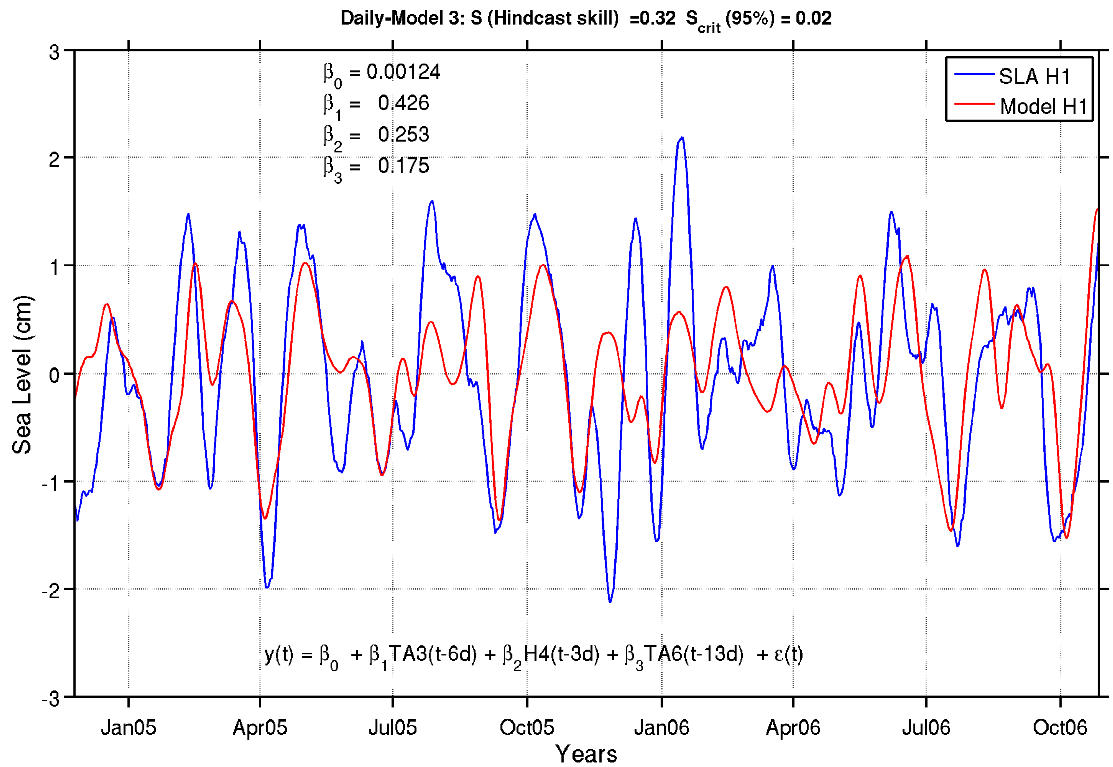

Figure 3.23: Daily AVISO - Model 3 for Predicting H1; Input Parameters: TA3, H4, TA6

3) There is a significant and moderate input from SLA south-east of Sri Lanka, with short (3 day) lags. This appears to originate next to Sumatra and propagate westward over a period of about 3 weeks.

4) There is a significant but weak input from winds and SLA from the south east coast of India, with lags of 11 to 13 days;

5) There is a significant but weak input from local winds with a lag of 0 to 1 days, here represented by wind stress curl, C2;

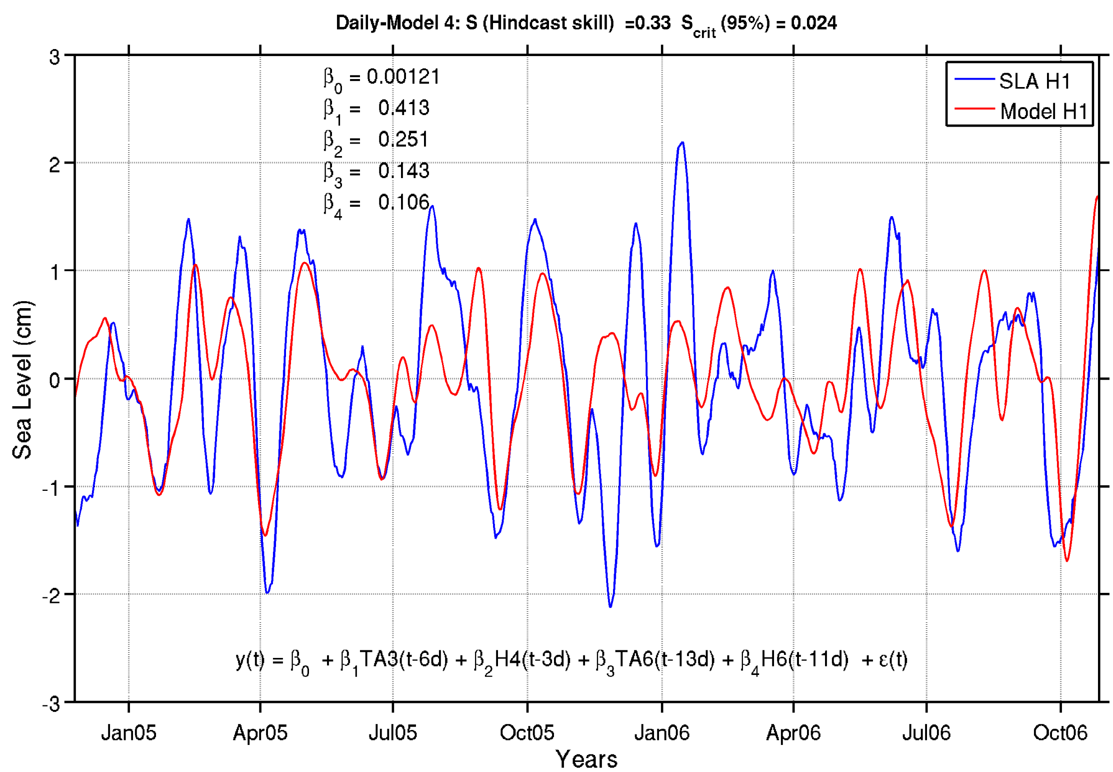

Figure 3.24: Daily AVISO - Model 4 for Predicting H1; Input Parameters: TA3, H4, TA6, H6

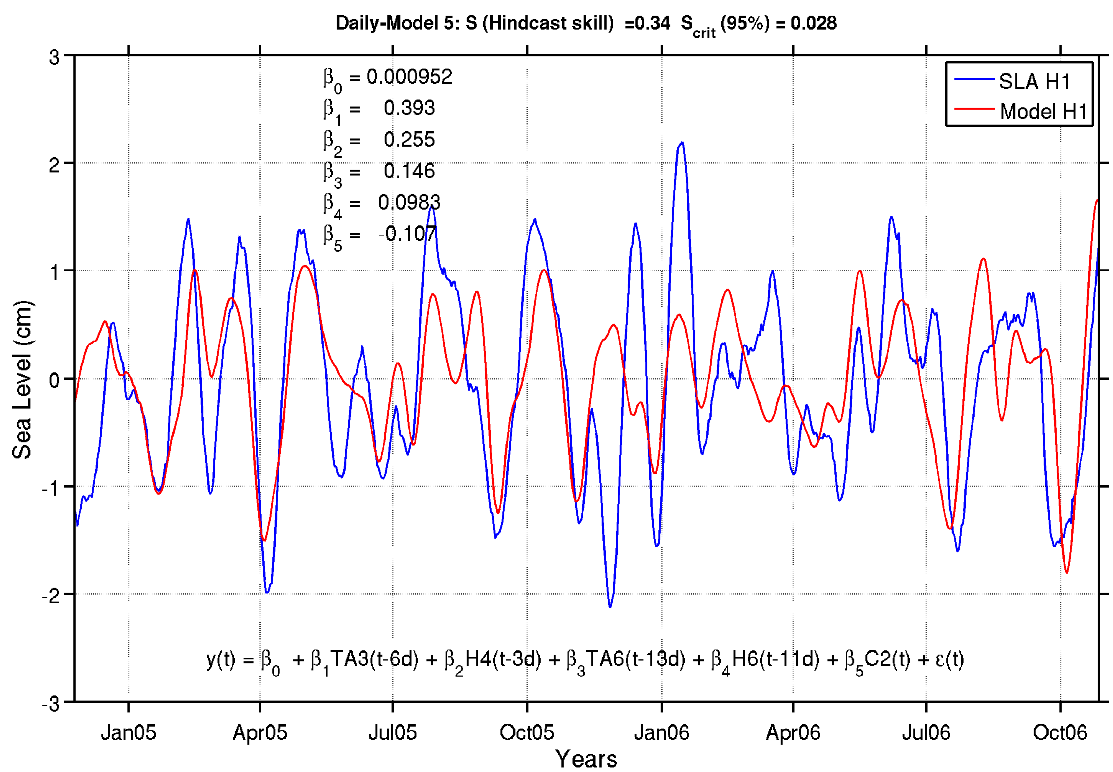

Figure 3.25: Daily AVISO - Model 5 for Predicting H1; Input Parameters: TA3, H4, TA6, H6, C2

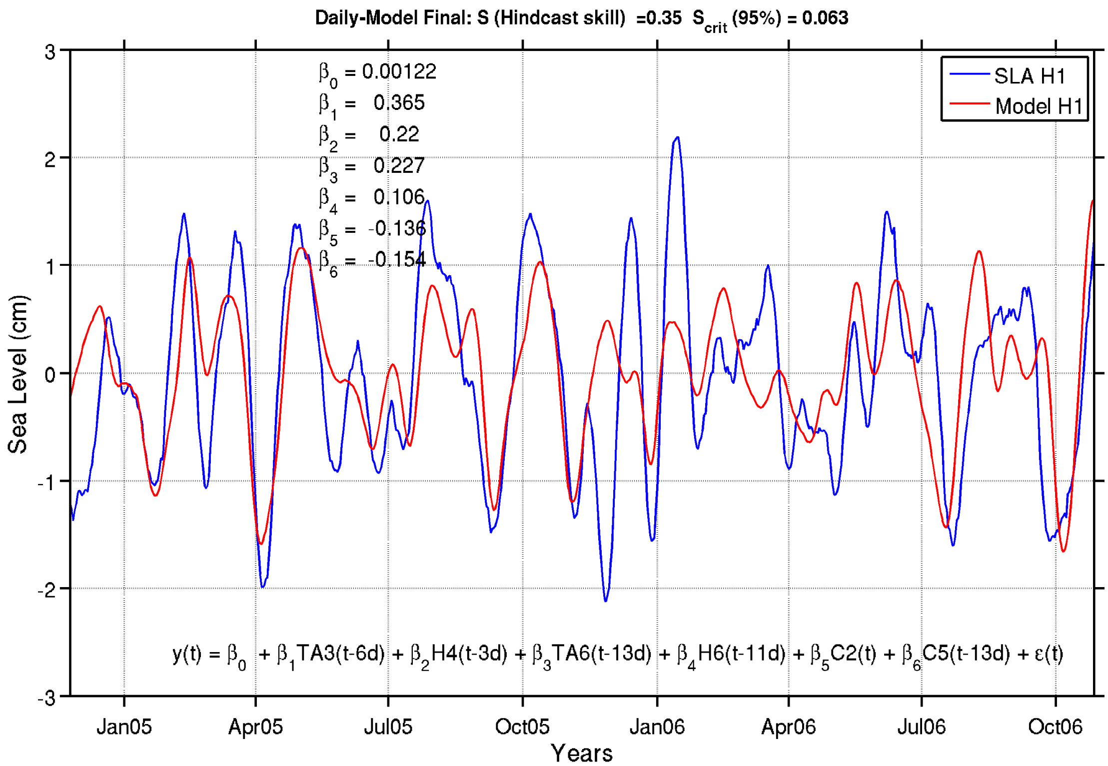

Figure 3.26: Daily AVISO - Final Model for Predicting H1; Input Parameters : TA3, H4, TA6, H6, C2, C5

Max. Correlation Weekly AVISO H1 with all other variables and corresponding Lags								
Wind Stress	H1	Lag	Wind Stress Curl	H1	Lag	Height	H1	Lag
TA1	0.2974	-7 days	C1	-0.2116	-7 days	H1	1.0000	0 days
TA12	0.3320	- 7 days	C12	-0.3316	-7 days	H2	0.7000	0 days
TA2	0.3420	- 7 days	**C2**	**-0.2858**	**-7 days**	H3	0.5840	0 days
TA3	**0.4873**	**-7 days**	C3	-0.3960	-7 days	**H4**	**0.3239**	**0 days**
TA4	0.4337	-7 days	C4	-0.4304	-7 days	H6	0.2102	-14 days
TA5	——-	———	**C5**	**-0.1982**	**-7 days**	H7(+ve)	0.2755	-21 days
TA6	**0.1973**	**-7 days**	C6	-0.2918	-7 days	H7(-ve)	-0.3369	+7 days

Table 3.1: Highest correlation of H1 with other time-series and corresponding Lag: Weekly AVISO SLA and weekly ECMWF winds. Shown in bold are the input variables selected by the regression models.

Max. Correlation Daily TA3 wind stress with other wind stress							
Wind Stress	TA1	TA12	TA2	TA3	TA4	TA5	TA6
TA3	0.4160	0.5532	0.5509	1.000	0.8379	-0.3357	0.4216
Lag	+1 day	+2 day	+ 1 day	0 day	0 day	+1 day	+1 day
Wind Stress Curl	C1	C12	C2	C3	C4	C5	C6
TA3	-0.3246	-0.6035	-0.4695	-0.7872	-0.7350	-0.1870	-0.5508
Lag	- 1 day	0 day	- 1 day	-1 day	0 day	- 3 day	+ 1 day

Table 3.2: Highest correlation of TA3 alongshore wind stress with other box wind stress and wind stress curl

Max. Correlation daily AVISO H1 with all other variables and corresponding Lags								
Wind Stress	H1	Lag	Wind Stress Curl	H1	Lag	Height	H1	Lag
TA1	0.3143	-5 days	C1	-0.2087	-6 days	H1	1.0000	0 days
TA12	0.3465	- 5 days	C12	-0.3452	-5 days	H2	0.6984	-1 days
TA2	0.3634	- 5 days	**C2**	**-0.2990**	**-6 days**	H3	0.5589	0 days
TA3	**0.5028**	**-6 days**	C3	-0.4121	-6 days	**H4**	**0.3263**	**-2 days**
TA4	0.4572	-6 days	C4	-0.4348	-6 days	**H6**	**0.2102**	**-11 days**
TA5	——-	———	**C5**	**-0.1966**	**-6 days**	H7(+ve)	0.2550	-21 days
TA6	**0.2122**	**-8 days**	C6	-0.2984	-6 days	H7(-ve)	-0.3466	+5 days

Table 3.3: Highest correlation of H1 with other time-series and corresponding Lag: AVISO Daily SLA and ECMWF daily Winds. Shown in bold are the input variables selected by the regression models.

Hierarchy of Models Predicting H1 (Weekly AVISO)						
Variables (Lags)	Inputs for Model 1 and 2		S	$Scri$	$S21$	$S21_{Cri}$
TA3 (-7 d)	**Model 1**	**TA3**	**0.2326**	**0.0103**	—	—
H4 (0 d)	**Model 2**	**TA3 + H4**	**0.2755**	**0.0161**	**0.0592**	**0.0108**
Inputs for Model 3			S	$Scri$	$S32$	$S32_{Cri}$
TA6 (-14 d)	**Model 3**	**TA3 + H4 + TA6**	**0.2954**	**0.0210**	**0.0282**	**0.0108**
Inputs for Model 4			S	$Scri$	$S43$	$S43_{Cri}$
C2 (0 d)	**Model 4**	**TA3 + H4 + TA6 + C2**	**0.3058**	**0.0255**	**0.0150**	**0.0109**
Inputs for Model 5			S	$Scri$	$S54$	$S54_{Cri}$
C5 (-14 d)	**Model 5**	**TA3 + H4 + TA6 + C2 + C5**	**0.3145**	**0.0502**	**0.0127**	**0.0110**

Table 3.4: Hierarchy of Models are Built with the inputs in the order of decreasing Correlation to predict H1. S is the hind-cast skill of the model representing the percentage of variance explained by regression model, for it to be significant it has to be greater than S_{Cri} for the 95% confidence level. Addition of an extra input parameter suppose going from Model 1 to Model 2, significantly explains more skill if $S21$ is higher than $S21_{Cri}$ and similar way Model 3 significantly explains more skill if $S32$ is greater than $S32_{Cri}$, with a 95% confidence. Similarly for $S43$, $S43_{Cri}$ and $S54$, $S54_{Cri}$

Hierarchy of Models Predicting H1 (Daily AVISO)						
Variables (Lags)	Inputs for Model 1 and 2		S	$Scri$	$S21$	$S21_{Cri}$
TA3 (-6 d)	**Model 1**	**TA3**	**0.2469**	**0.0097**	——	——
H4 (-3 d)	**Model 2**	**TA3 + H4**	**0.2885**	**0.0151**	**0.0585**	**0.0106**
Inputs for Model 3			S	$Scri$	$S32$	$S32_{Cri}$
TA6 (-13 d)	**Model 3**	**TA3 + H4 + TA6**	**0.3167**	**0.0197**	**0.0412**	**0.0104**
Inputs for Model 4			S	$Scri$	$S43$	$S43_{Cri}$
H6 (-11 d)	**Model 4**	**TA3 + H4 + TA6 + H6**	**0.3268**	**0.0239**	**0.0150**	**0.0104**
Inputs for Model 5			S	$Scri$	$S54$	$S54_{Cri}$
C2 (0 d)	**Model 5**	**TA3 + H4 + TA6 + H6 + C2**	**0.3379**	**0.0279**	**0.0167**	**0.0105**
Inputs for Model 6			S	$Scri$	$S65$	$S65_{Cri}$
C5 (-13 d)	**Model 6**	**TA3 + H4 + TA6 + H6 + C2 + C5**	**0.3505**	**0.0542**	**0.0194**	**0.0108**

Table 3.5: Similar to 3.4, however with daily AVISO SLA and daily ECMWF winds. Shown in bold are the input variables selected by the regression models.

Chapter 4: DISCUSSION

In the last section, regression models helped to clarify some of the connections between sea level along the Indian west coast and signals in other regions that were first identified using lagged correlations. There remains a puzzle as to the cause of a 6 day lag between the west coast SLA and winds south of India and throughout the Indian basin. This puzzle is part of a more general difficulty in interpreting the results of correlations, due to the significant inter-correlations between the different input variables [Table 3.2]. Although the multivariate regression models help to differentiate the signals from various key locations, again the inter-correlation of the input variables limits our ability to asses the relative importance of the inputs. This section focuses on separating these signals using coherence and phase computations to identify the dominant frequencies in the system, and the application of an additional band-pass filter to examine the coherent wind and sea-level connections in the narrower 40-60 day period band. Hovmoller diagrams also provide a visual means to interpret the statistics. Finally, we investigate the possibility that basin-wide winds create multiple signals that combine to generate the observed lag of around 6 days in the correlations between west coast SLA and large scale winds.

Fig 4.1 - Fig 4.5 show the coherence between H1 and other heights (H2, H3, H4 , H6 and H7). Coherence and phase plots of H1 with H2 and H3 suggest that there is very high coherence at all the frequencies with periods greater than 30 days. [Note: The AVISO filtering of SLA reduces signals with periods less than 30 days.] The phase plot shows that the lag (blue dots) is close to 0 to 2 days, and not statistically different from 0 (confidence limits are shown as red dots). This result is consistent with our correlations of H1 with other west coast heights. The coherence plot for H1 and H4 has a peak between 50 and 60 days and for periods >70 days. The phase plot suggests that the lag between H1 and H4 is approximately 0 to 2 days, but again not distinguishable from 0. The coherence plot between H1 and H7 shows that there is significant coherence for the higher periods with a lag of about 3-4 weeks. This result is consistent with the results obtained from previous correlations [Table 3.3, Table 3.1]. The coherence plot of H1 and H6 suggests that there exist barely significant correlations with periods between 30 to 60 days. The corresponding lags(blue dots) are close to 12 days, which is again consistent with the lags obtained from correlations (-11 days)[Table 3.3]. The noticeable difference between signals coming through H4 and H6 is that H4 has a wider range of coherent frequencies above 50 days. In fact, the highest coherence comes from periods greater than 70 days, whereas H6 is more limited to the band between 30 and 50 days. If the SLA signal from H4 roughly represents Equatorial signals arriving as reflected Rossby waves, these may be the source of signals at H1 with lower frequencies and periods of 70-120 days.

The propagation of signals from the south east coast of India (H6) to H1 and from Sumatra (H7 through H4) to H1 are investigated with Hovmoller plots of AVISO weekly SLA. In Fig 4.6, boxes X1-X3 (on the west coast), X4 (south of Sri-Lanka), X5-X8 (along the Rossby wave guide path going to the east of Sri-Lanka) are chosen to investigate the Rossby pathway. Boxes X1-X4 and Y5-Y6 (going around Sri-Lanka to the east coast of India) are chosen to investigate the signals coming from the south-east coast of India.

Fig 4.7 shows the Hovmoller plot of the Rossby pathway for a 2-year subset of the 10-year period. Significant propagation of both high and low signals between X8 and X4 can be seen from Dec 2004 to May 2005, from Aug 2005 to Nov 2005, and from March 2006 to Jan 2007. The figure shows that it takes 3 to 5 weeks for the SLA signal to travel from X8 (west of Sumatra) to X4 (south of Sri Lanka), consistent with our previous results [Fig 3.13, Fig 4.5, Table 3.3]. The signal then propagates very quickly from X4 to X1, in less than a week.

Fig 4.8 shows the Hovmoller diagram for the east coast signal. X1-X4 are the same in Fig 4.7 and Fig 4.8. The propagation of the signal is not as robust as it was in case of the Rossby wave path and only some of the propagating signals reach the west coast. However, propagating signals can be observed in Feb 2005, May

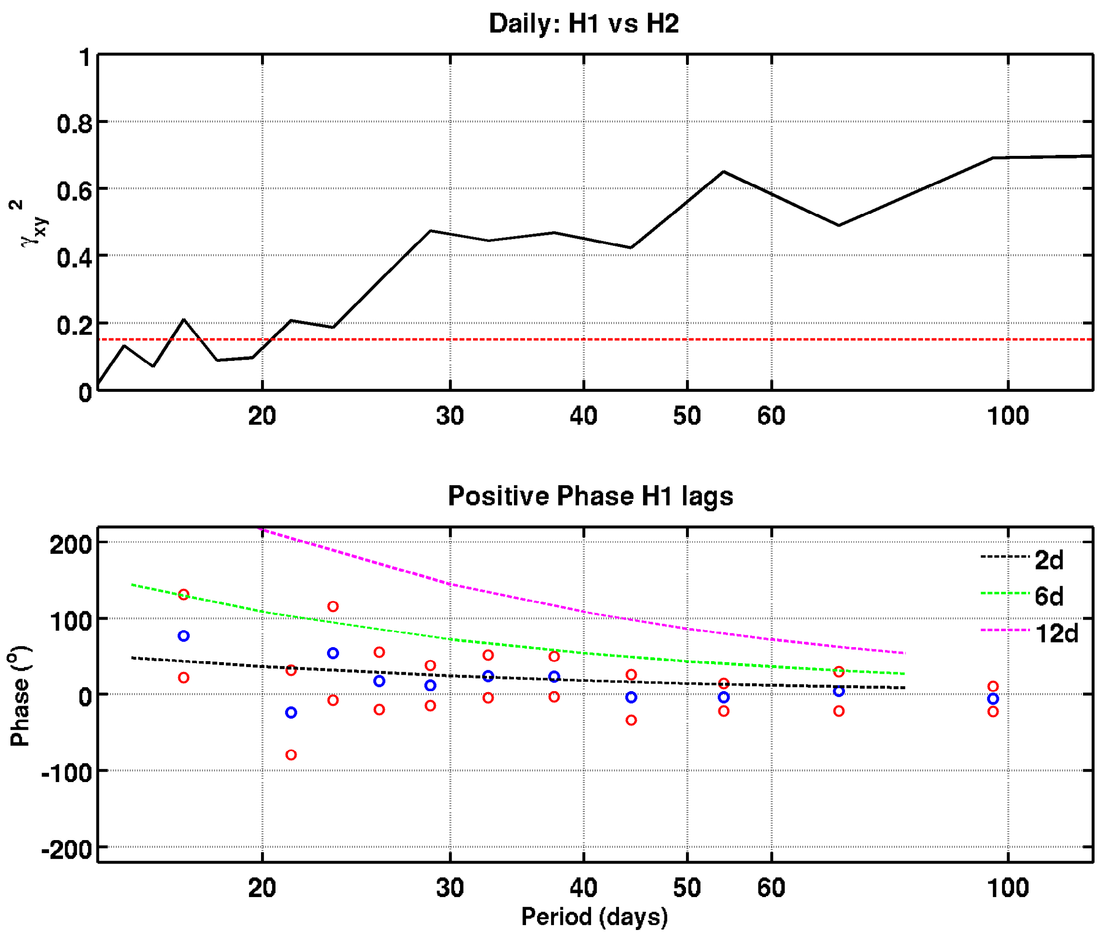

Figure 4.1: Daily AVISO - Coherence and phase between H1 and H2. Dashed red line for the coherence and the red circles for the phase represent 95% significance levels. Black, Green and magenta lines represent corresponding values of phases and periods for a constant lag of 2 days, 6 days and 12 days respectively.

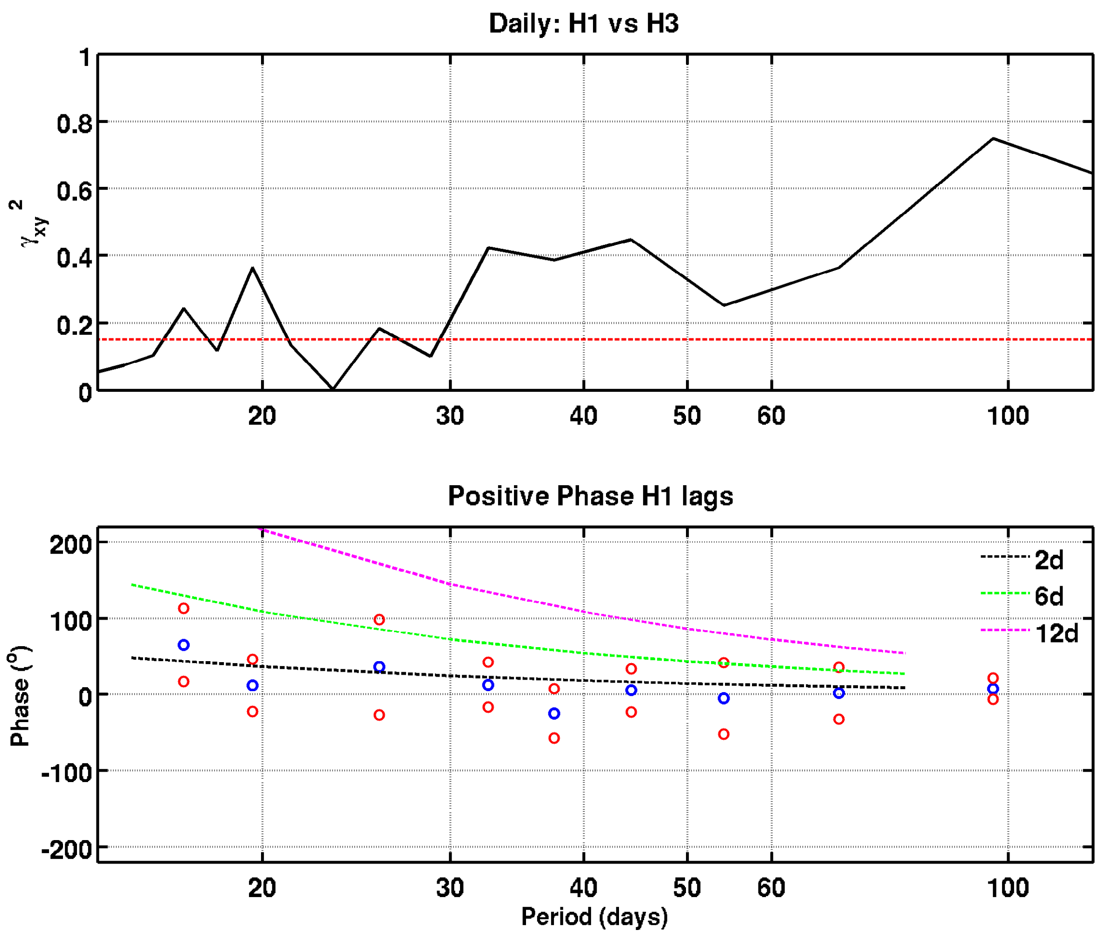

Figure 4.2: Daily AVISO - Coherence and phase between H1 and H3. Dashed red line for the coherence and the red circles for the phase represent 95% significance levels. Black, Green and magenta lines represent corresponding values of phases and periods for a constant lag of 2 days, 6 days and 12 days respectively.

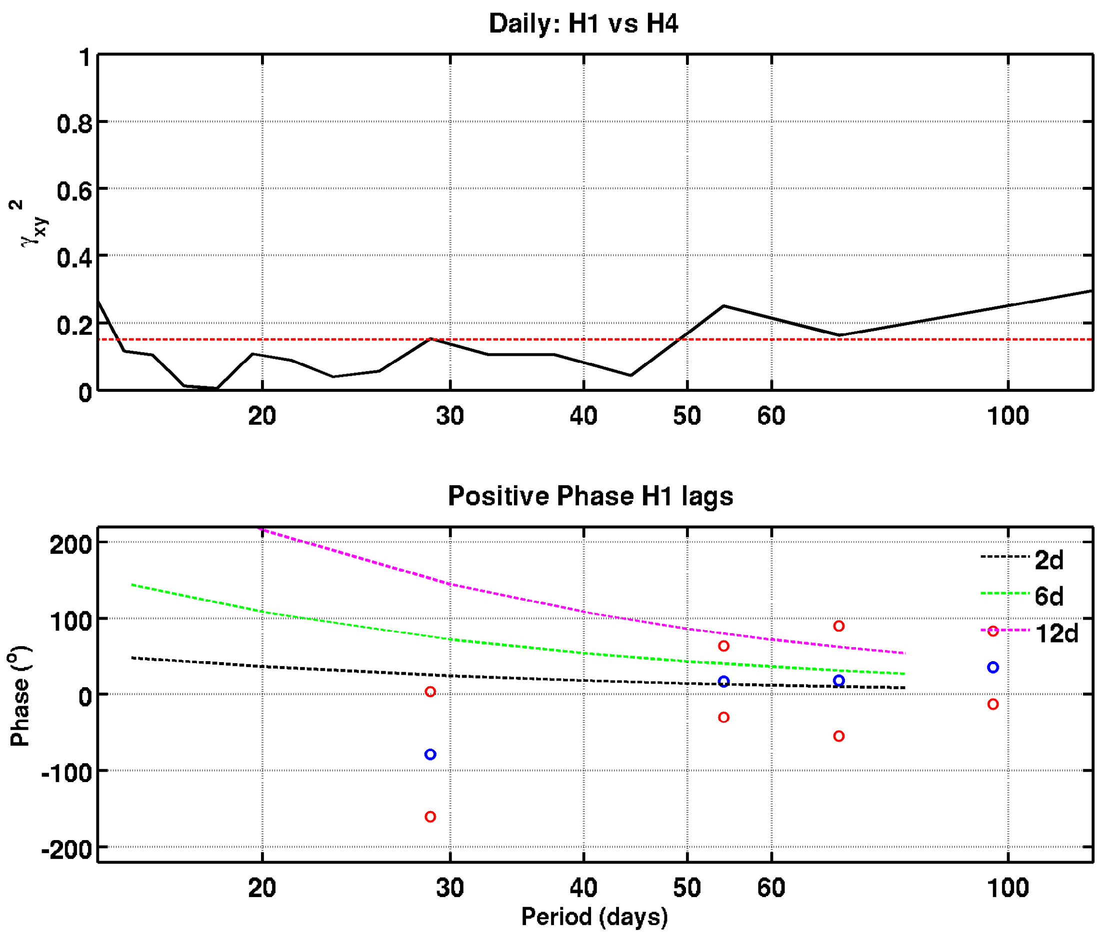

Figure 4.3: Daily AVISO - Coherence and phase between H1 and H4. Dashed red line for the coherence and the red circles for the phase represent 95% significance levels. Black, Green and magenta lines represent corresponding values of phases and periods for a constant lag of 2 days, 6 days and 12 days respectively.

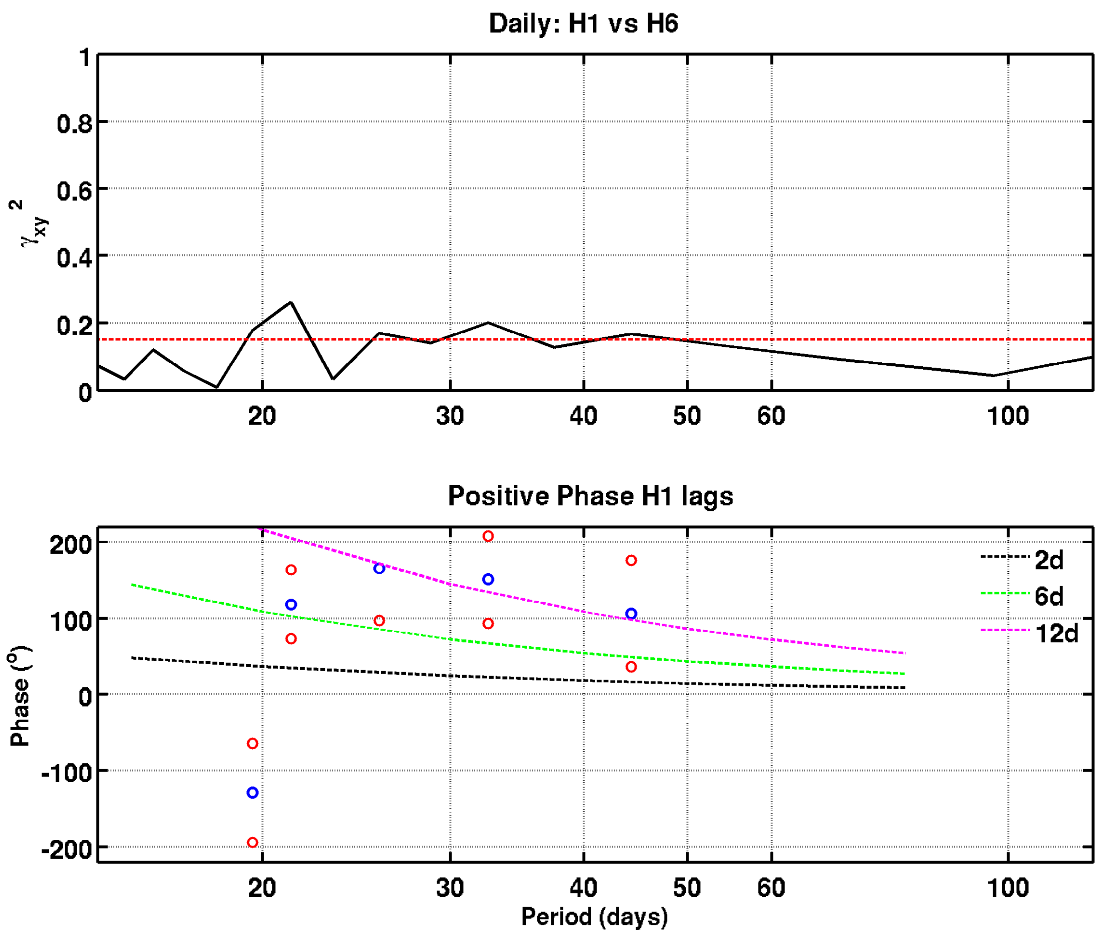

Figure 4.4: Daily AVISO - Coherence and phase between H1 and H6. Dashed red line for the coherence and the red circles for the phase represent 95% significance levels. Black, Green and magenta lines represent corresponding values of phases and periods for a constant lag of 2 days, 6 days and 12 days respectively.

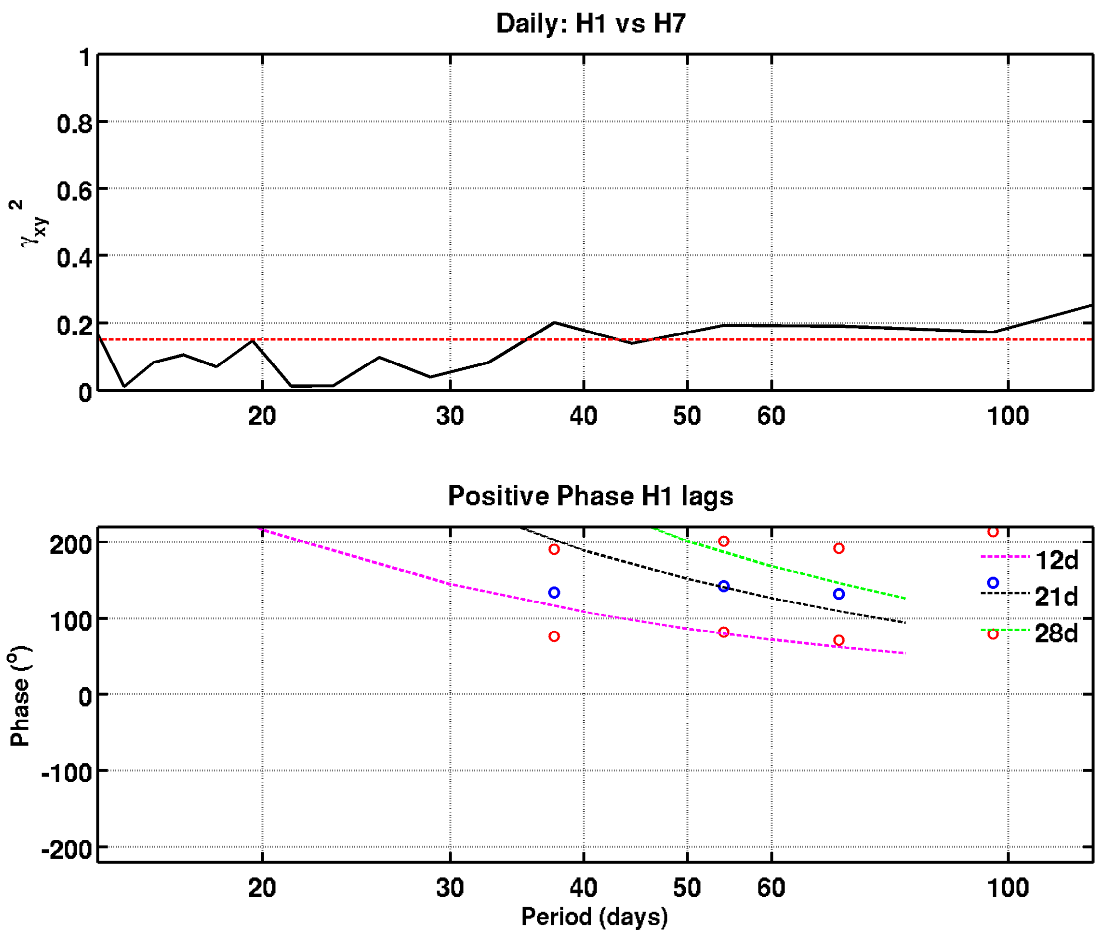

Figure 4.5: Daily AVISO - Coherence and phase between H1 and H7. Dashed red line for the coherence and the red circles for the phase represent 95% significance levels. Black, Green and magenta lines represent corresponding values of phases and periods for a constant lag of 12 days, 21 days and 28 days respectively.

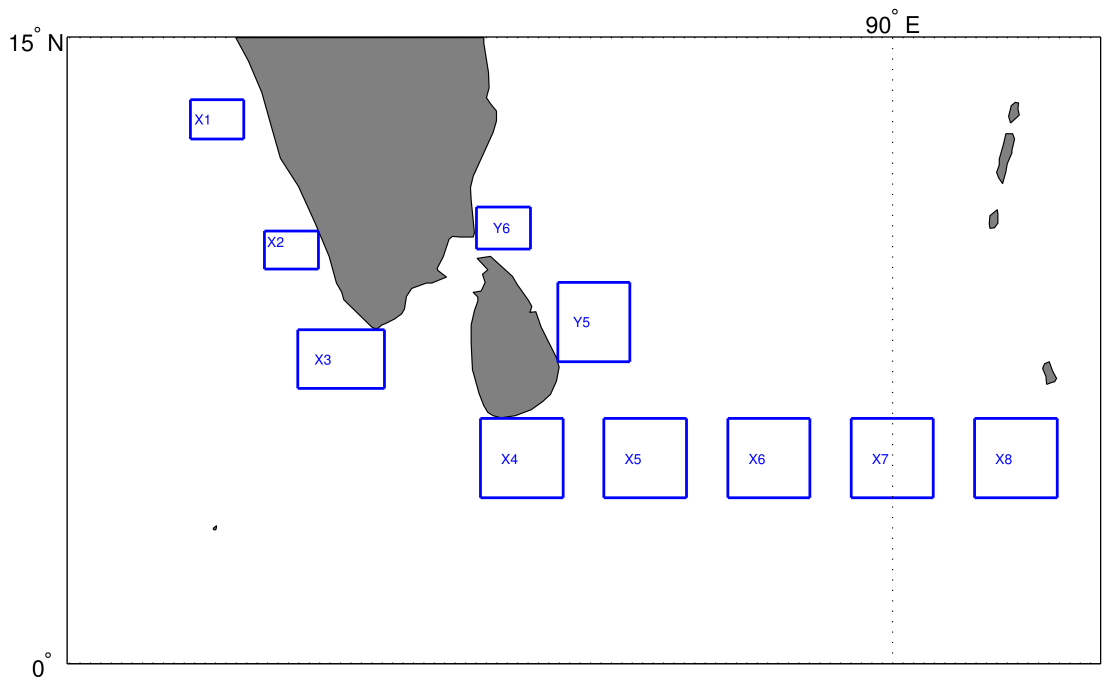

Figure 4.6: Boxes X1-X8 represent a Rossby wave path way and Boxes X1-X4-Y5-Y6 represent coastal trapped signal coming from the east coast of India

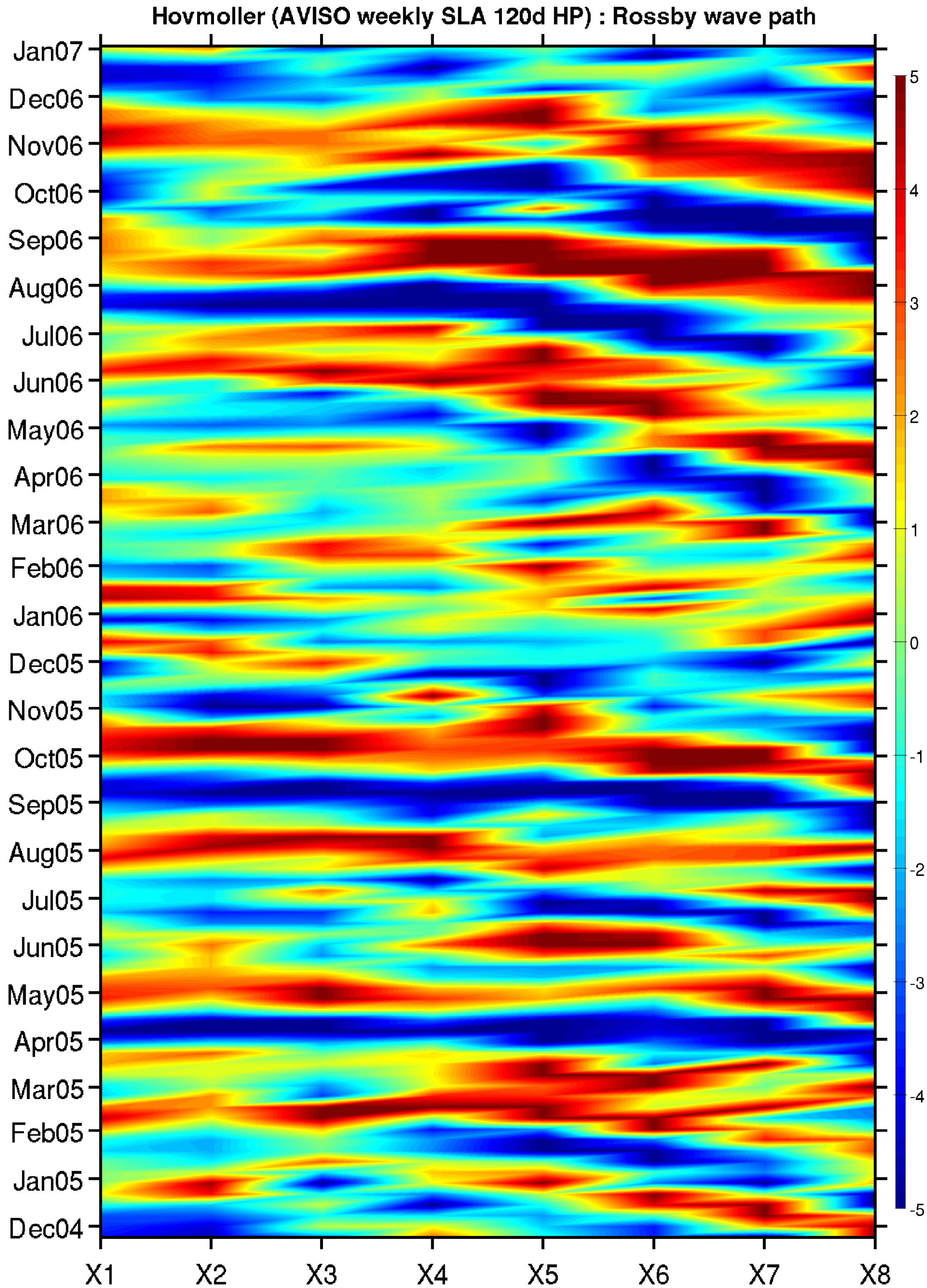

Figure 4.7: Hovmiller plot from AVISO weekly SLA(cm); X1-X3 are on the west coast of India; X4 is at the tip of Sri- Lanka and X5-X8 are boxes going to the east.

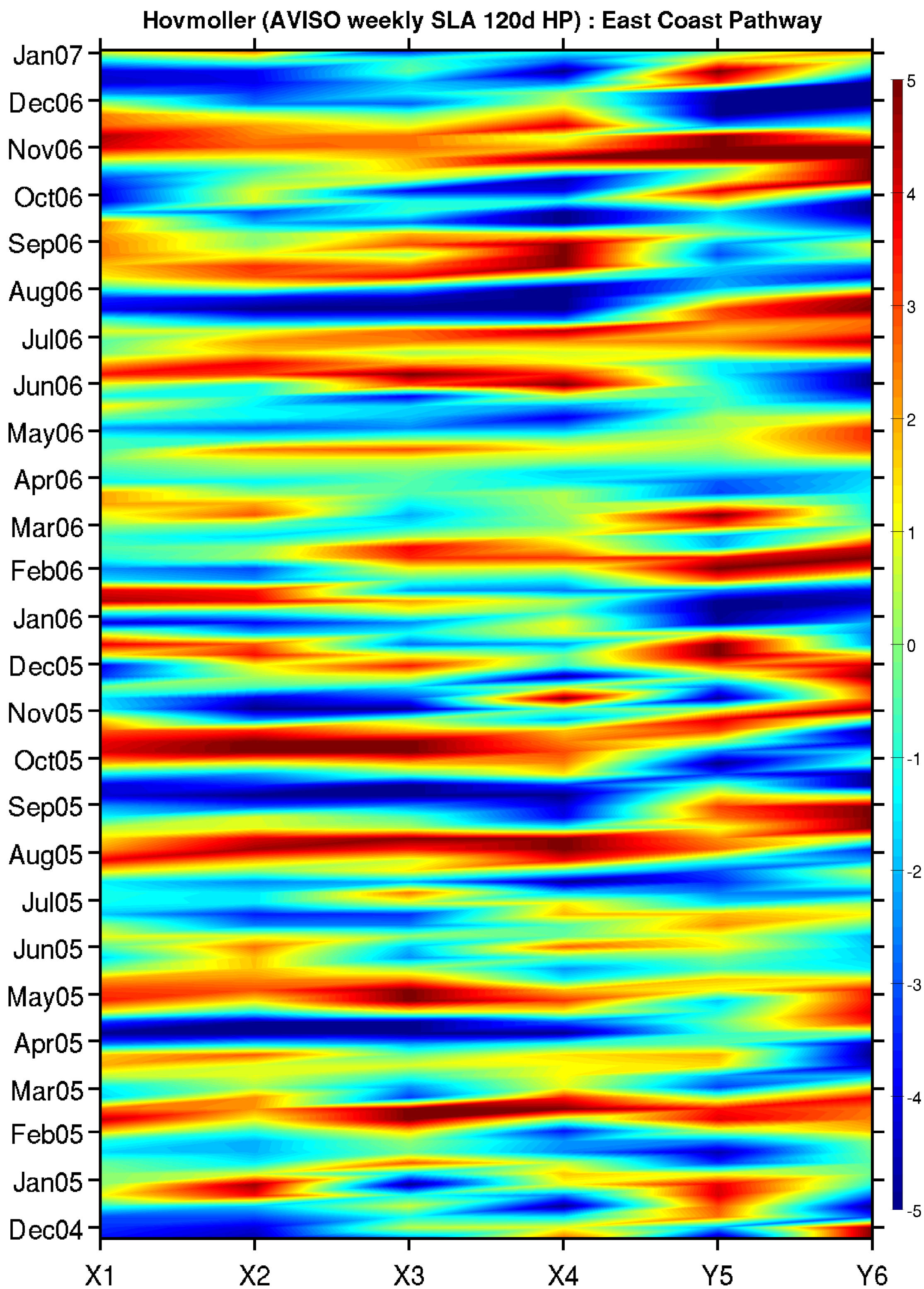

Figure 4.8: Hovmiller plot from AVISO weekly SLA(cm); X1-X3 are on the west coast of India; X4 is at the tip of Sri- Lanka and Y5-Y6 are boxes going around Sri-Lanka to the east coast of India

2005 and Nov 2006. The travel time from Y6 to H1 is roughly 2 weeks, which is consistent with the results from correlations, regression models and the coherences.

X4 is the primary site where the two signals combine, one coming from the south-east coast of India and another as a reflected Rossby wave from the east of Sri-Lanka. The Hovmoller plots show that the signals from the Rossby wave path dominate the signals coming from the east coast of India. For example, a downwelling signal starts from the east coast of India (Y6) around Nov-Dec 2005 and reaches X4 in early Dec 2005. However, during that same time an upwelling (low sea level) signal from the Rossby wave pathway reaches X4, canceling most of the signal coming from the east coast of India. There is also the possibility that winds at the tip of India either reinforce or decrease the distant signals coming from either pathway. For example in Fig 4.7, Aug 2005 and mid Oct 2005, the downwelling signal was reinforced as it moved from X5 to X3.

In summary, propagation can be seen on the Rossby wave path with a lag of 3 to 5 weeks from Sumatra to H1; propagation can also be seen on the east coast pathway with a lag of about 2 weeks. However, the propagation from the east coast pathway does not occur as often as along the Rossby wave pathway. This result provides a possible explanation for a result found in a modelling study by *Suresh et al.* [2013]. They found that the correlation between intra-seasonal coastal sea level and equatorial forcing decreases as we move along the coastal waveguide from the northern Bay of Bengal to the eastern coast of Sri Lanka. The correlations then increase as we move along the waveguide from south of Sri Lanka to the west coast of India. The increased connection between the west coast of India and the equator could be explained by the signals arriving along the Rossby wave pathway.

Coherences of alongshore wind stress with H1 SLA have also been computed and are presented in Fig 4.9 - Fig 4.14. The coherence plot for TA1 shows that the maximum contribution comes from the periods 35 to 65 days and the phase plot shows that the lags corresponding to those periods are between 0 to 2 days. The point to note here is that the lag found in the previous correlation of H1 with TA1 is 5 days, which is longer than expected for a coastal response to the local winds. However, multivariate regression models suggest a lag of around 0 days using local forcing. Note that we previously used C2 in the regression model to represent the local forcing, since it explained the greatest variance of all local forcing variables. However TA1 with 0 day lag explained almost as much variance, as did the other local wind variables. Thus, the coherence results combine with the regression model to support the importance of local wind forcing with lags of 0 to 2 days.

Moving from local winds along the west coast to the winds south of India and Sri Lanka, coherence magnitudes of H1 with TA12, TA2, TA3 and TA4 again show similar peaks for periods of 30-35 to 65 days. However, the lags increase from 0-2 days locally to 6 days in the south at TA3 and TA4. The coherence plots for TA3 and TA4 are very similar and the 6 day lag obtained from the coherence is consistent with the lags from previous correlations and the multivariate regression models.

Along the south-east coast of India, the coherence plot for TA6 winds shows two peaks; one at 30-35 days and another in the 45-65 day band. The phase plot shows that the corresponding lag is close to 8-12 days. The combined coherence results from H6 (lags closer to 12 days) and TA6 (lags of 8-12 days) with the multivariate regression models [Table 3.5] (lags of 11-13 days) provide support for the visual estimates of 1-2 week travel times from the Hovmoller diagrams, connecting the western and the south-east coasts of India.

In summary, the coherence analysis is consistent with the multivariate regression models. However, a puzzle still remains: The previous correlations between winds at all locations and SLA at H1 produced lags of 5 to 7 days. This is in contrast to the shorter lags for local winds and longer lags for winds along the south-east coast of India obtained from regression models, coherence calculations and Hovmoller diagrams.

A possible solution to this puzzle is suggested by the basin-wide scale of the winds. If these winds produce simultaneous signals with the same frequency at different locations, these signals will arrive at H1 with different travel times and

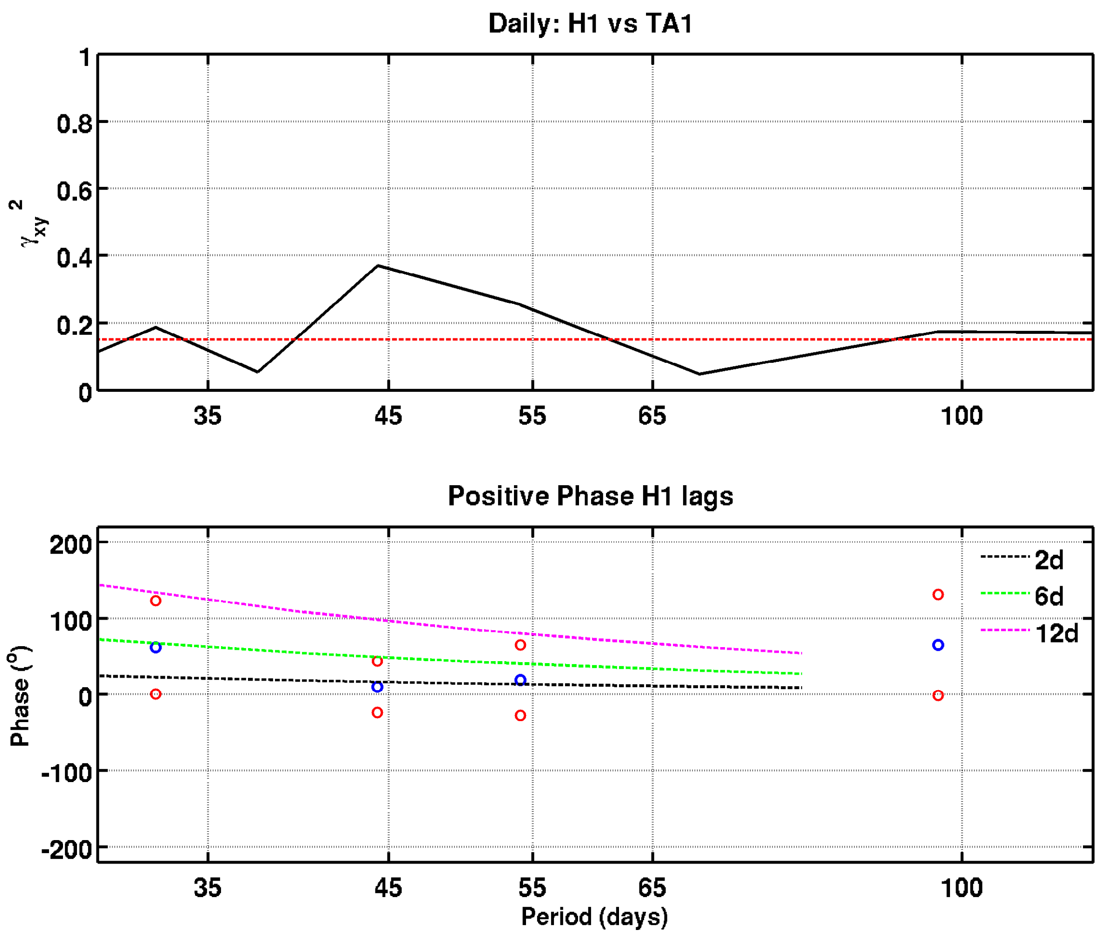

Figure 4.9: Daily AVISO - Coherence and phase between H1 and TA1. Dashed red line for the coherence and the red circles for the phase represent 95% significance levels. Black, Green and magenta lines represent corresponding values of phases and periods for a constant lag of 2 days, 6 days and 12 days respectively.

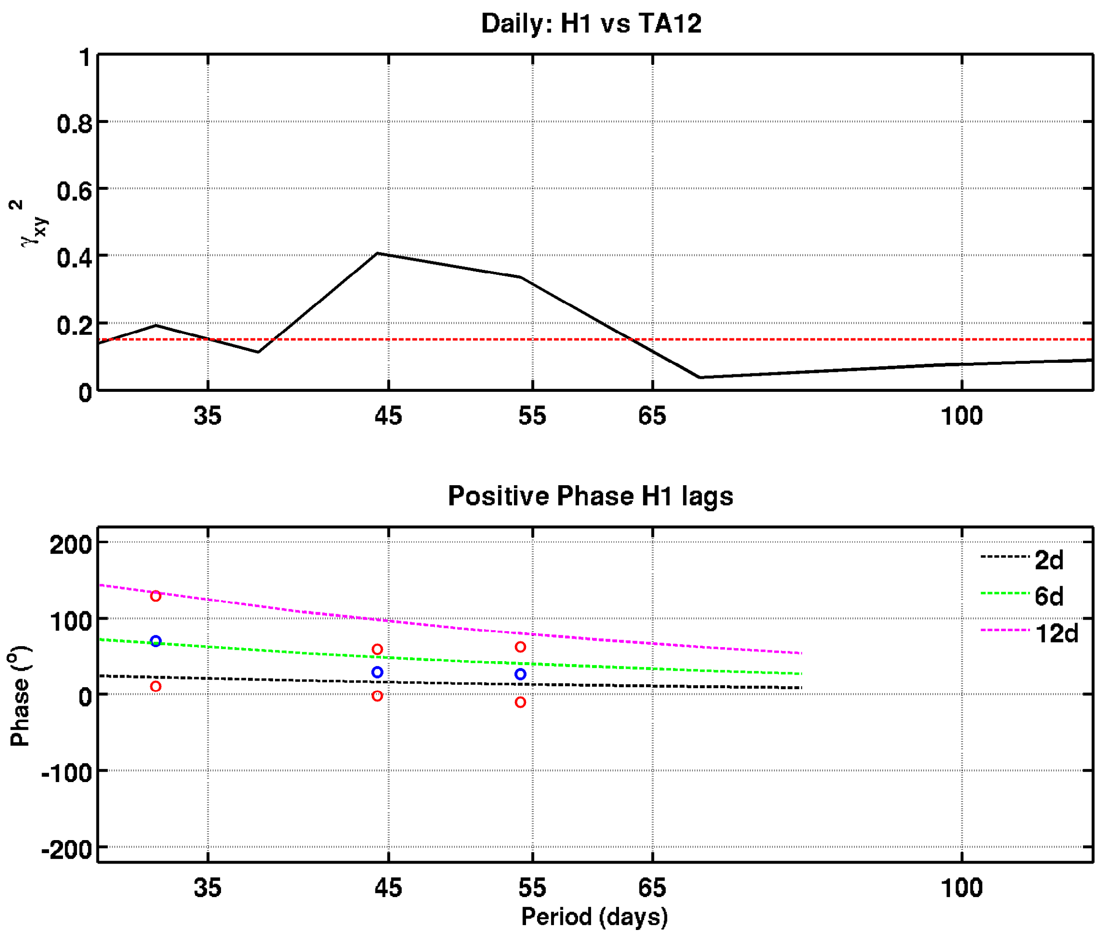

Figure 4.10: Daily AVISO - Coherence and phase between H1 and TA12. Dashed red line for the coherence and the red circles for the phase represent 95% significance levels. Black, Green and magenta lines represent corresponding values of phases and periods for a constant lag of 2 days, 6 days and 12 days respectively.

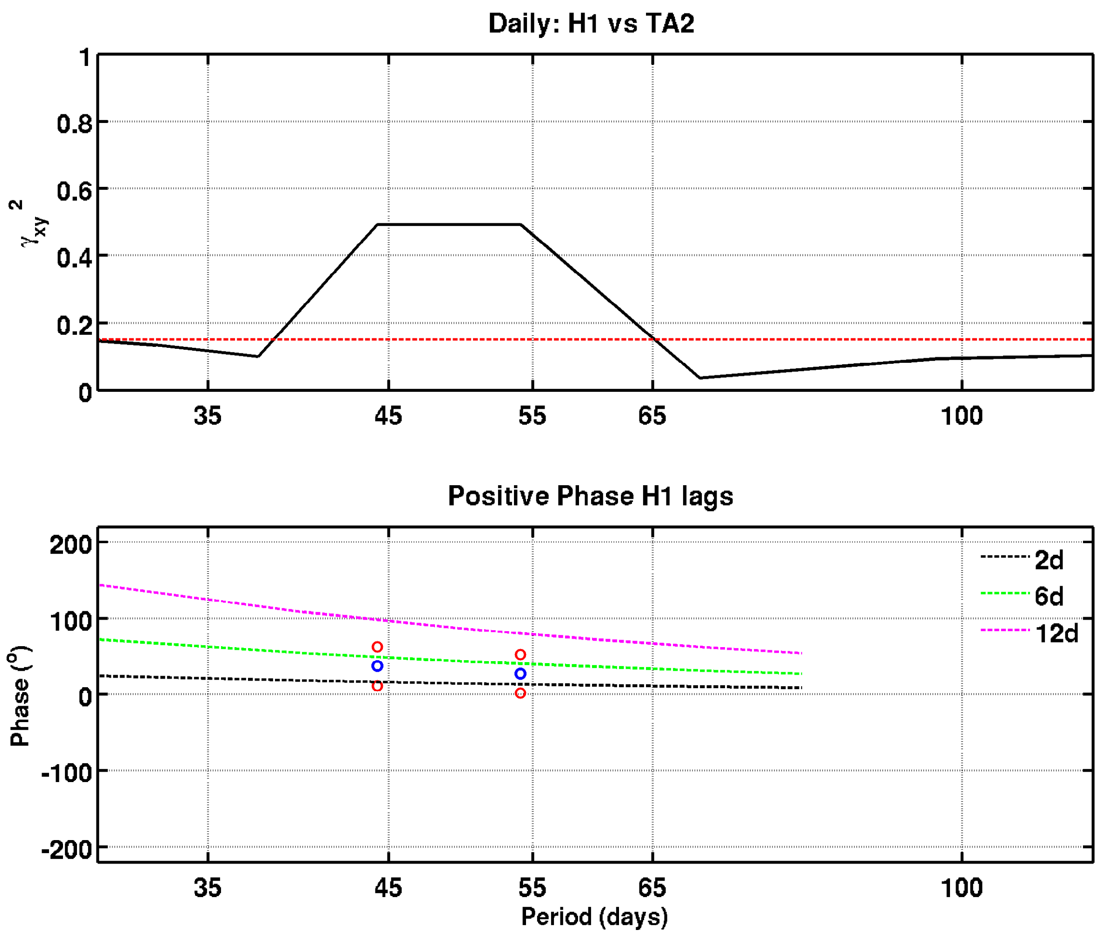

Figure 4.11: Daily AVISO - Coherence and phase between H1 and TA2. Dashed red line for the coherence and the red circles for the phase represent 95% significance levels. Black, Green and magenta lines represent corresponding values of phases and periods for a constant lag of 2 days, 6 days and 12 days respectively.

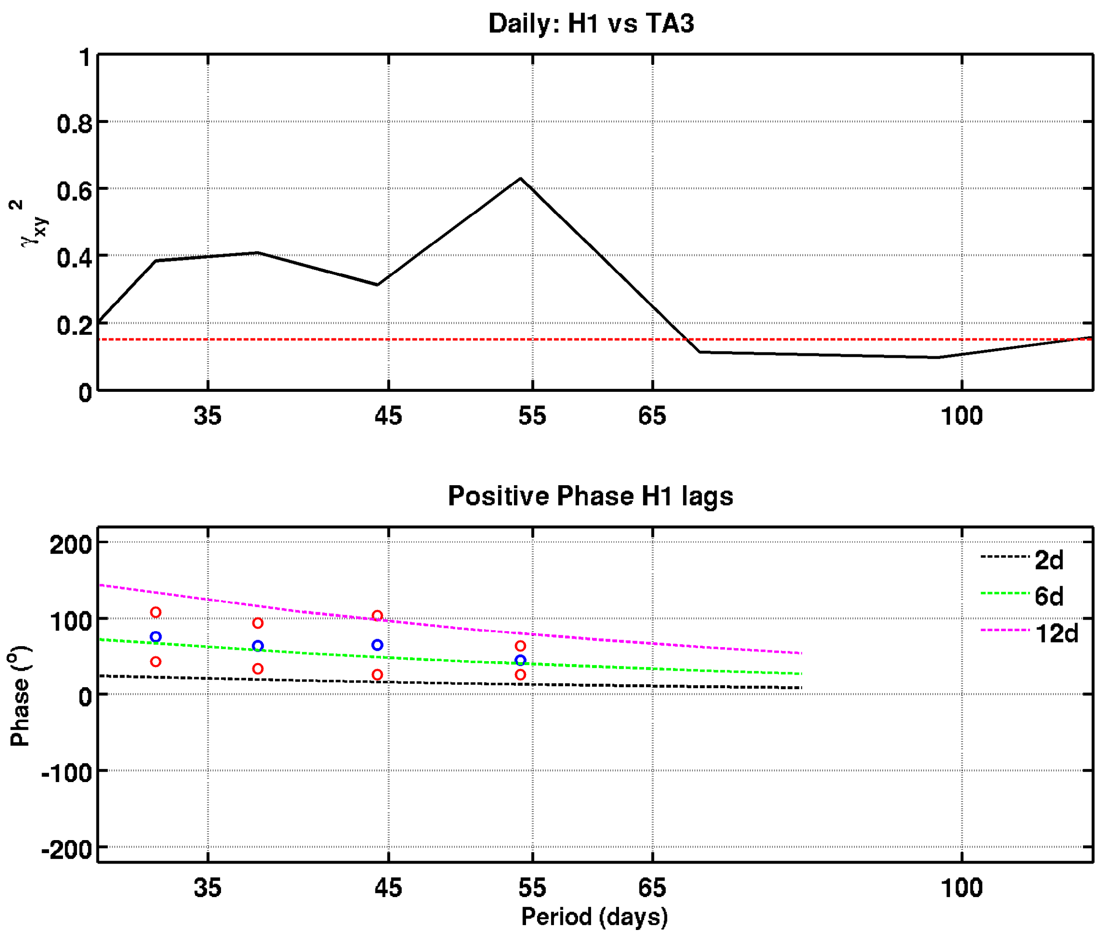

Figure 4.12: Daily AVISO - Coherence and phase between H1 and TA3. Dashed red line for the coherence and the red circles for the phase represent 95% significance levels. Black, Green and magenta lines represent corresponding values of phases and periods for a constant lag of 2 days, 6 days and 12 days respectively.

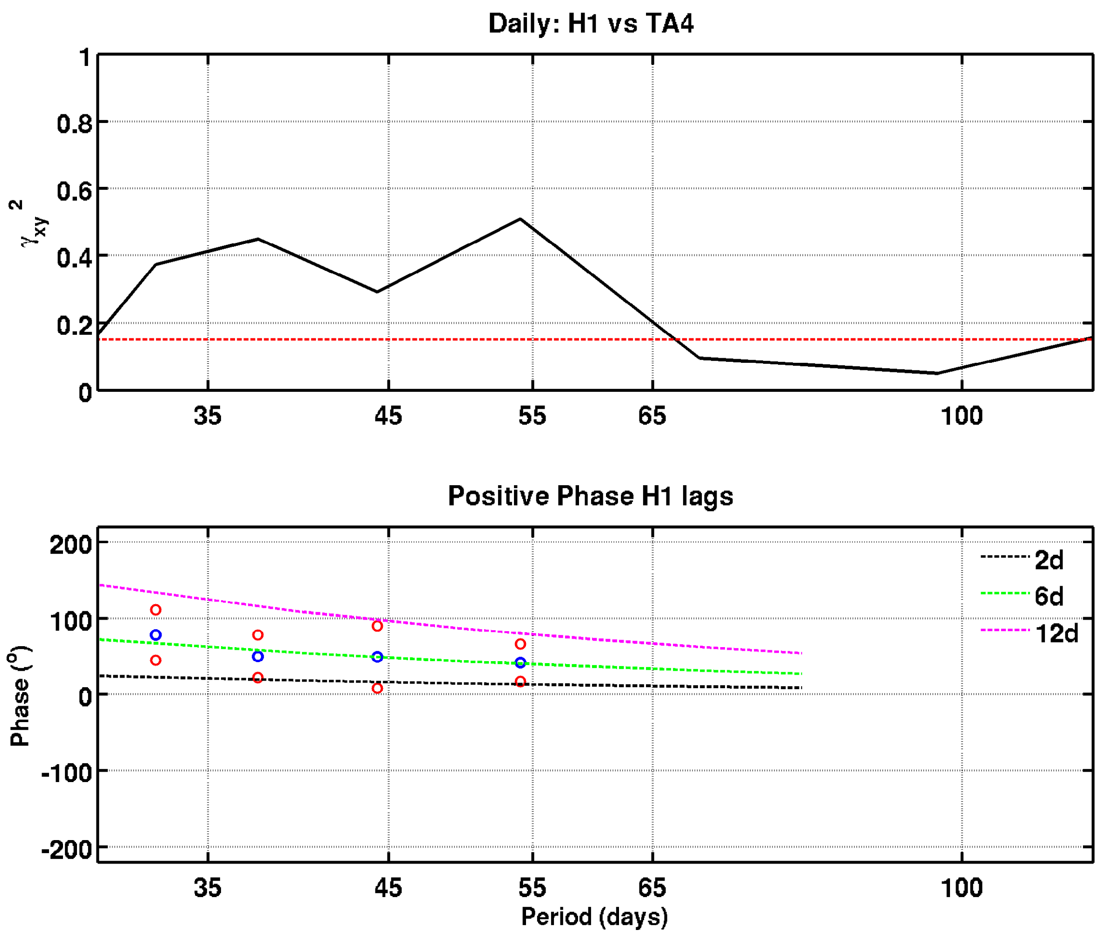

Figure 4.13: Daily AVISO - Coherence and phase between H1 and TA4. Dashed red line for the coherence and the red circles for the phase represent 95% significance levels. Black, Green and magenta lines represent corresponding values of phases and periods for a constant lag of 2 days, 6 days and 12 days respectively.

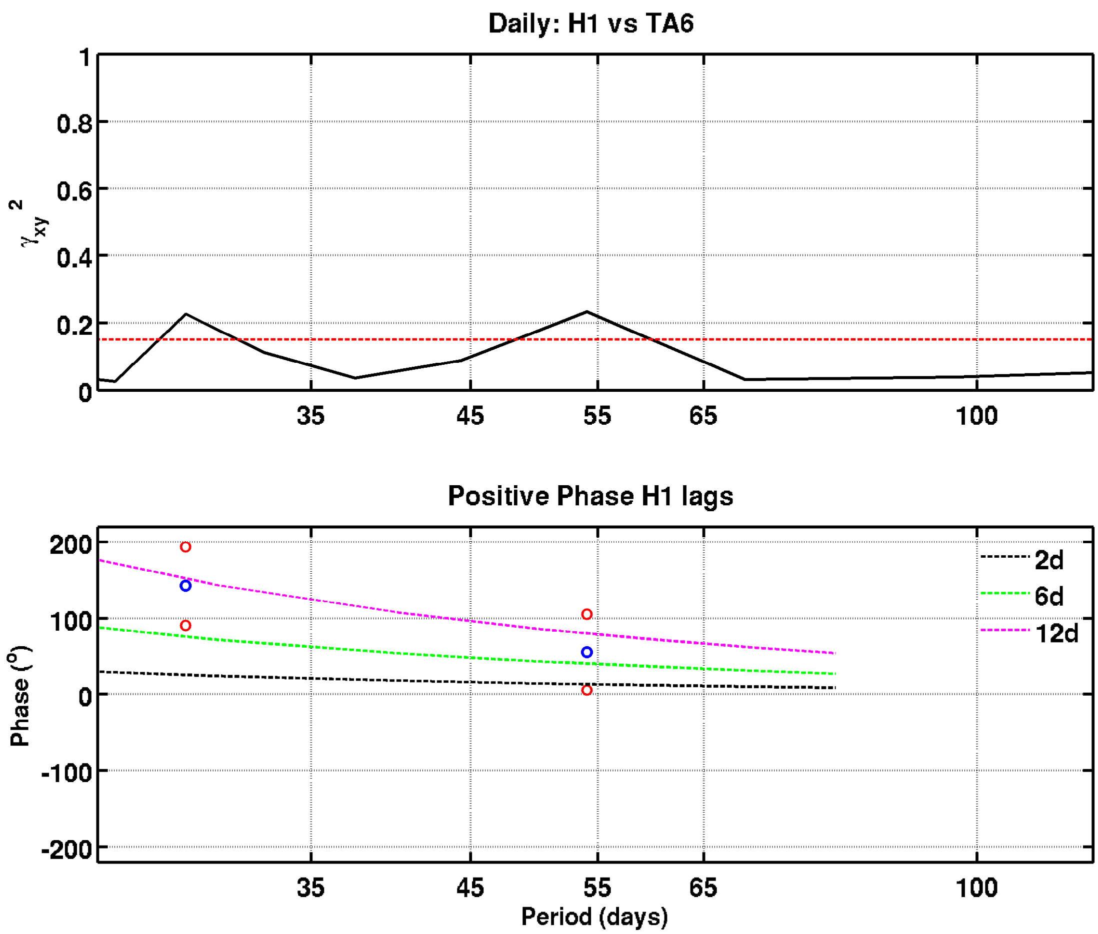

Figure 4.14: Daily AVISO - Coherence and phase between H1 and TA6. Dashed red line for the coherence and the red circles for the phase represent 95% significance levels. Black, Green and magenta lines represent corresponding values of phases and periods for a constant lag of 2 days, 6 days and 12 days respectively.

corresponding phase lags. The combination of these signals can create an artificial lag between the basin scale winds and the signal at H1. Below we use correlations between winds at different locations to show their basin scale nature. Coherences extend this to show the dependence of correlations on periods. This leads to an examination of whether the use of a narrower band of periods eliminates the artificial lags. Finally, we develop an idealised mathematical model that describes the creation of an artificial lag by combinations of distant and local signals.

TA3 has the highest correlation with H1 among all other wind variables. Its lag of 6 days lies between the 5 day lag of H1 with local winds and the 7 day lag of H1 with more distant winds from the south-east coast of India. Thus, we use TA3 as an initial representation of the large-scale winds. Table 3.2 shows the correlation of TA3 with all other possible wind variables. We can see that TA3 and TA4 are highly correlated with each other with almost 0 lag. There are also significant correlations between TA3 and the winds from the west and south-east coasts of India with lags of 1 to 2 days.

The above results from lagged correlations are consistent with coherence and lag calculations of TA3 with all other winds in Fig 4.15 - Fig 4.20. The coherence of TA3 with TA1, TA12 and TA2 show high coherences for all the frequencies with a lag of 0 to 2 days. Even the winds from the south-east coast of India show significant coherences for a wide range of frequencies, again with a lag of 0 to 2 days. The coherence plots and correlation tables suggest that TA3 and TA4 are most likely the best representatives of the basin-scale signal.

In the previous coherence plots for H1 and winds, we see the more realistic lags for periods of 35-65 days. However, the previous correlation calculations included all of the periods from 30-120 days. Our next question is whether the lag for the local wind forcing will decrease (closer to 0) if we band pass filter the data to include only a 40-60 day band. Fig 4.21 - Fig 4.25 show the correlations of the H1 sea levels with all other variables after the data have been band-pass filtered to keep periods between 40 and 60. The first change in the results is an increase in the correlations of all of the wind variables with H1. There is also a significant

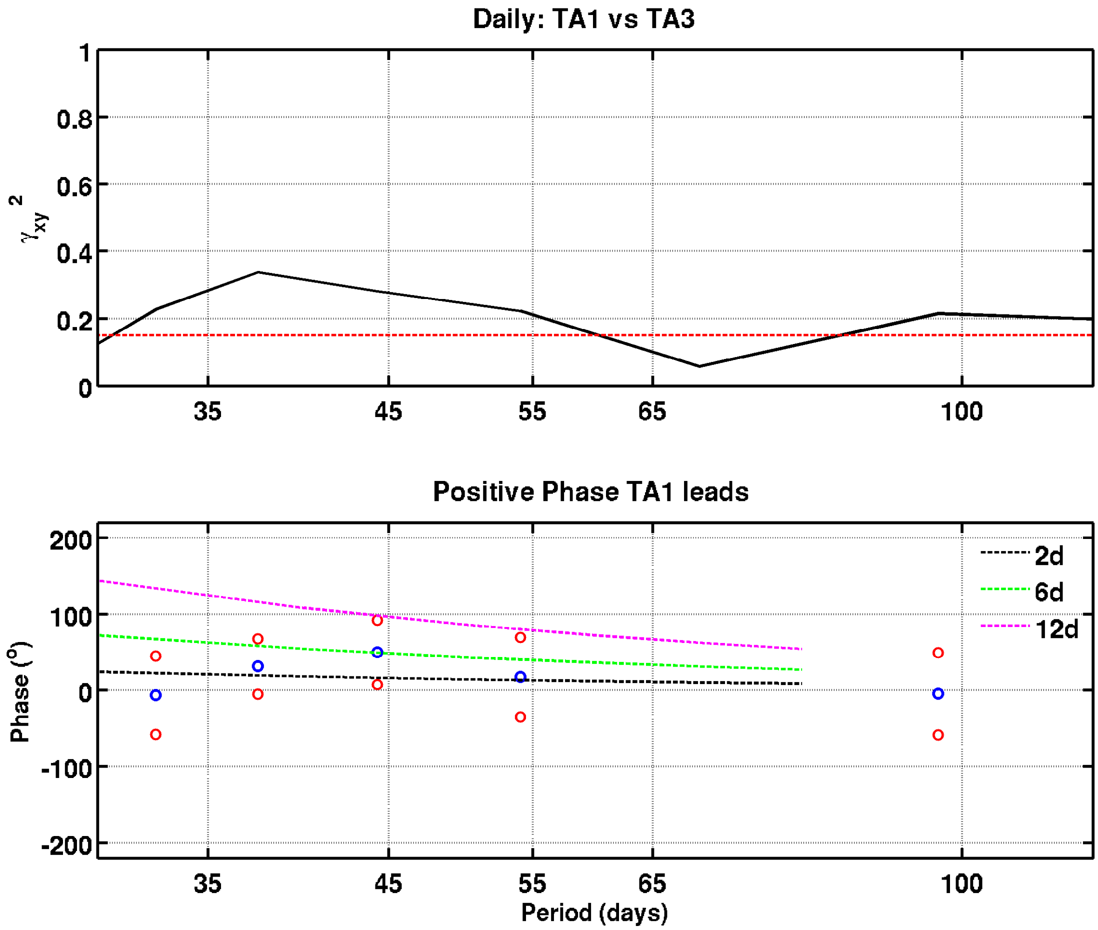

Figure 4.15: Daily- Coherence and phase between TA1 and TA3. Dashed red line for the coherence and the red circles for the phase represent 95% significance levels. Black, Green and magenta lines represent corresponding values of phases and periods for a constant lag of 2 days, 6 days and 12 days respectively.

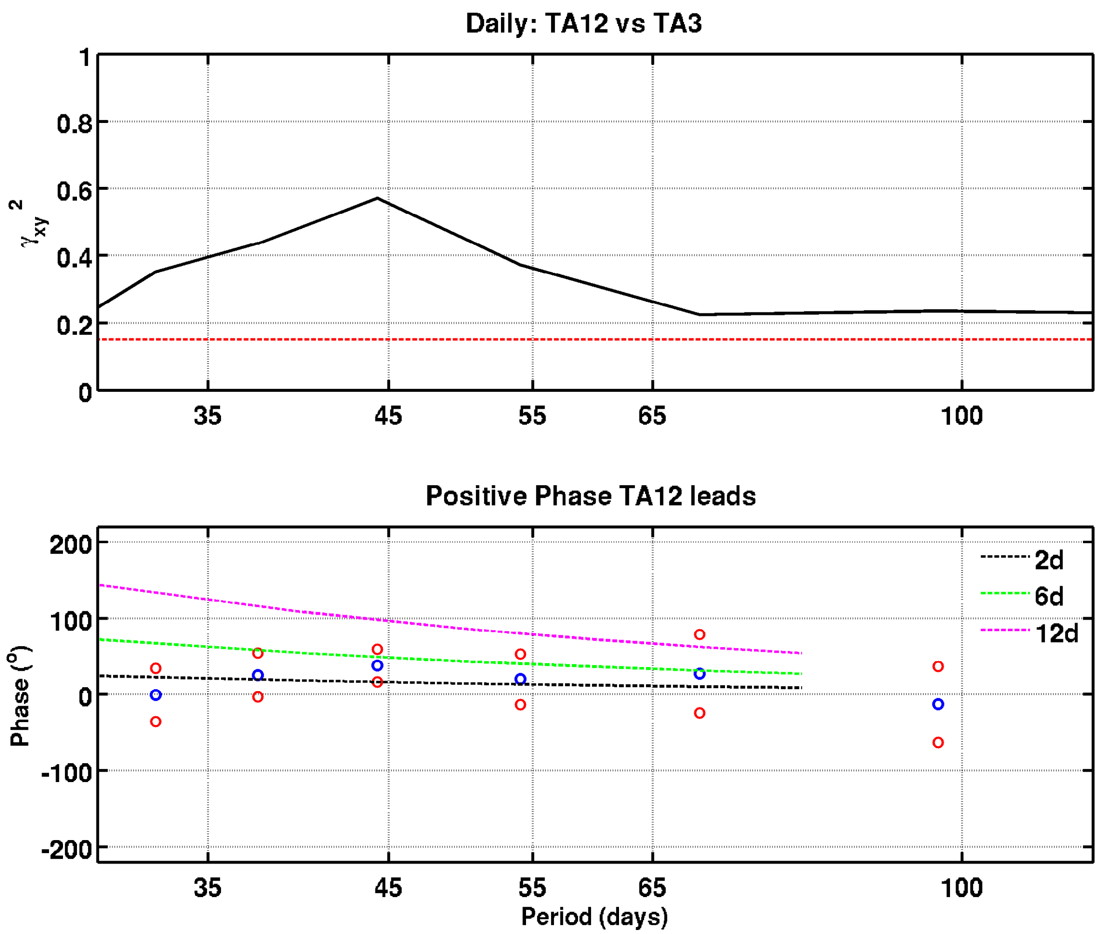

Figure 4.16: Daily - Coherence and phase between TA12 and TA3. Dashed red line for the coherence and the red circles for the phase represent 95% significance levels. Black, Green and magenta lines represent corresponding values of phases and periods for a constant lag of 2 days, 6 days and 12 days respectively.

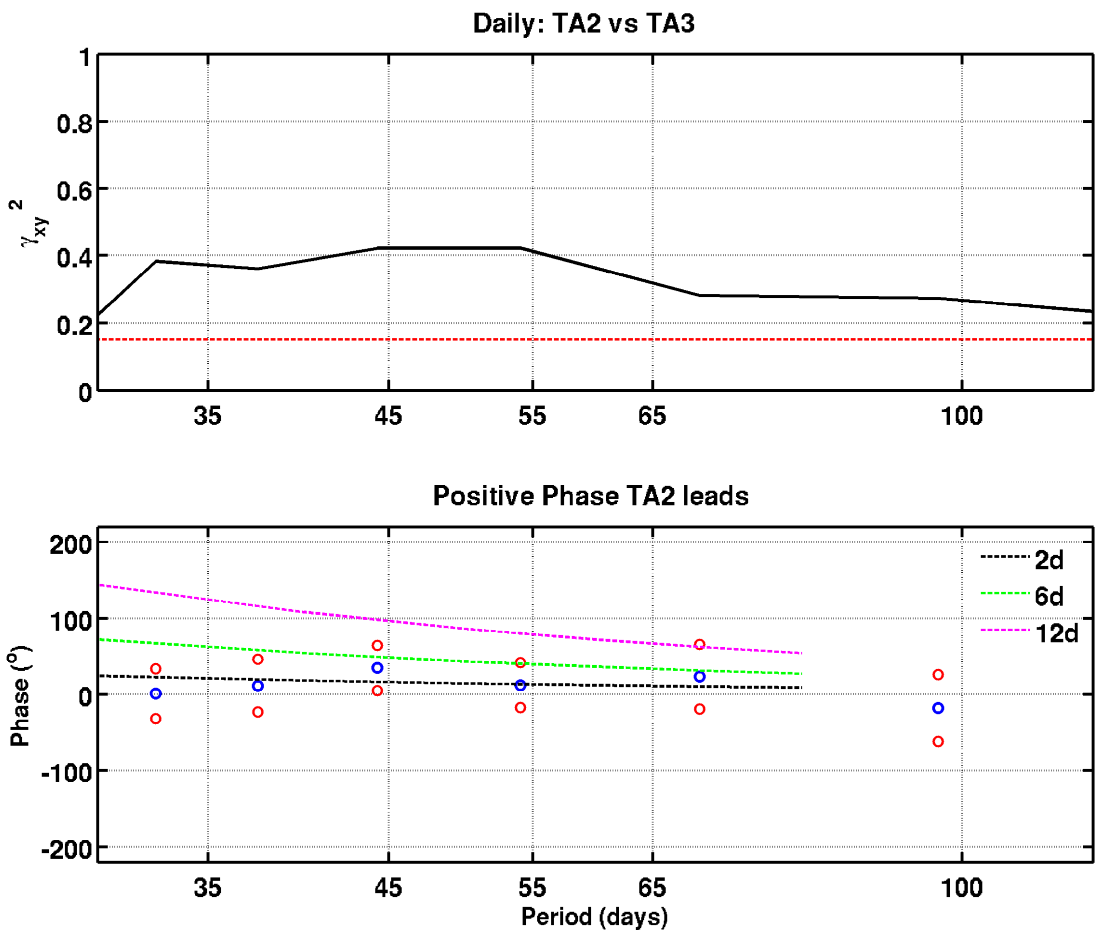

Figure 4.17: Daily - Coherence and phase between TA2 and TA3. Dashed red line for the coherence and the red circles for the phase represent 95% significance levels. Black, Green and magenta lines represent corresponding values of phases and periods for a constant lag of 2 days, 6 days and 12 days respectively.

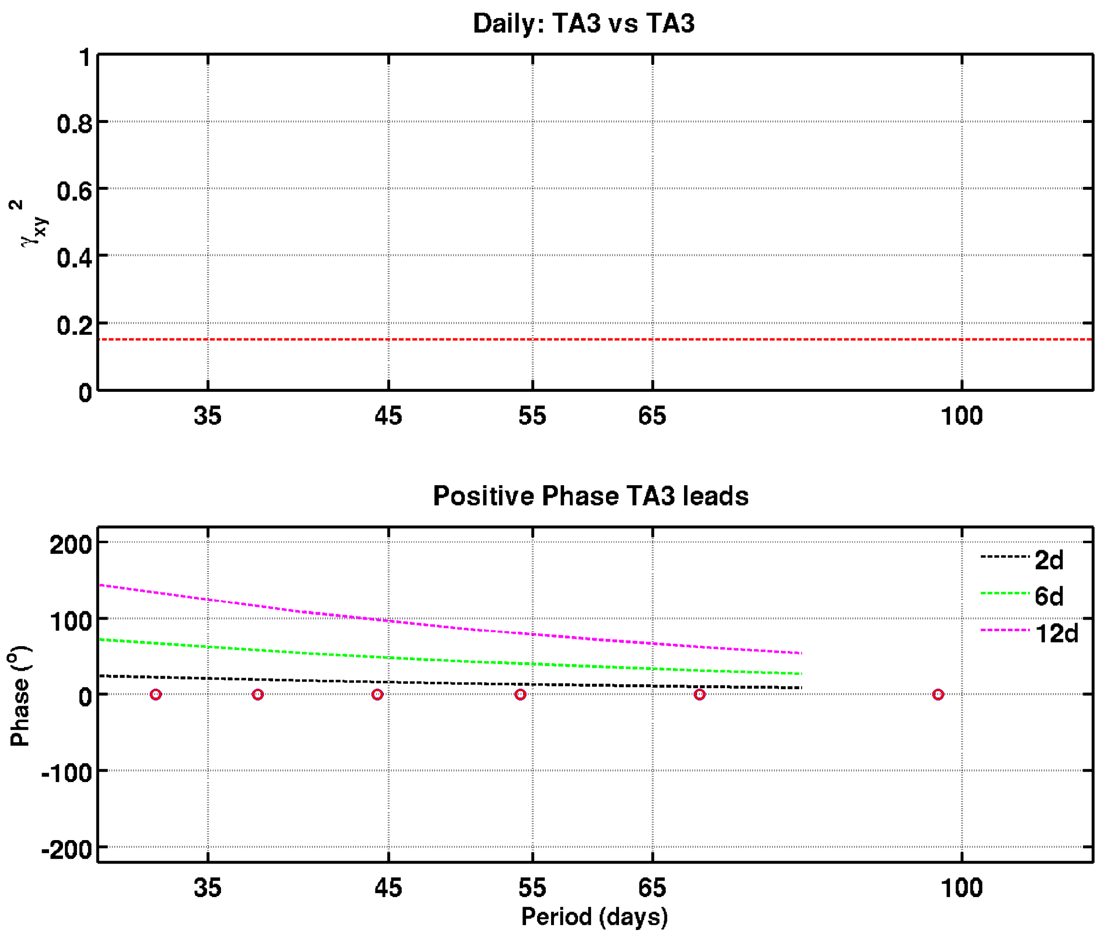

Figure 4.18: Daily - Coherence and phase between TA3 and TA3. Dashed red line for the coherence and the red circles for the phase represent 95% significance levels. Black, Green and magenta lines represent corresponding values of phases and periods for a constant lag of 2 days, 6 days and 12 days respectively.

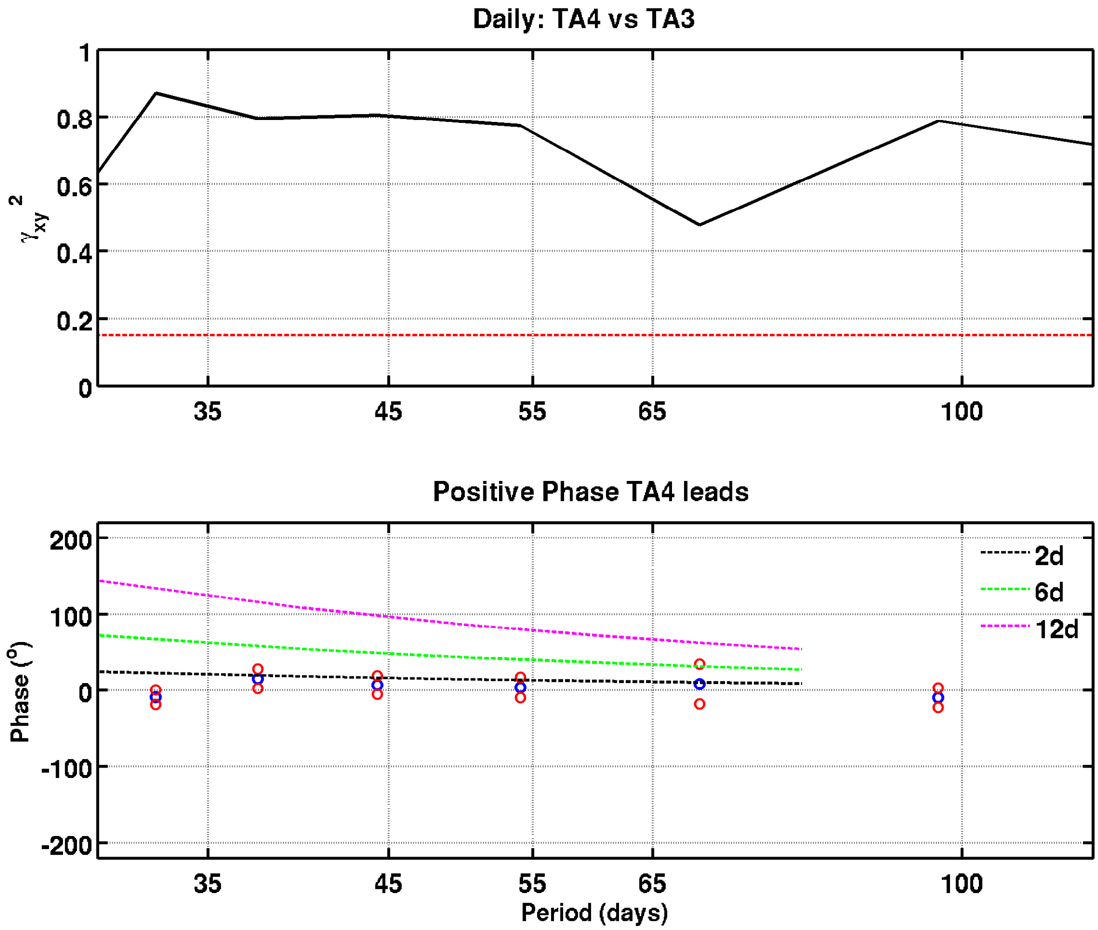

Figure 4.19: Daily - Coherence and phase between TA4 and TA3. Dashed red line for the coherence and the red circles for the phase represent 95% significance levels. Black, Green and magenta lines represent corresponding values of phases and periods for a constant lag of 2 days, 6 days and 12 days respectively.

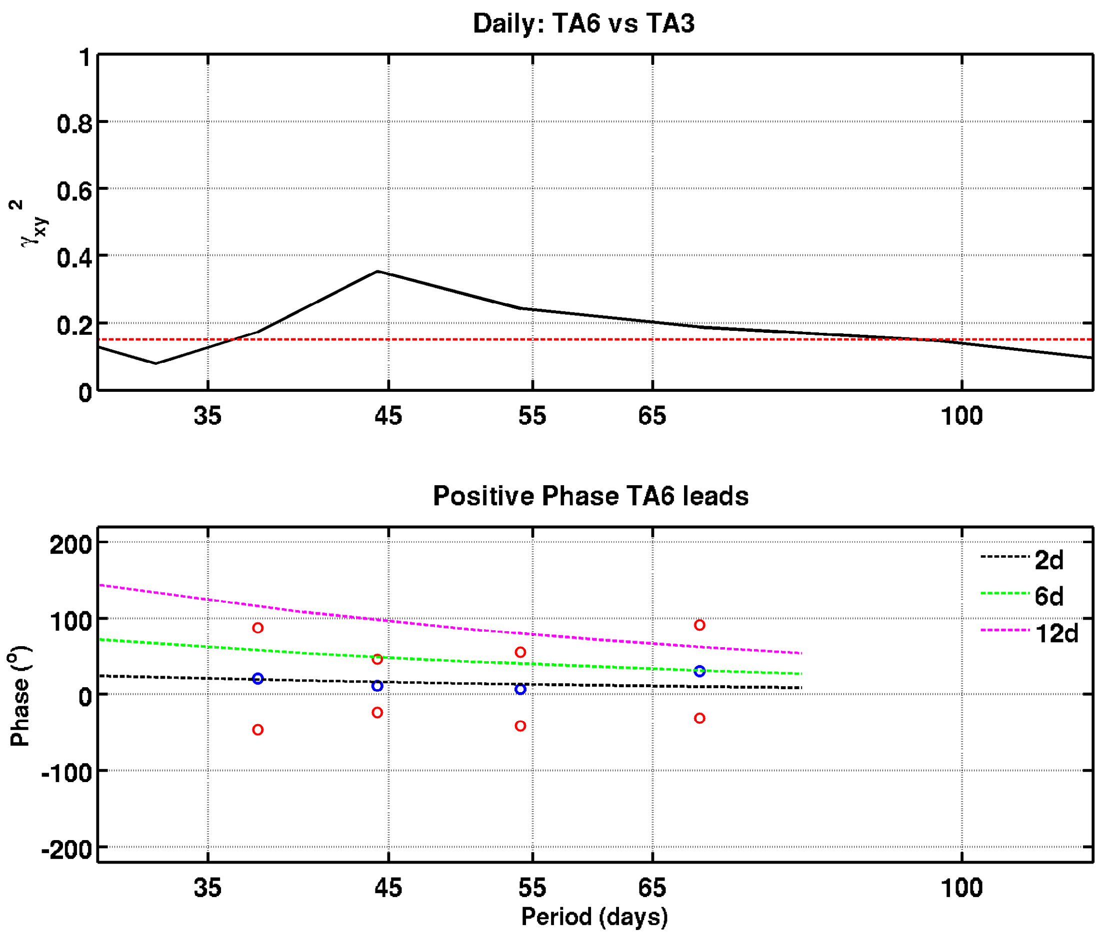

Figure 4.20: Daily - Coherence and phase between TA6 and TA3. Dashed red line for the coherence and the red circles for the phase represent 95% significance levels. Black, Green and magenta lines represent corresponding values of phases and periods for a constant lag of 2 days, 6 days and 12 days respectively.

decrease in the lag between the local winds and sea level, from 5 days to 2 days. This demonstrates that the periods outside of the 40-60 day band contributed to the longer lags of the previous correlations between H1 and local winds. Using the 40-60 band-pass filtered data set in the final model derived in Section 3 (using the same lags) now explains 55% of the total variance compared to the previous 35%, a significant increase.

Our interpretation of the above results is as follows: Winds at all locations used in our analysis are significantly correlated with the basin-scale winds, which are represented by TA3 and TA4 winds. This basin-wide signal produces a lag of 6 days with the SLA on the west coast of India. Hence, when SLA on the west coast is correlated with the winds at any location, the correlations and corresponding lags are primarily due to the basin scale wind relationship, as represented by the 6 day lag at TA3. However, multivariate regression models and coherence plots help to separate this basin-scale signal and give a more realistic lag due to the interaction of SLA and winds within a narrower band of periods. Normalized spectra for H1 SLA and TA3 winds in Fig 3.6 show coincident peaks in energy with periods of 50-60 days (the dominant MJO signal in the basin). The coherence plots of H1 and winds produce more realistic lags for that band and we suggest that the regression models allow signals with those lags to contribute significantly to the explained variance. This is because the strong signal at TA3 explains any and all variance with lags of 6 days, allowing signals with different lags to contribute significantly. However this still leaves open the question of how the basin-scale winds produce a lag of 6 days with SLA along the west coast of India?

A hypothetical explanation consists of the combinations of multiple signals forced by the basin-scale winds. In the Indian Ocean, we have shown that winds are coherent over the intra-seasonal band over most of the basin. Consider large scale winds blowing to the east between the tip of India and the equator. These winds will generate two different SLA signals: low sea level at the tip of India due to upwelling and high sea level at the Equator due to downwelling (exactly opposite in sign). Both of these signals will ultimately reach to the west coast of

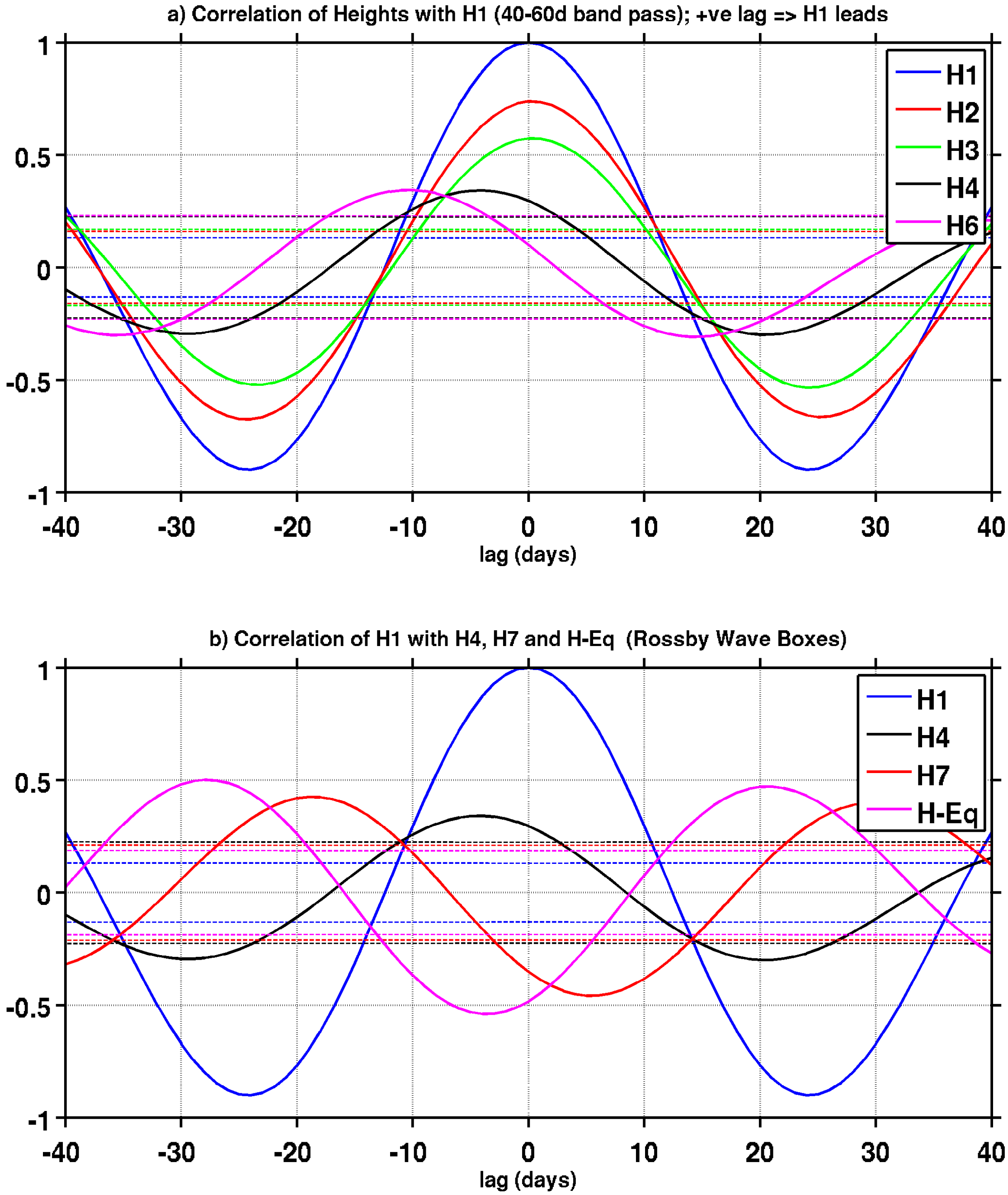

Figure 4.21: Correlation of H1 with all other heights(Daily AVISO) (40-60 day band pass filtered); +ve lag means H1 leads

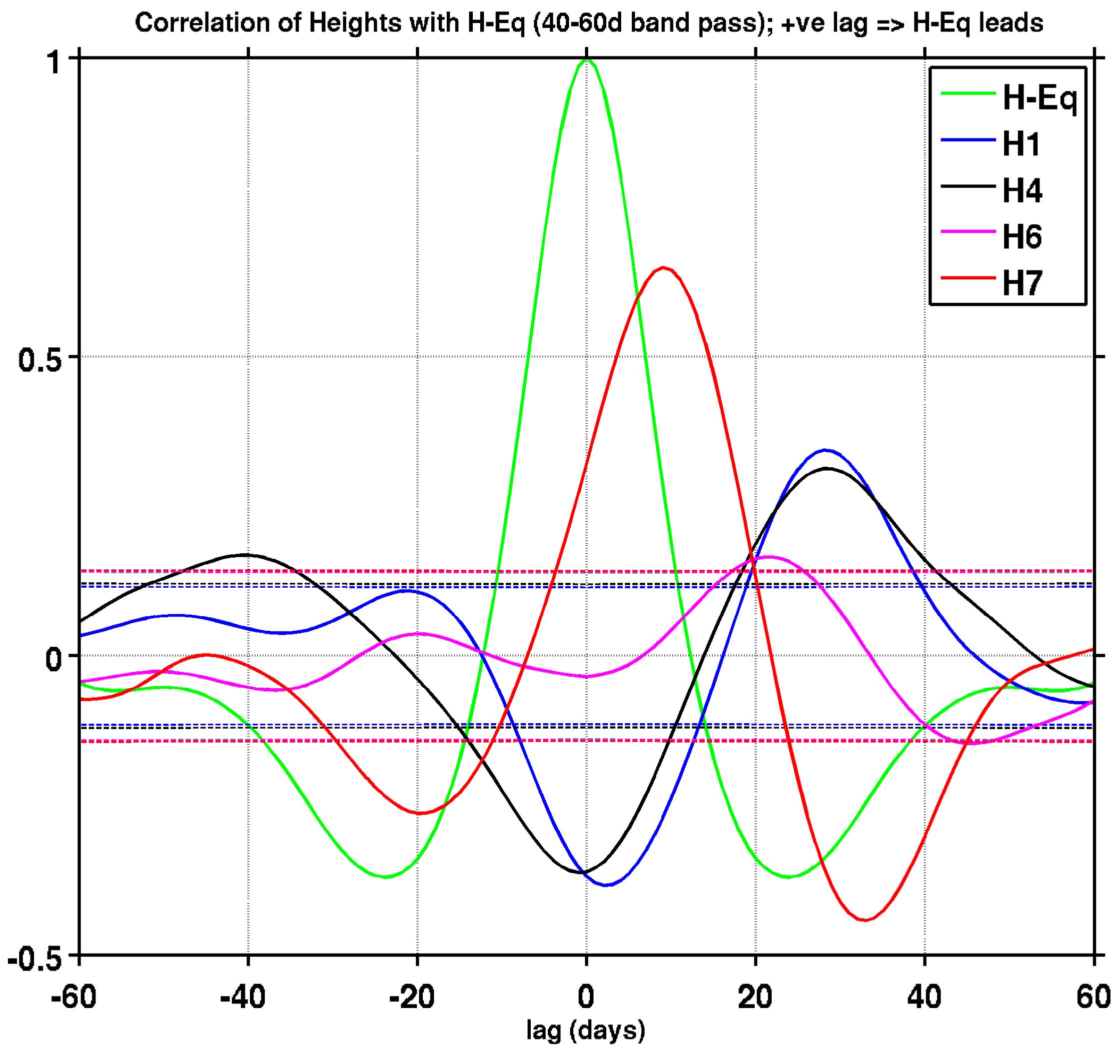

Figure 4.22: Correlation of H-Eq with all other heights(Daily AVISO) (40-60 day band pass filtered); +ve lag means H1 leads

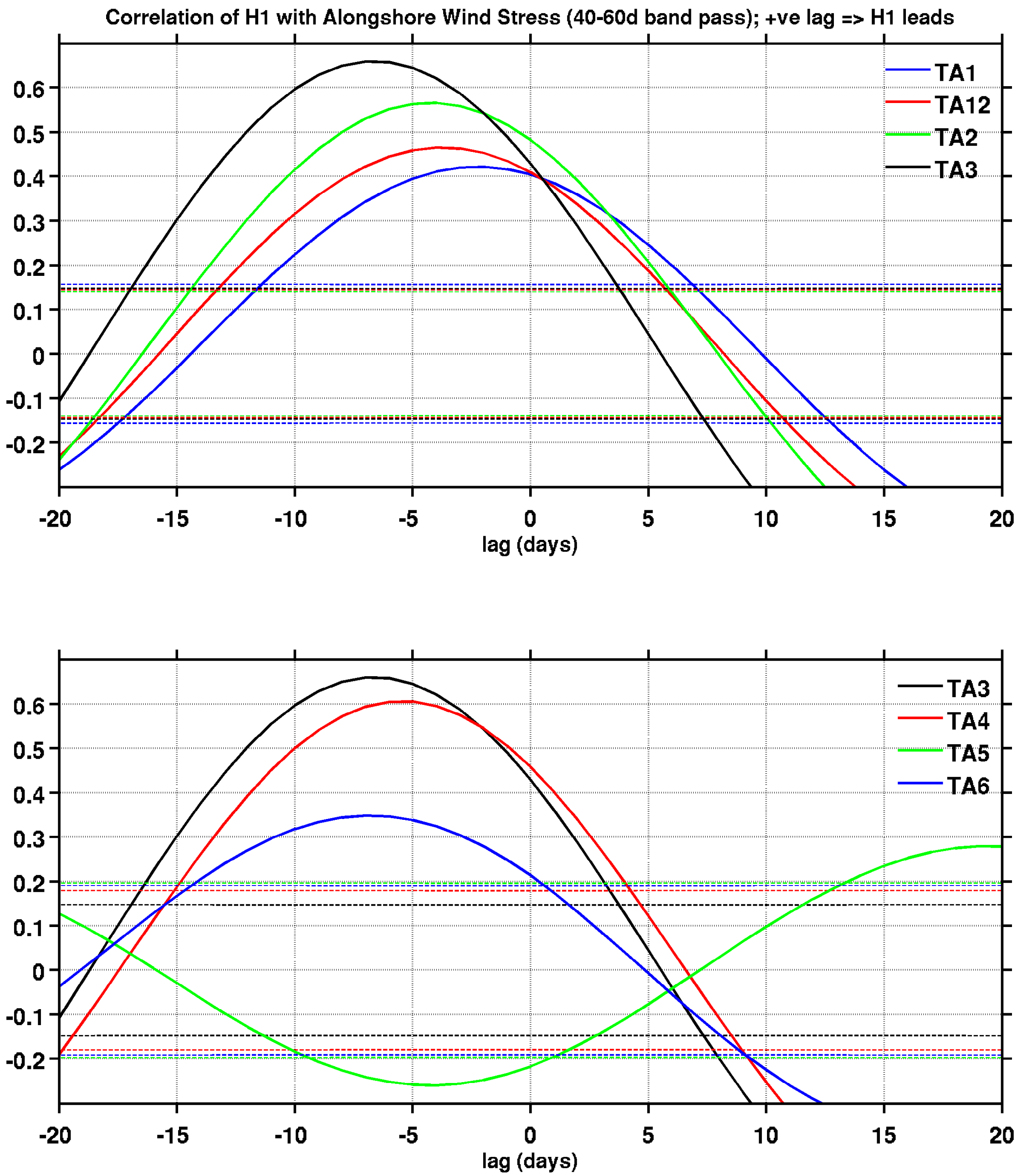

Figure 4.23: Correlation of daily AVISO H1 with alongshore Wind Stress with 40-60 day band pass days filtered; +ve lag means H1 leads

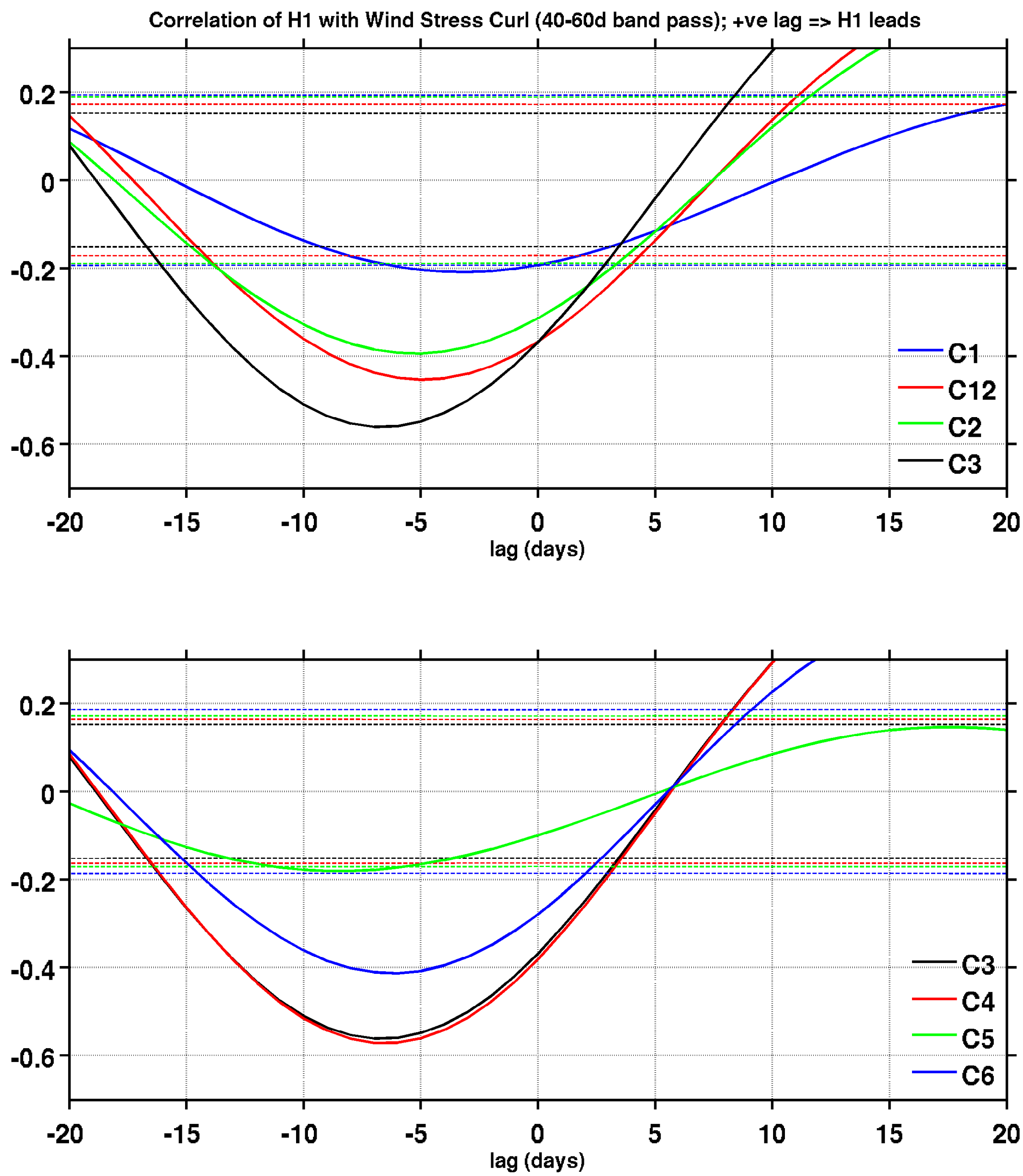

Figure 4.24: Correlation of daily AVISO H1 with alongshore Wind Stress curl with 40-60 day band pass days filtered; +ve lag means H1 leads

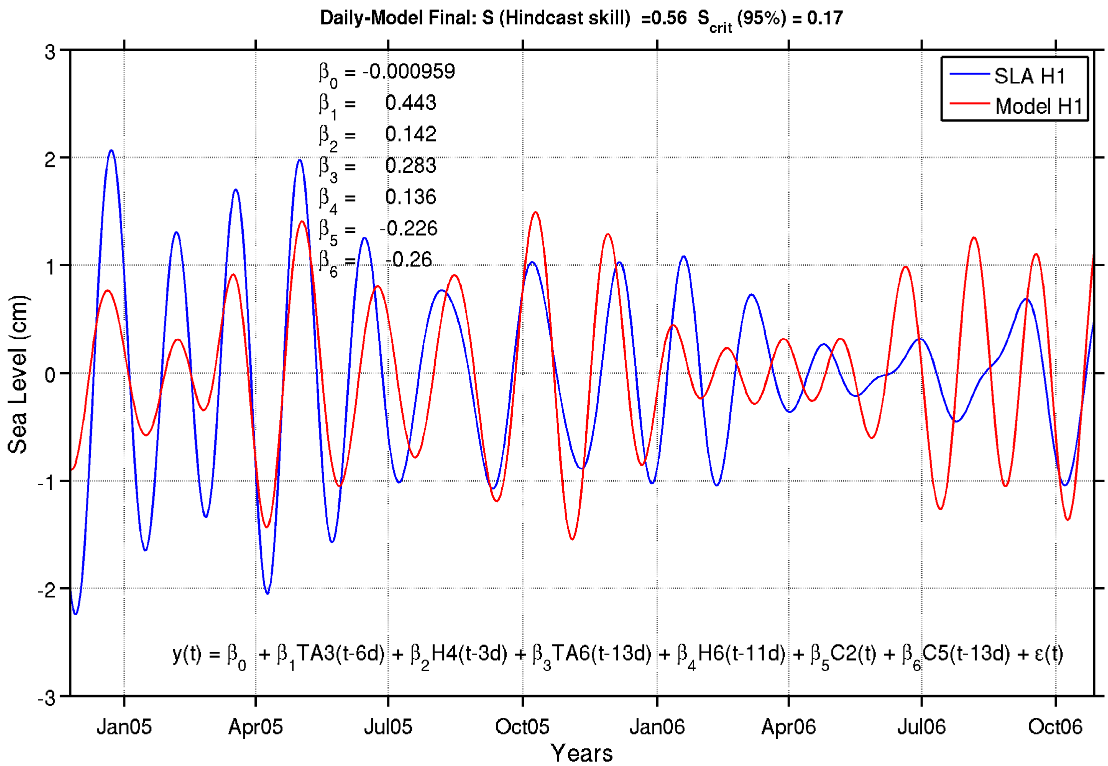

Figure 4.25: Daily AVISO 70 day High pass filtered- Final Model for Predicting H1; input Parameters : TA3, H4, TA6, H6, C2, C5

India following pathways shown in Fig 1.3. The fact that the SLA on the west coast is a combination of the two signals can create an observed but artificial lag. The observed lag depends upon the travel times to reach H1, and the frequency and relative amplitudes of the arriving signals. In this model, many aspects of real ocean SLA generation and propagation are ignored (response time and amplitude, dissipation, frequency-dependent phase velocity). The purpose of the theoretical model is simply to test the hypothesis that two signals produced by basin-scale winds at the tip of India and along the equator with opposite signs could combine after travelling from their generation locations to create an artificial observed lag (similar to the 6 day lag observed here).

Consider $\overset{\frown}{Y}1$ to be a signal created at the tip of India, whereas $\overset{\frown}{Y}2$ is a signal created at the equator which takes time τ to reach the location where both signals combine to give an observed lag Γ, which is 6 days. We assume that the amplitudes A and B remain constant during the travel time for a given frequency.

$$\overset{\frown}{Y}1 = A\ \sin(2\pi f t) = A\ \sin(\varepsilon) \tag{4.1}$$

$$\overset{\frown}{Y}2 = B\ \sin(2\pi f(t-\tau)) = B\ \sin(\varepsilon - \Delta) \tag{4.2}$$

$$\overset{\frown}{Y} = \overset{\frown}{Y}1 + \overset{\frown}{Y}2 = A\ \sin(\varepsilon) + B\ \sin(\varepsilon - \Delta) \tag{4.3}$$

$$\overset{\frown}{Y} = C\ \sin(2\pi f(t-\Gamma)) = C\ \sin(\varepsilon - \delta) \tag{4.4}$$

Here, ε (=$2\pi ft$), Δ (=$2\pi f\tau$) and δ (=$2\pi f\Gamma$) are corresponding phases in the wave equation. Equating 4.3 and 4.4:

$$A\ \sin(\varepsilon) + B\ \sin(\varepsilon - \Delta) = C\ \sin(\varepsilon - \delta) \tag{4.5}$$

$$C = \sqrt{A^2 + B^2 + 2AB\ \cos(\Delta)} \tag{4.6}$$

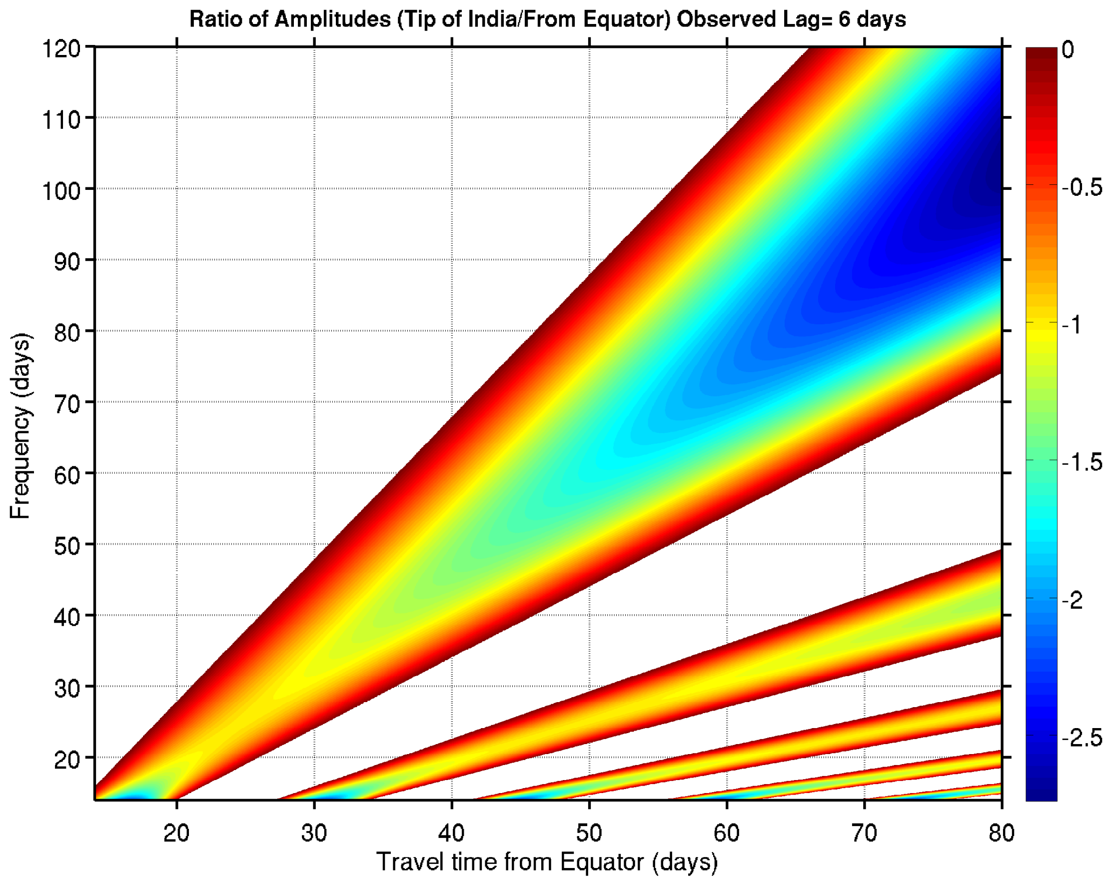

Figure 4.26: Basin wide scale signal assuming a lag of 6 days with SLA on the west coast of India; x-axis is the travel time from equator to reach the tip of India; y-axis is the possible frequencies; z-axis represent the ratio of the amplitudes and the constraint is the ratio has to be negative

$$\tan(\delta) = \frac{B\ \sin(\Delta)}{A + B\ \cos(\Delta)} \tag{4.7}$$

$$\frac{A}{B} = (\frac{\tan(\Delta)}{\tan(\delta)} - 1)\cos(\Delta) \tag{4.8}$$

The travel time τ and the frequency of the winds f is varied (corresponding to Δ=$2\pi f\tau$ in Eq. 4.8) to get a solution where the amplitude ratio ($\frac{A}{B}$) is negative. Fig 4.26 shows possible solutions for travel time and corresponding frequencies which result in a lag of Γ (= 6 days here). For an estimated travel time of 4 to 6 weeks from the Equator to western India, periods of 20 to 80 days can produce an artificial lag of 6 days [Fig. 4.7]. Given the idealized nature of this model we do not expect correspondence of exact values. The model simply shows that a realistic band of frequencies and estimates of travel times could produce artificial lags such as seen in the correlation between SLA at H1 and basin scale winds.

Chapter 5: CONCLUSION

Analysis of 10 years of altimeter sea level anomaly data and the ECMWF winds on intra-seasonal time scales of 30-120 days are consistent with previous studies that report the presence of CTW dynamics along the west coast of India. Sea level at H1 is correlated with sea level and alongshore winds farther south along the coastal wave guide. Sea level at H1 is also moderately well correlated with the sea level east of Sri-Lanka and along the Sumatra coast, implying a more distant connection to the Equator. Sea level at H1 is also weakly correlated with sea level and winds along the south east coast of India. Regression models, coherence calculations and Hovmoller diagrams help to identify the corresponding lags between H1 and the distant signals. Short lags of 0-2 days are found between H1 and the local sea level and winds. Lags of 3 to 5 weeks are found for sea level between Sumatra and Sri Lanka (H4), followed by a lag of several days between Sri Lanka and H1. Between the south-east coast of India and H1, the lags are 11 to 13 days for sea level and winds respectively.

The strongest influence on sea level at H1, as determined by correlation and regression models, is from winds south of the tip of India and Sri Lanka. The puzzle is the lag of 6 days for the maximum correlation between the winds south of India and sea level at H1. This 6 (5-7) day lag is found between H1 and winds at all locations examined. We suggest that this is due to the fact that intra-seasonal winds over the Indian Ocean basin are large-scale and well correlated everywhere. For reasons that are not well understood, these large scale winds are best correlated with sea level at H1 at a lag of 6 days. Thus, correlations between H1 and any winds in the basin represent correlations with the basin-scale winds and produce lags close to 6 days.

Coherence calculations present a somewhat more realistic picture of the lags. In the band with periods between 35-65 days, high coherences between H1 and local alongshore winds identify lags of 0-2 days, more realistic for a coastal response to local winds. High coherences between H1 and the south-east coast of India correspond to lags of 11-13 days for the same band of periods. We expect longer lags such as these between the south-east and the west coasts of India. The above results are consistent with the regression models. Coherence calculations between sea level at H1 and winds south of India continue to show lags of approximately 6 days, consistent with both the correlations and the regression models. A final band-pass filtering of winds and sea levels to reduce periods outside of the 40-60 day band brings the lags from the correlation calculations of H1 sea level and winds into agreement with the coherence calculations. In particular, the lag between local winds and sea level at H1 reduces to a more realistic 0-2 days.

The 6 day lag between sea level at H1 and and winds south of India appear unrealistic for CTW propagation and remain a puzzle. One possible explanation is offered by the combination of different signals arriving at H1 from both local and distant regions, forced by the same basin scale winds.

Bibliography

Amol, P., Shankar, D., Aparna, S.G., Shenoi, S.S.C., Fernando, V., Shetye, S.R., Mukherjee, A., Agarvadekar, Y., Khalap, S. and Satelkar, N.P. (2012), Observational evidence from direct current measurements for propagation of remotely forced waves on the shelf off the west coast of India, *J. Geophys. Res.* (117), C05017, doi:10.1029/2011JC007606.

Babu, M.T., Sarma, Y.V.B., Murty, V.S.N. and Vethamony, P. (2003), Spatio-temporal structure of the East India Coastal Current from satellite altimetry, *J. Geophys. Res.* (114), C02013, doi:10.1029/2008JC004807.

Bakun, A., Roy, C., and Lluch-Cota, S. (1991), Coastal upwelling and other processes regulating ecosystem productivity and fish production in the western Indian Ocean, *,Large marine ecosystems of the Indian Ocean: Assessment, sustainability and management. Massachusettes:* Blackwell Sciences Inc., p. 103141.

Brink, K. H., Beardsley, R. C., Niiler, P.P., Abbott, M., Huyer, A., Ramp, S., Stuart, D., (1991), Statistical properties of nearsurface flow in the California Coastal Transition Zone, *J. Geophys. Res.*: Oceans (19782012), 96(C8), 14693-14706.

Chelton, D., (1983), Effects of sampling errors in statistical estimation, Deep Sea Research Part A, *Oceanographic Research Papers* 1983. Pages 1083-1103, ISSN 0198-0149.

Chelton, D. B., Schlax, M. G., Samelson, R. M., (2011), Global observations of nonlinear mesoscale eddies, *Progress in Oceanography*, 91(2), 167-216.

Clarke, A. J., Liu, X., (1994), Interannual Sea Level in the Northern and Eastern Indian Ocean, *J. Phys.Oceanogr.* (6), 24, 12241235.

Denbo, D. W., Allen, J. S., (1987),Largescale response to atmospheric forcing of shelf currents and coastal sea level off the west coast of North America: MayJuly 1981 and 1982, *J. Geophys. Res.*: Oceans (19782012), 92(C2), 1757-1782.

Ducet, N., Le Traon, P. Y., Reverdin, G., (2000), Global high resolution mapping of ocean circulation from TOPEX/POSEIDON and ERS-1/2, *J. Geophys. Res.* 105, 1947719498.

Durand, F., Shankar, D., Birol, F. and Shenoi, S.S.C. (2009), Spatio-temporal structure of the East India Coastal Current from satellite altimeter, *J. Geophys. Res.* (114), C02013, doi:10.1029/2008JC004807.

Emery, W. J., Thomson, R. E., (2004), Data Analysis Methods in Physical Oceanography, *Elsevier, 2nd Ed.* 2004. Pages 533-539.

Girishkumar, M.S., Ravichandran, M., and Han, W., (2013), Observed intraseasonal thermocline variability in the Bay of Bengal, *J. Geophys. Res*, 118, 33363349, doi:10.1002/jgrc.20245.

Han, W., McCreary, J. P., D.L.T. Anderson, A.J. Mariano (1999), Dynamics of the Eastern Surface Jets in the Equatorial Indian Ocean, *J. Geophys. Res.* (29), 2191-2209.

Le Traon, P. Y.,Nadal, F.,Ducet, N., (1998), An improved mapping method of multisatellite altimeter data, *Atmos. Oceanic Technol.* 15, 522534.

Manjusha, U., Jayasankar, J., Remya, R., Ambrose, T.V. and Vivekanandan, E. (2013), Influence of coastal upwelling on the fishery of small pelagics off Kerala, south-west coast of India, *Indian Journal of Fisheries,* 60 (2). pp. 37-42.

McCreary, J.P., Kundu, P.K., Molinari, R.L. (1993), A numerical investigation of dynamics, thermodynamics and the mixed layer processes in the Indian Ocean., *Prog. In Oceanog.* (31), 181-244.

McCreary, J.P., Han, W., Shankar, D., and Shetye, S. R. (1996), Dynamics of the East India Coastal Current. 2. Numerical solutions., *J. Geophys. Res.* (101), C02013, 1399314010.

Potemra, J.T., Luther, M.E., and OBrien, J.J. (1991), The Seasonal Circulation of the Upper Ocean in the Bay of Bengal, *J. Geophys. Res* 96(C7), 12667-12683.

Rao, R.R., Girish Kumar, M.S., Ravichandran, M., Rao, A.R., Gopalakrishna, V.V. and Thadathil, P. (2010), Interannual variability of Kelvin wave propagation in the wave guides of the equatorial Indian Ocean, the coastal Bay of Bengal and the southeastern Arabian Sea during 1993-2006, *Deep-Sea Res* (114), I:57, 1-13.

Saji, N.H., Goswami, B.N., Vinayachandran, P.N., Yamagata, T., (1999), A dipole mode in the tropical Indian Ocean 199798, *Nature* (401), 360-363.

Schott, F.A., McCreary, J.P., (2001), The monsoon circulation of the Indian Ocean, *Prog. Oceanogr.* 82 (12), 1-123.

Shankar, D. and Shetye, S.R. (1997), On the dynamics of Lakshadweep high and low in the south-eastern Arabian Sea, *J. Geophys. Res.* (102), 0148-0227/97/97JC00465.

Shankar, D. (2000), Seasonal cycle of sea level and currents 1along the coast of India, *Current Science* 78(3), 279-288.

Shankar, D., Aparna, S.G., McCreary, J.P., Suresh, I., Neetu, S., Durand, F., Shenoi, S.S.C., and Al Saafani, M.A. (2010), Minima of interannual sea-level variability in the Indian Ocean, *Progress in Oceanography*, 84(3), 225-241.

Shenoi, S.S.C. (2010), Intra-seasonal variability of the coastal currents around India: A review of the evidences from new observations, *Indian J. Geo-Marine Sci.* 39(4), 489-496.

Shetye, S.R., Gouveia, A.D., Shankar, D., Shenoi, S.S.C., Vinayachandran, P.N., Sundar, D., Michael, G.S. and Nampoothiri, G. (1996), Hydrography and circulation in the western Bay of Bengal during the northeast monsoon, *J. Geophys. Res.* (101), 1401114025, doi: 10.1029/95JC03307.

Suresh, I., Vialard, J., Lengaigne, M., Han, W., McCreary, J., Durand, F. and Muraleedharan, P.M. (2012), Origins of winddriven intraseasonal sea level variations in the North Indian Ocean coastal waveguide, *J. Geophys. Res.* (40), 5740-5744, doi:10.1002/2013GL058312.

Vialard, J., Shenoi, S.S.C., McCreary, J.P., Shankar, D., Durand, F., Fernando, V. and Shetye, S.R. (2009), Intraseasonal response of Northern Indian Ocean coastal waveguide to the Madden-Julian Oscillation, *Geophys. Res. Lett.* (36), L14606, doi:10.1029/2009GL038450.

Vinayachandran, P.N., Shetye, S.R., Sengupta, D. and Gadgil, S. (1996), Forcing mechanisms of the BoB circulation, *Current Science* (114), 71(10), 753-763.

Webster, P.J., Moore, A.M., Loschnigg, J.P., Leben, R.R., (1999), Coupled ocean-atmosphere dynamics in the Indian Ocean during 199798, *Nature* (401), 356-360.

Matsuno, T. (1966), Quasi-geostrophic motions in the equatorial area, *J. Meteor. Soc. Japan* 44(1), 25-43.

APPENDICES

Appendix A: Appendices

A.1 Planetary Waves

A.1.1 Rossby Waves

The dispersion relation for barotropic mid-latitude Rossby waves can be obtained from the shallow water Quasi Geostrophic Potential Vorticity (QGPV) equations with the following assumptions.

1) Nearly Geostrophic flow :

$$u \simeq -\frac{g}{f}\frac{\partial \eta}{\partial y}\,;\ v \simeq \frac{g}{f}\frac{\partial \eta}{\partial x} \tag{A.1}$$

2) Small Meridional displacement:

$$f = f_0 + \beta_0\, y\,;\ \Delta y \ll \frac{f_0}{\beta} \Rightarrow \beta\Delta y \ll f_0 \tag{A.2}$$

3) Small changes in bottom depth:

$$H \simeq H_0 - h_B(x, y) \Rightarrow \frac{h_B}{H_0} \ll 1 \tag{A.3}$$

4) Variations on to the free surface are small:

$$|\eta| \ll H_0 \tag{A.4}$$

The dispersion relation for the linear barotropic Rossby waves, in a background state of rest and nearly flat bottom can be written as follows:

$$\sigma \;=-\frac{\beta\, k}{k^2+l^2+\dfrac{1}{\lambda_0^2}} \tag{A.5}$$

Where $\lambda_0 = \dfrac{C_0}{f_0} = \dfrac{\sqrt{gH_0}}{f_0}$ is the barotropic deformation radius, and k and l are the zonal and the meridional wave numbers.

The eastward phase speed can be written as :

$$C = \frac{\sigma}{k} = -\frac{\beta}{k^2+l^2+\dfrac{1}{\lambda_0^2}} \tag{A.6}$$

It shows that the phase always propagates westward (i.e.,$k < 0$). The group velocity can be written as:

$$\vec{C_g} = \frac{\partial\sigma}{\partial\vec{k}} = \frac{\beta}{\left(k^2+l^2+\dfrac{1}{\lambda_0^2}\right)^2} \;\; \{(k^2-l^2-\frac{1}{\lambda_0^2})\,,\, 2kl\} \tag{A.7}$$

For long waves $(k^2+l^2) \ll \dfrac{1}{\lambda_0^2}$, so from the above equation $\vec{C_g} \to \{-\beta\,\lambda_0^2, 0\}$, meaning energy propagation is zonal and westward at a non-dispersive phase speed. For short waves, $(k^2+l^2) \gg \dfrac{1}{\lambda_0^2}$ from the above equation, the group velocity can be written as:

$$\begin{aligned} \vec{C_g} &= \frac{\beta}{(k^2+l^2)^2} \;\; \{(k^2-l^2-\frac{1}{\lambda_0^2})\,,\, 2kl\} \\ &< \frac{\beta}{k^2+l^2} \;\; \{1\,,\, 2\} \\ &\ll \beta\lambda_0^2 \;\; \{1\,,\, 2\} \end{aligned}$$

We see that the magnitude of short wave group velocity is much smaller than that of the long wave.

In the presence of stratification there are different internal vertical modes. The dispersion relation for the n^{th} vertical mode can be written as follows:

$$\sigma_n = -\frac{\beta\, k}{k^2 + l^2 + \dfrac{1}{\lambda_n^2}} \tag{A.8}$$

where, λ_n, is the n^{th} internal Rossby radius of deformation. The phase speed and group velocity results described above for barotropic mode apply to any internal mode, with λ_0 replaced by λ_n.

When the stratification is depth independent,

$$\lambda_n = \frac{C_n}{f_0} = \frac{N_0\, H_0}{n\, \pi\, f_0} \tag{A.9}$$

where, $N = -\dfrac{g}{\rho_0}\,\dfrac{d\bar{\rho}}{dz}$ is the buoyancy frequency and N_0 is a constant value of N. When N varies with depth, as in the real ocean, C_n (and hence λ_n) must in general be determined numerically.

In basin-scale oceanography we are generally concerned with meridional scales that are much larger than any internal deformation radius:

$$l^2 \ll \lambda_n^2 \tag{A.10}$$

Under this condition, when $k^2 \gg \lambda_n^2$ (short waves),

$$\vec{C}_g \simeq \{\frac{\beta}{k^2}\,,\, 0\} \tag{A.11}$$

In this, the energy propagation is zonal and eastward, and the waves are dispersive.

A.1.2 Kelvin Waves

Kelvin waves are trapped to a lateral boundary in the form of a coast or the equator, along which the energy propagates in the direction of the phase propagation. The waves can be barotropic (n=0) or baroclinic (n>0, with the assumption that the cross-shore velocity is 0 at the boundary, the dispersion relation for these waves can be written as:

$$\sigma_n = C_n \, k; \tag{A.12}$$

with C_n defined as in $(A.9)$. The waves are non-dispersive (the phase speed doesn't depend on the wave number) and coastal Kelvin waves decay exponentially away from the boundary with decay scale λ_n (defined in $A.9$) In the northern hemisphere ($f_0 > 0$), the waves propagate with the boundary on the right.

A.1.3 Coastal Trapped Waves

Coastal trapped waves can be divided into 3 main categorise :

I) Homogeneous fluid with the continental shelf as a function of off-shore direction (x); They can also be sub-categorized into two categorize: 1) Free 2) Forced. In general these types of waves are called "Continental Shelf Waves (CSW)".

II) Stratification without the continental shelf; i.e. assuming a flat-bottom condition. Internal Kelvin waves (discussed above) comes under this category.

III) Non-homogeneous (Stratification) flow with the continental shelf as a function of off-shore direction (x) along with a the presence of wind forcing and friction. This is most general form of coastal trapped waves.

Suppose, the continental shelf has an off-shore structure given by :

$$h(x) = \begin{cases} \mathrm{e}^{2\lambda x} & \text{if } \; 0 \leq x \leq L \\ H & \text{if } \; x > L \end{cases}$$

The dispersion relation for the above case for a homogeneous flow with no wind forcing can be written as :

$$\sigma = \frac{2\,\lambda\, l\, f}{k^2 + l^2 + \lambda^2} \tag{A.13}$$

And the phase speed in the alongshore direction is:

$$C = \frac{\sigma}{l} = \frac{2\,\lambda\, f}{k^2 + l^2 + \lambda^2} \tag{A.14}$$

After applying proper boundary conditions, the above solution gives modes in the off-shore (x) direction. The first mode is the fastest. For long waves, the waves become non-dispersive. For small wave number $l(\rightarrow 0)$:

$$C = \frac{\sigma}{l} = \frac{2\,\lambda\, f}{k^2 + \lambda^2} \tag{A.15}$$

A.1.4 Equatorial Waves

Equatorial waves are trapped along the equator with zonal and vertical propagation. Equatorial Kelvin waves propagate very fast from west to the east. More slowly moving Rossby waves propagate to the west (fastest Rossby wave ∼1/3 speed of Kelvin wave). For higher frequencies there exist inertio-gravity waves, very similar to the mid-latitude Poincare Waves which travel even faster than the eastward propagating equatorial Kelvin Waves. In between these inertio-gravity waves and Rossby waves there exist another class of waves called as Yanai waves or mixed Rossby-gravity waves which may propagate either to the east or to the west.

For an equatorial β-plane ($\cos(\varphi) = 1$, $\sin(\varphi) \simeq \varphi = y/a$, $f = \beta\, y$), linearised shallow water equations for a motionless basic state for mean depth h_e are (Following *Matsuno* [1966]):

$$\frac{\partial u^{'}}{\partial t} - \beta\, y\, v^{'} = -\frac{\partial \Phi^{'}}{\partial x} \tag{A.16}$$

$$\frac{\partial v^{'}}{\partial t} + \beta\, y\, u^{'} = -\frac{\partial \Phi^{'}}{\partial y} \tag{A.17}$$

$$\frac{\partial \Phi^{'}}{\partial t} + gh_e \left(\frac{\partial u^{'}}{\partial x} + \frac{\partial v^{'}}{\partial y}\right) = 0 \tag{A.18}$$

Where as the $\Phi^{'} = gh$ is the geopotential disturbance.

For the case of equatorial Kelvin waves, $v^{'}$ is assumed to be 0, substituting in the above equations:

$$\frac{\partial u^{'}}{\partial t} = -\frac{\partial \Phi^{'}}{\partial x} \tag{A.19}$$

$$\beta\, y\, u^{'} = -\frac{\partial \Phi^{'}}{\partial y} \tag{A.20}$$

$$\frac{\partial \Phi^{'}}{\partial t} + gh_e \frac{\partial u^{'}}{\partial x} = 0 \tag{A.21}$$

Rearranging and rewriting in terms of u' using the above three equations we get:

$$\frac{\partial^2 u^{'}}{\partial^2 t} - gh_e \frac{\partial^2 u^{'}}{\partial^2 x} = 0 \tag{A.22}$$

$$\frac{\partial\, \partial u^{'}}{\partial y\, \partial t} - \beta\, y\, \frac{\partial u^{'}}{\partial x} = 0 \tag{A.23}$$

Solving the above two equation and applying the boundary condition that solution is bounded in y-direction, we obtain only an eastward propagating Kelvin wave mode :

$$u^{'}_{Kelvin} = \mathrm{e}^{-(\beta\, y^2/2\sqrt{gh_e})}\, F(x - \sqrt{gh_e}\, t) \tag{A.24}$$

This mode moves eastward with the long wave speed, c (assuming $c = \sqrt{gh_e}$) with a decay scale away from the equator:

$$L_{eq} = \big(\frac{c}{\beta}\big)^{1/2} \tag{A.25}$$

which is the equatorial Rossby radius of deformation. For a baroclinic equatorial Kelvin wave, the dispersion relation can be written as :

$$\sigma_n = c_n\, k \tag{A.26}$$

For a barotropic mode, the phase speed ($c_0 \sim 200\, m/s$) is around a few hundreds of meters/second where as the first baroclinic mode of equatorial Kelvin wave travels with approximately ($c_1 \sim 200\, cm/s$) a few hundreds centimetres/second.

Now considering other cases where $v^{'}$ is not 0. Rearranging *Eq A14- A16* in terms of $v^{'}$ we obtain :

$$\frac{1}{gh_e}\,\frac{\partial^3 v^{'}}{\partial^3 t} + \frac{\beta^2 y^2}{gh_e}\,\frac{\partial v^{'}}{\partial t} - \frac{\partial}{\partial t}\Big(\frac{\partial^2 v^{'}}{\partial^2 x} + \frac{\partial^2 v^{'}}{\partial^2 y}\Big) - \beta\,\frac{\partial v^{'}}{\partial x} = 0 \tag{A.27}$$

Assuming a wavelike solution in the zonal-direction and substituting into the above equation:

$$v^{'} = V_0(y)\, \exp\left[i(k\, x - \sigma\, t)\right] \tag{A.28}$$

We get,

$$\frac{\partial^2 V_0(y)}{\partial^2 y} + \Big(\frac{\sigma^2}{gh_e} - \frac{\beta^2 y^2}{gh_e} - \frac{\beta\, k}{\sigma} - k^2\Big)\, V_0(y) = 0 \tag{A.29}$$

Here beyond a certain value of y, the above form of the equation implies exponentially growing behaviour. Equatorward of that latitude, the function $V_0(y)$ will be oscillatory in y. Let $c^2 = gh_e$ and $y = \big(\frac{c}{\beta}\big)^{1/2}\,\xi$, then the above equation in it's non-dimensionalised form can be written as :

$$\frac{\partial^2 V_0}{\partial^2 \xi} + \Big(\frac{\sigma^2}{\beta\, c} - \frac{k^2\, c}{\beta} - \frac{c\, k}{\sigma} - \xi^2\Big)\, V_0 = 0 \tag{A.30}$$

This is the Hermite equation in mathematics and the only solution that is bounded at infinity is of the form:

$$V_0 = V_{0j}(\xi) = \frac{\exp\left(-\xi^2/2\right)}{\sqrt{2^j\, j!\ \pi^{1/2}}}\, H_j(\xi) \tag{A.31}$$

Where $H_j(\xi)$ is called as Hermite polynomial with the orthogonality condition:

$$\int_{-\infty}^{\infty} V_{0j}\, V_{0i}\, \mathrm{d}\xi = \delta_{ij} \tag{A.32}$$

Hermite polynomials are generated as:

$$H_j(\xi) = (-1)^j\ \exp\left(\xi^2/2\right) \frac{\partial^j\ \left(\mathrm{e}^{-\xi^2/2}\right)}{\partial^j \xi} \tag{A.33}$$

$$\begin{aligned}
\Rightarrow H_0 &= 1 \\
H_1 &= 2\,\xi \\
H_2 &= 4\,\xi^2 - 2 \\
H_3 &= 8\,\xi^3 - 12\,\xi \\
H_4 &= 16\,\xi^4 - 48\,\xi^2 + 12 \\
\vdots\ &= \qquad \vdots \\
H_n &= (-1)^n\ \exp\left(\xi^2/2\right) \frac{\partial^n\ \left(\mathrm{e}^{-\xi^2/2}\right)}{\partial^n \xi}
\end{aligned}$$

Each of these are bounded and satisfy the equation below:

$$\frac{\partial^2 V_0}{\partial^2 \xi} + \left[(2j+1) - \xi^2\right] V_0 = 0 \tag{A.34}$$

Comparing *Eq A.28* and *Eq A.32*, so that our solution should correspond to one of these eigenfunctions:

$$\frac{\sigma^2}{\beta\, c} - \frac{k^2\, c}{\beta} - \frac{c\, k}{\sigma} = 2j + 1 \quad (j = 1, 2, 3, \dots) \tag{A.35}$$

Rearranging,

$$\sigma^2 = c^2 \left[k^2 + \frac{(2j+1)}{L_{eq}^2} \right] + \frac{\beta\, k}{\sigma}\, c^2 \tag{A.36}$$

Where, $L_{eq} = \big(\frac{c}{\beta}\big)^{1/2}$, which is the equatorial Rossby radius of deformation.

Eq. A34 is a cubic in σ, where as it's a quadratic in terms of wave number k, so re-writing the dispersion relation after solving the quadratic in k :

$$k = -\frac{\beta}{2\sigma} \pm \frac{1}{2} \Big[\Big(\frac{\beta}{\sigma} - \frac{2\sigma}{c} \Big)^2 - 8\, j\, \frac{\beta}{c} \Big]^{1/2} \tag{A.37}$$

In general, the solution for the above dispersion relation can be divided into three categorize:

I) At Higher Frequencies, $\sigma \sim o(kc)$, and if the gravity wave speed is much greater than the Rossby wave speed, $c > \frac{\beta}{k^2}$, we obtain approximate dispersion relation for the Poincare waves (inertio-gravity waves).

$$\sigma^2 = c^2 \left[k^2 + \frac{(2j+1)}{L_{eq}^2} \right] \tag{A.38}$$

II) At Lower Frequencies i.e, for small σ, we obtain an approximate dispersion relation for the equatorial Rossby wave modes :

$$\sigma \; = -\frac{\beta\, k}{k^2 + (2j+1)/L_{eq}^2} \tag{A.39}$$

III) For the case of $j = 0$:

$$k = -\frac{\beta}{2\sigma} \pm \frac{1}{2} \Big(\frac{\beta}{\sigma} - \frac{2\sigma}{c} \Big) \tag{A.40}$$

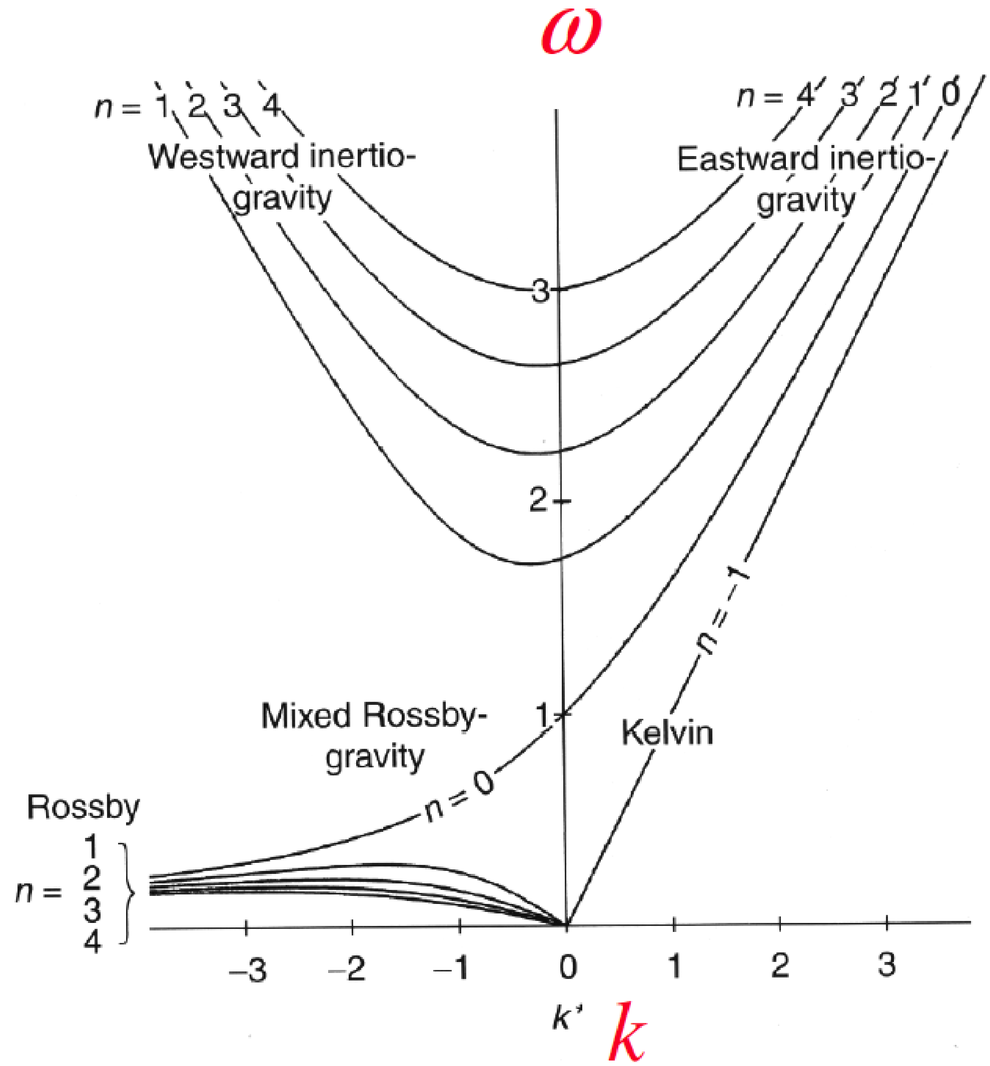

Figure A.1: Dispersion Relations for the Equatorial β-plane. The x-axis represents the wave number and the y-axis is the frequency σ, [*Matsuno*, 1966]

Two roots are then :

$$k_1 = -\frac{\sigma}{c}; \;\; k_2 = -\frac{\beta}{\sigma} + \frac{\sigma}{c} \tag{A.41}$$

The first solution gives an unbounded solution for the zonal velocity in y-direction so must be rejected. The second solution; looks like a Rossby wave at low frequencies i.e., $\sigma \simeq -\frac{\beta}{k}$ while for large frequencies , it looks alike a pure gravity wave, $\sigma \simeq k\,c$. This single wave is often called as the *mixed-Rossby-gravity wave or the Yanai* wave.

Summary of equatorial waves:

I) Rossby waves only propagate to the west, whereas their energy may propagate to the east or west.

II) Yanai waves can have eastward or westward phase propagation but has only eastward energy propagation

III) Kelvin waves propagate to east and are non-dispersive with same speed of phase and energy propagation.

IV) Poincare waves can be categorized into eastward propagating and westward propagating waves. There exist a minimum and a maximum frequency for these modes of waves to exist and the minimum frequency at which they exits won't be at k=0, rather it's slightly shifted to the left because of β, [Fig A.1].

A.2 Computation of N*

There is no robust methodology to compute the effective sample size (N*). However a practical solution which is at least an improvement over the assumption that $N* = N$, is used to estimate value of N*. The effective number of degrees of freedom (N*) at the sample interval Δt is proportional to $N\Delta t$, where N is the total number of observations.

The effective sample size is used to estimate the significance level for correlation between two time-series at different lags. Here we use the Artificial Skill Method (ASM) to compute the effective sample size between two time-series when they are correlated with each other.

As per the above assumption the effective sample size is proportional to the record length:

$$N^* = \nu' \, \Delta t \, N = \nu \, N \tag{A.42}$$

Where as $\nu = \nu' \, \Delta t$ and N is the total number of observations. Consider a lagged regression Model with a lag $\tau_k \, (= k \, \Delta t)$:

$$y(t_n) = \sum_{m=0}^{M} \beta_{mk} \, X_m(t_n + \tau_k) + \hat{\varepsilon_k}(t_n) \tag{A.43}$$

Here, M is the total number of input parameters used in the model and the ε_k represents the error associated with the model corresponding to the lag τ_k. The expected value of skill(fraction of variance explained by the model) of the regression model can be written as:

$$\langle \hat{S_k} \rangle = S_k + S_A(\tau_k) \tag{A.44}$$

Sample skill $\langle \hat{S_k} \rangle$ is a positively biased estimate of the true skill S_k of the postulated regression model, whereas $S_A(\tau_k)$ represents artificial skill due to sampling errors given by:

$$S_A(\tau_k) \simeq \frac{M}{N^*} \tag{A.45}$$

At long lags τ_k, the true skill S_k is assumed to go to 0. Hence,

$$\langle \hat{S_k} \rangle = S_A(\tau_k) \simeq \frac{M}{N^*} = \frac{M}{\nu\, N} \tag{A.46}$$

Here ν represents the degrees of non-independence of the observations which is an intrinsic property of the process of interest and hence it is independent of lags τ_k. Assuming there is no missing observations the effective number of independent samples($N*$) is replaced by N^*_k given by $N^*_k = N- \mid k \mid$:

$$\nu = \frac{M}{\langle N_k\, \hat{S_k} \rangle} \tag{A.47}$$

The above expression is valid only at long lags where the true skill of the postulated model is assumed to be 0. The factor ν can be estimated by replacing the value in the denominator with a sample average of $N_k\, \hat{S_k}$ over a large number of "long" lags, both negative and positive where the true skill of the postulated model is zero, for the processes that are adequately resolved by data records. The expected value in the denominator can be estimated by the arithmetic average over K positive and K negative lags,

$$\hat{A} = \frac{1}{2K} \sum_{k=k_1}^{k_1+K-1} \left[N_k\, \hat{S_k} + N_{-k}\, \hat{S_{-k}} \right] \tag{A.48}$$

An estimate of ν can be obtained by replacing the denominator of *A.45* with $\hat{A}$.

$$\nu = \frac{M}{\hat{A}} \tag{A.49}$$

The effective number of independent samples at any particular lag τ_k can then be estimated as:

$$N^*_k = \nu\, N_k \tag{A.50}$$

Defining a range for the lags which constitute the *long* lags is practically difficult. The lower cut-off has to be such that true skill of the lagged regression model is zero and the upper cut-off should avoid very long lags at which S_k can be very noisy because of the small number of samples, N_k. In this analysis, we assumed 60-80% of the record length to be an approximation for making the arithmetic average which constitutes *long* lags.

For the case of estimating the confidence intervals over the lagged correlation between two time series, the ASM is used with a 2 parameter univariate regression model (M=1) to compute the effective size of independent samples (N*).

For the case of estimating the critical Skill [*Eq 2.4*] while building the hierarchy of models (Suppose from Model 1 with skill S1 going to Model 2 with Skill S2) we need to have an estimate of the effective number of independent samples (N*). Here again the same method is used as above with a 2 parameter univariate regression model, with one timeseries (Y) as the actual dataset and another as the model regression output ($\hat{Y}$) [*Eq 2.1*], to first estimate the individual values of independent sample sizes for each of the two models, N_1^* and N_2^*. For estimating the critical skill to check the significance of increment in the variance explained while going from model 1 to model 2, the value of N* used in the [*Eq 2.4*] is chosen to be the highest among N_1^* and N_2^*.